NASA Contractor Report 2961

The Aerodynamic Design of an Advanced Rotor Airfoil

James A. Blackwell, Jr., and Bobby L. Hinson

CONTRACT NAS1-14597
MARCH 1978

NASA

NASA Contractor Report 2961

The Aerodynamic Design of an Advanced Rotor Airfoil

James A. Blackwell, Jr., and Bobby L. Hinson
Lockheed-Georgia Company
Marietta, Georgia

Prepared for
Langley Research Center
under Contract NAS1-14597

National Aeronautics
and Space Administration

**Scientific and Technical
Information Office**

1978

TABLE OF CONTENTS

THE AERODYNAMIC DESIGN OF AN ADVANCED ROTOR AIRFOIL

By James A. Blackwell, Jr. and Bobby L. Hinson

LOCKHEED-GEORGIA COMPANY

SUMMARY

An advanced rotor airfoil has been designed utilizing supercritical airfoil technology and advanced design and analysis methods. The design was accomplished using a physical-plane, viscous, transonic inverse design procedure, and a constrained function minimization technique for optimizing the airfoil leading-edge shape. Performance analysis was accomplished using a method which solves the full potential-equation in a body-oriented coordinate system, and includes boundary layer displacement effects. The unified design and analysis methodology is assessed as adequate for the present rotor-section design, and should be extensible to the design of sections with operating conditions not significantly different from those considered herein.

The new airfoil was designed subject to stringent aerodynamic design criteria for improving the performance over the entire rotor operating regime. The section is predicted to achieve most of the aerodynamic performance objectives which ensure an improved design. The airfoil exhibits low pitching-moment characteristics in spite of a small amount of nose camber. Nose-droop was found to be necessary in order to obtain a low-speed ($M=0.4$) maximum lift coefficient of 1.5. The section is predicted to achieve a drag-rise Mach number of 0.81 at zero-lift conditions. The maximum thickness-to-chord ratio of the new airfoil is 10%.

INTRODUCTION

The design of new airfoil sections with improved aerodynamic performance for use in helicopter rotors has progressed relatively slow in the past. This lack of rapid progress is due in part to the complexity of the rotor-section design requirements. The rotor airfoil must yield good performance over a wide spectrum of operating conditions such as those sketched in figure 1. Region I is representative of operating conditions for the forward moving rotor blade in forward flight. The second region represents conditions for the retreating blade in forward flight. Region III is indicative of rotor section operating conditions for the helicopter in hover. A second reason for the lack of rotor section design progress has been the lack of advanced airfoil concepts. As a result, work to improve rotor sections initially took the form of minor modifications to conventional NACA airfoils. Typical of this type of research is that discussed in reference 1.

Recently, several new airfoil concepts have been developed that indicate potential gains in rotor performance may be possible in the operating regions of figure 1. For example, in Region I significant progress has been made over the last ten years in increasing the airfoil drag-rise Mach number through the application of "peaky" and "supercritical" airfoil technology. Early applications (1969) of supercritical airfoil technology to rotor airfoil design (ref. 2) indicated large gains in drag-rise Mach number was possible, with respect to conventional airfoils, at low lift coefficients. Unfortunately, the maximum-lift characteristics (Region II) of this section were disappointingly low. Relative to Region II, new airfoil designs by Wortmann (ref. 3) and Liebeck (ref. 4) have shown that the maximum lift of the airfoil can be significantly increased through proper design. These airfoils are not suitable, however, for rotor applications due to poor performance at the operating conditions of Region I. The work does indicate, however, that there is potential for improving rotor performance in Region II through the application of technology developed in this area.

Several attempts (ref. 5) have been made to synthesize the above advanced concepts developed for improving the performance in a single region into a

unified approach. This approach would yield good performance over the entire helicopter flight regime. This work has met with some success. The primary limiting factor in implementing the synthesized design approach and, hence, in achieving improved overall airfoil performance has been the lack of an adequate analytical design and analysis methodology

Over the past five years, significant advances have been made in theoretical methods for the design and analysis of airfoil sections. Examples of these are the viscous, transonic design program of Carlson (ref. 6), the airfoil-optimization program of Vanderplaats and Hicks (ref. 7), and the viscous, transonic-analysis program of Bauer, et al (ref. 8). The use of these advanced analytical programs will substantially increase the rotor-section designers chance of developing a new airfoil that will best suit his particular helicopter mission and result in optimum rotor performance.

It is the objective of this report to present results on the application of some new methods to design a new rotor airfoil on the basis of a representative set of design criteria. Emphasis in this task is placed not only on achieving specific results, but also on both developing and evaluating the complete set of methods for the sample case. The total methodology is defined to include the design logic and the coupled use of design and analysis tools.

The presentation of the results will parallel the overall rotor-airfoil design procedure illustrated in figure 2. The discussion will begin with an in-depth description of the technology elements within the design process necessary for accomplishing the airfoil design. The next sections will describe the development of the new rotor airfoil resulting from application of the technology elements, along with the predicted performance characteristics of the airfoil. Finally, the value of the design logic, the computer codes, and the coupled application of the two will be assessed.

SYMBOLS

a_n, b_n	coefficients and exponents in equation (1)
c	airfoil chord, m
C_d	section drag coefficient
C_ℓ	section lift coefficient
C_{ℓ_α}	lift-curve slope, $dC_\ell/d\alpha$
C_m	section pitching-moment coefficient about quarter chord
C_n	section normal-force coefficient
C_p	pressure coefficient, $(P-P_\infty)/q_\infty$
C_p^*	pressure coefficient for local Mach number of 1.0
H_i	boundary layer incompressible form factor
M	freestream Mach number
M_D	drag-rise Mach number ($dC_d/dM = 0.1$)
M_S	local Mach number immediately upstream of shock
M_T	Mach number for pitching moment break, or Mach tuck ($dC_m/dM = -.25$)
P	static pressure, N/m^2
q	dynamic pressure, N/m^2
R_N	Reynolds number based on freestream conditions and airfoil chord
t	maximum thickness of airfoil, m
u, v	velocity components in x, y directions, m/s
x, y	coordinates along and normal to airfoil chord, m
x_T	laminar boundary layer transition location, m
y_o	airfoil ordinate at $x = 0$, m (see eq. (1))
α	angle of attack, degrees
δ^*	boundary layer displacement thickness, m

Subscripts:

c	camber or mean-line
ℓ	lower surface, or local
t	thickness distribution
u	upper surface
∞	freestream conditions

ROTOR DESIGN OBJECTIVES

In order to guide the design of a new, advanced airfoil for rotor application, a synthesized set of design objectives were developed utilizing the requirements for advanced rotors presented in references 5, 9 and 10. The design objectives have been divided into two categories: geometric constraints and aerodynamic-performance objectives.

Geometric Constraints

In order to achieve a practical rotor-section design, the following geometric constraints were imposed:

1. The airfoil shape must be as easy to manufacture and maintain in the field as shapes currently in use.
2. Minimum t/c of 10% - from structural considerations.
3. Airfoil trailing-edge cutoff thickness greater than 0.2% chord but less than 0.5% chord.
4. Minor airfoil contour deviations, typical of manufacturing tolerances, and moderate variations in leading-edge roughness should have negligible effect on aerodynamic characteristics.

Aerodynamic Performance Objectives

A prioritized list of aerodynamic performance objectives for the advanced rotor section is given in table 1. In general, these are representative of criteria for an outer span airfoil for a medium-performance helicopter main rotor. The first priority performance objectives were to be satisfied as closely as possible. The second and third priority objectives were to have appropriately weaker influence on the design. The sequence of the itemized numbers on the objectives in table 1 is also an indication of priority — the lower numbers having higher priority. To assist in visualizing the aerodynamic performance objectives, most objectives are graphically illustrated in figure 3.

AERODYNAMIC DESIGN CRITERIA

As previously indicated, several advanced-airfoil concepts have been developed that offer potential performance gains in one of the rotor operating regions of figure 1. In this section, an attempt will be made to synthesize these advanced airfoil concepts into a unified set of aerodynamic design criteria that, when applied, will yield a rotor section with improved performance over the entire helicopter flight regime. As background to the presentation of the aerodynamic design criteria in each operating region, the performance of existing airfoil-concepts applicable to rotorcraft will be discussed to assess the merits and weaknesses of each concept. The relative performance characteristics were determined using the transonic analysis program of reference 8.

The airfoils chosen for this background concept-comparison are:

- o NACA 0010 airfoil
- o NACA 64A010 airfoil
- o NASA 11% symmetrical supercritical airfoil
- o FX69-H-098 airfoil

All of the selected airfoils are approximately 10% thick with the exception of the 11% supercritical airfoil. Sketches of these airfoils are provided in figure 4 and a comparison of the airfoil slope distributions is given in figure 5. The NACA 0010 airfoil is representative of airfoils used on rotors up until the last decade, and exhibits good performance characteristics in all three operating regions. The NACA 64A010 airfoil is representative of airfoil sections designed to promote extensive regions of laminar flow over the forward portion of the airfoil and, hence, reduce the airfoil profile drag. The NASA 11% symmetrical supercritical airfoil (ref. 2) was developed in 1969 to improve the high-speed/low-lift performance of rotor sections using the supercritical airfoil concepts developed by Dr. R. T. Whitcomb of NASA. The FX69-H-098 airfoil was developed by Dr. F. X. Wortmann (ref. 5) in an attempt to improve rotor section performance in all three operating regions.

The assessment of existing airfoil performance and the discussion of the aerodynamic design criteria will be divided into three parts which are consistent with the three operating regions in figure 1.

Region I — High Mach Number/Low Lift

Existing Airfoil Performance Assessment. - A comparison of the theoretical performance characteristics for the airfoils shown in figure 4 at typical Region I design conditions is presented in figure 6. Analysis of the data indicates that the lowest value of drag coefficient was obtained for the 11% supercritical airfoil. This is due to the airfoil having a shock wave substantially weaker ($M_S = 1.10$) than the other airfoils ($M_S = 1.20$ to 1.22). The conclusion to be reached from this assessment is that in the specification of design criteria for Region I, the criteria should be heavily weighted toward supercritical concepts.

Design Criteria. - In this section, the aerodynamic design criteria pertinent to achieving the aerodynamic performance objectives in Region I (objectives no. 3, 8, and 12 in table I) will be discussed. Several of these criteria are illustrated in figure 7 in terms of the required pressure distribution shapes. The paragraph number of the individual design criteria which follow are keyed to the numbers depicted in figure 7.

1. *In order to achieve good drag-rise characteristics, a rapid change in curvature must occur near the airfoil leading-edge on both the upper and lower airfoil surfaces.* The presence of the required leading-edge curvature is evidenced by the "peaky" subcritical pressure distribution near the airfoil leading-edge (fig. 7(a)). At transonic speeds, the rapid change in curvature produces supersonic expansion waves that, when acting in concert with design criteria no. 2 (to follow), results in a near isentropic or isentropic recompression of the supercritical flow.

The chordwise location of the subcritical pressure-distribution peak (fig. 7(a)) is very important. The closer the location of the pressure-

distribution peak to the leading edge, the higher the drag-rise Mach number will be. By moving the region of rapid curvature closer to the nose of the airfoil, a considerable reduction in curvature over the crest region of the airfoil can occur. This reduces the supervelocities over the crest region resulting in a delay of the drag-rise Mach number.

The magnitude of the subcritical pressure peak is also very important. If the pressure peak is too large, an adverse gradient occurs over the forward portion of the airfoil at transonic speeds. Further, a subcritical peak that is too large may result in excessive subcritical creep drag (objective no. 12, table I). The correct level of subcritical pressure peak is one that produces a near flat pressure distribution back to the shock at transonic speeds (fig. 7(b)).

The effect that these criteria have on airfoil geometry is depicted in figure 8. The locations of the rapid change of curvature on the airfoil upper and lower surfaces that are pertinent to Region I are denoted as points B and D respectively. For the lower surface the rapid change in curvature is located right at the airfoil leading-edge. On the upper surface, the chordwise location of the rapid change in curvature must be compromised with Region II design criteria (to follow) which requires that point B be located as far aft as possible. For the current design, a compromise location of approximately 10% chord was selected for the upper surface position of the rapid change in curvature and the attendant subcritical pressure distribution peak.

2. *The surface Mach number preceding the shock waves on the upper and lower airfoil surfaces must be less than 1.16 at the design point for Region I ($M = 0.83$, $C_\ell = 0$).* The weak shock wave can be obtained by using "supercritical" design concepts. The mechanism whereby the shock strength is reduced using this concept is illustrated in figure 9. A single strong supersonic expansion wave is generated near the airfoil leading edge by a rapid increase in surface curvature. Through proper airfoil shaping, the expansion wave reflects from the sonic line as a compression wave, strikes the surface, and reflects back toward the sonic

line as a compression wave. The compressive effect following the compression wave results in a substantial reduction in Mach number preceeding the shock. Using this design concept, the strength of the shock wave can be diminished to near-isentropic or to an isentropic flow recompression. A full discussion of this subject can be found in reference 11.

To obtain the favorable recompression described above, the airfoil shape following the regions of rapid curvature (points B and D, fig. 8) back to the airfoil crests (points C and E, fig. 8) must be designed such that the curvature in these regions is minimized. This can be achieved by locating the airfoil crest (at the angle of attack corresponding to $C_\ell = 0$) for each surface as far aft as possible.

The effects of applying this design criteria to the airfoil geometry and slope diagram is demonstrated in figure 8. As can be seen, a flattened effect occurs in the airfoil geometry over regions B to C and D to E. The low values of curvature in these regions can be seen from inspecting the slope diagrams.

3. The pressure recovery following the shocks on the airfoil surfaces (fig. 7(b)) should be mild. Several candidate upper-surface pressure-distribution shapes and their calculated (ref. 12) boundary-layer characteristics are illustrated in figure 10. Shape no. 1 is indicative of the type of design pressure distribution currently used on supercritical airfoils for transport application. This shape provides a maximum amount of boundary-layer recovery following the shock. However, this shape also results in a deterioration of boundary-layer conditions near the airfoil trailing-edge. The geometric shape of the airfoil upper surface that produces pressure distribution no. 1 is one that has a large slope at the airfoil trailing-edge. Pressure distribution no. 2 is representative of Stratford-type (ref. 13) pressure recoveries. This shape aggravates the boundary-layer conditions near the shock but vastly improves the conditions near the trailing-edge. For conditions where the shock is stronger than that shown in figure 10, pressure distribution no. 2 would precipitate earlier separation at the shock. There is also

an attendant increase in profile drag (computed using a Squire and Young-type expression) for shape no. 2. The upper surface geometric shape that corresponds to pressure distribution no. 2 is one that has a near zero trailing-edge slope. Pressure distribution no. 3 appears to be the best compromise pressure recovery. Pressure recovery no. 3 is also highly desirable from Region II design considerations, to be presented later, which require the boundary-layer conditions near the airfoil trailing-edge be as well behaved as possible.

4. *The flow must remain attached over the entire airfoil surface.*

5. *To achieve well behaved boundary-layer characteristics at the airfoil trailing-edge, the trailing-edge pressure coefficient should be minimized as much as possible (more negative).* The aerodynamic effect of this requirement is indicated in figure 11 where similar upper-surface pressure recoveries with differing values of trailing-edge pressure coefficient are shown along with their accompanying calculated boundary-layer characteristics. As can be seen, pressure distirbution no. 1 has vastly superior boundary-layer characteristics near the airfoil trailing edge. It is also interesting to note that this is accomplished with no increase in profile drag. The geometric effect resulting from minimizing the trailing-edge pressure coefficient is that the trailing-edge included angle of the airfoil basic thickness form is reduced.

6. *The airfoil trailing-edge bluntness should be less than one-half the boundary layer thickness at the trailing-edge.* This criterion (ref. 14) ensures that excessive base drag due to the blunt trailing-edge will not occur. This criterion is important to achieving aerodynamic performance objective no. 12 in table 1.

7. *In order to achieve a low drag level at Mach numbers below the onset of drag-rise (objective no. 12, table I), the upper and lower surface boundary-layers must remain laminar back to approximately 30% chord.* Since subcritical pressure peaks (ref. 7(a)) are required near the leading-edge to achieve a high drag-rise Mach number, it does not

appear that aerodynamic performance objective no. 12 can be fully achieved. This is due to the adverse pressure gradients associated with the leading-edge pressure peaks precipitating earlier boundary-layer transition. Furthermore, there is considerable debate within the helicopter industry as to whether or not the rotor-section environment will even permit any length of laminar flow to occur. However, if there is a possibility of achieving laminar flow, every effort should be made to limit the height and severity of the leading-edge pressure peaks without degrading the drag-rise characteristics. It should be noted, however that the flow should be turbulent prior to entering the shock waves (fig. 7(b)) in order to minimize the adverse effects of shock-wave/boundary-layer interaction.

Region II — Low Mach Number/High Lift

Existing Airfoil Performance Assessment. - A comparison of the low-speed high-lift theoretical aerodynamic characteristics for the airfoils in figure 4 is presented in figure 12. This particular comparison is felt to be indicative of the several performance requirements given in table I for Region II. The data in figure 12 are inviscid since this angle of attack is slightly beyond the maximum lift point for several of the airfoils. Analysis of the results in figure 12 indicates several important facts:

1. As can be seen in figure 12(a), where the upper surface leading-edge pressure distributions are shown, a localized region of transonic flow occurs near the leading-edge of the airfoils terminated by strong shock waves ($M_S = 1.6$ to 2.2). As the boundary-layer interacts with the shock wave, its ability to negotiate the remainder of the adverse pressure gradient (fig. 12(b)) is considerably weakened. Of course, the stronger the shock the greater the tendency of the boundary layer to separate. Of the pressure distributions presented in figure 12(a), it is obvious that the FX69-H-098 airfoil has the weakest shock (even though its lift coefficient is 10% higher).

In order to maximize the high-lift characteristics of a new airfoil, it is obvious that the airfoil must be designed to minimize the strength

of the leading-edge shock. From the above considerations, it would appear reasonable that this will best be achieved by biasing the leading-edge shape toward the underlying concepts used in the development of the FX69-H-098 airfoil (ref. 5).

2. The upper surface pressure distribution for the NASA 11% supercritical airfoil over the last 20% of the chord is considerably more adverse relative to the other airfoils. This feature is undesirable, due to the higher tendency of the flow to separate. In addition, the trailing-edge pressure coefficient of the NASA 11% supercritical airfoil is more positive than for the other airfoils, which results in a higher probability of the flow separating as it approaches the trailing-edge. Both of the above occurrences can be traced to the airfoil's large included trailing-edge angle (see fig. 4). From these observations it appears that the new design should minimize the adverse pressure gradients near the trailing-edge and the trailing-edge pressure coefficient in order to delay trailing-edge separation and thus attain a higher value for the maximum lift coefficient.

3. The pitching-moments shown for the four airfoils at $\alpha = 12^{\circ}$ and $M = 0.4$ (fig. 12) are reasonably low indicating that aerodynamic performance objective no. 7 (table 1) should easily be obtained if the new airfoil is not too far from the airfoil concepts presented here.

Design Criteria. - The aerodynamic design criteria for Region II operating conditions will be presented in this section. Several of the aerodynamic criteria to be discussed below are illustrated in figure 13. The paragraph numbers of the individual design criteria which follow are keyed to the numbers shown in figure 13.

1. The Mach number ahead of the leading-edge shock should be less than 1.4 at the conditions corresponding to maximum lift at $M = 0.40$. For shock Mach numbers in excess of 1.4, the condition of the boundary layer is substantially weakened and flow separation occurs at the shock (ref. 15), or near the airfoil trailing-edge thereby limiting the maximum lift of the airfoil. To minimize the strength of the leading-edge shock at these

high-lift/low-speed conditions, "supercritical" design concepts similar to those discussed for Region I can be used. This approach was first recognized by Wortmann (refs. 5 and 16).

The mechanism that reduces the shock strength when supercritical design concepts are used is sketched in figure 14. As can be seen, the mechanism is the same as that shown in figure 8 for Region I. As with Region I, maximum isentropic recompression is achieved for Region II when the crest is as far aft on the airfoil as possible. This is accomplished by allowing a large change in curvature to occur behind the crest for the high angle of attack condition. This causes a visual "corner" to occur on the airfoil. (See point B in figure 8.)

2. *The pressure distribution ahead of the leading-edge shock should be shaped to promote isentropic recompression (fig. 13(a)).* In order to achieve a level of supervelocity over the forward part of the airfoil that culminates in a shock strength no greater than 1.4, the curvature of the airfoil must be low following the leading-edge. This gives the appearance of a flat over the leading-edge region as shown in figure 8 between points A and B. The upper surface design distribution in figure 13(a) cannot be achieved with a symmetrical airfoil if the requirements for Region I are also recognized. The most powerful geometric parameter that can be used to achieve the proper design upper surface pressure distribution is nose droop.

3. *Pressure recovery following the shock should be designed to maintain attached flow up to 90% chord for the condition corresponding to maximum lift.* This criterion is partially achieved by moving the airfoil maximum thickness point as far forward as possible. This results in the majority of flow deceleration taking place over the forward portion of the airfoil where the boundary layer is thin. A forward maximum-thickness location also allows a smaller included trailing-edge angle which in turn produces a more negative trailing-edge pressure coefficient. This has the effect of minimizing the pressure drop between the leading and trailing edges and reduces the tendency of the flow to separate. It should be

noted that this criterion is in conflict with the design criteria of Region I where it is desirable to have the maximum thickness as far rearward as possible. Obviously a compromise must be made.

4. *In order to achieve aerodynamic performance objective no. 1, the design pressure distribution (fig. 13(b)) must be constrained such that the pitching-moment coefficient is minimized.* To achieve a low value of the pitching moment, the amount of airfoil camber must be minimized and the camber must be limited to a forward region of the airfoil. Alternatively, reflex camber may be applied at the trailing edge. No camber would of course be ideal; however, as noted earlier, a moderate amount of nose droop will be required to achieve aerodynamic performance objective no. 2.

Region III — Moderate Mach Number/Moderate Lift

Existing Airfoil Performance Assessment. - A comparison of the theoretical performance characteristics for the airfoils in figure 4 at typical hover conditions (Region III) is presented in figure 15. This comparison is representative of aerodynamic performance objective no. 5.

Analysis of the results in figure 15 indicates that the FX69-H-098 airfoil has the lowest drag coefficient of the four airfoils shown. As can be seen, the FX69-H-098 airfoil has a very small region of supercritical flow which is isentropically recompressed without a shock whereas significant shocks are present on the other three airfoils. It would appear from the results in figure 15 that for Region III design, the design concepts for the new airfoil should be biased toward the concepts used in designing the FX69-H-098 airfoil in order to obtain a minimum drag at $M = 0.60$, $C_\ell = 0.60$.

Design Criteria. - The airfoil aerodynamic design criteria for Region III operating conditions are illustrated in figure 16. The paragraph numbers of the individual design criteria which follow are keyed to the numbers depicted in figure 16.

1. *In order to meet the target drag level of $C_d = .0080$ at $M = 0.60$ and $C_\ell = 0.60$ (aerodynamic performance objective no. 5), the wave drag must be virtually zero.* Wave-drag minimization requires that the entire pressure distribution be subcritical or if supercritical flow is present then the flow must either recompress isentropically or the shock waves must be very weak.

2. *The lower surface pressure distribution should be shaped to promote laminar flow and hence reduce the airfoil profile drag.* The drag coefficient level of 0.0080 at $M = 0.60$ and $C_\ell = 0.60$ can not be achieved without a substantial portion of laminar flow over the airfoil lower surface.

3. *The flow must remain attached to the airfoil trailing edge.*

DESIGN AND ANALYSIS METHODOLOGY

The aerodynamic design considerations previously discussed dictate the design of an airfoil section with good performance at conditions which produce extensive regions of supercritical flow over the airfoil. Therefore, the required theoretical design-and-analysis methodology must be able to treat transonic flows. A number of transonic airfoil design and analysis techniques are currently available. The design methods can be classified as either direct or inverse procedures.

In a direct design approach, a minimization scheme is coupled with an analysis method in order to design airfoils that are in some sense optimized for specific flight conditions. An extremely versatile direct design method is currently under development at NASA-Ames (ref. 7). The Ames optimization technique can be coupled with any theoretical analysis method; however, the transonic inviscid analysis method of Jameson (ref. 17) is currently used since a transonic viscous analysis module would be prohibitively costly. Viscous effects which are very important in transonic flow are therefore neglected. A further difficulty encountered in the application of the Ames program is the necessity for analytically defining the airfoil shape. The proper choice of shape functions is critical to a successful design.

Inverse design methods have been formulated using both hodograph equations (ref. 18) and by solving the problem in the physical plane (refs. 6 and 19). Since hodograph formulations are applicable only to shock-free flows, they are of limited usefulness in transonic design. Furthermore, the methods are difficult to implement and they require excessive user expertise. Physical-plane solutions suffer computational difficulties in the leading-edge region which are usually avoided by prescribing the geometry in the first few percent of the airfoil chord and designing to a specified pressure distribution over the remainder. An additional weakness of the inverse transonic design method of reference 19 is the small disturbance approximation to the full equations. Carlson's method (ref. 6), however, uses the full potential equation formulation. Viscous effects are taken into account by designing a "fluid" airfoil with a

thick trailing edge and then removing the computed displacement thickness to yield the actual airfoil shape. The Carlson method is also easy to use, yields good results, and computation time is small.

The approach that was selected for designing the rotor airfoil involves the use of the Carlson inverse method for designing the aft region of the airfoil (approximately the aft 85% chord) and use of the Ames optimization technique to design the leading edge (where viscous effects are relatively unimportant).

The transonic viscous analysis method of Bauer, et al at New York University (ref. 8) was selected for analysis of the airfoil at design and off-design conditions because it is probably the most widely used and accepted viscous transonic airfoil analysis method. The program is essentially the Jameson code used in the Ames optimization procedure coupled with a Nash-Macdonald turbulent boundary layer method. The NYU method has proven to be fairly accurate, is easy to use, and computations are inexpensive.

In the sections that follow, the individual methods will be discussed in detail and then their combination into a unified design and analysis procedure will be presented. The predictive accuracy of the individual methods is evaluated in Appendix A. An assessment of the value of their application in this exercise is also included at the conclusion of the rotor design and evaluation phase.

Transonic-Airfoil Inverse-Design Method

An inverse design method applicable to airfoils with supercritical flow regions which are terminated by shock waves has recently been developed by Carlson (ref. 6) at Texas A&M University. Briefly, the method involves the solution of the full 2-D potential equation and boundary conditions. A stretched Cartesian computational grid is used in the method. The potential equation and boundary conditions are written in finite-difference form and the resulting nonlinear algebraic equations are solved by successive line over-relaxation. Viscous effects are treated by using the Nash-Macdonald integral boundary-layer method to compute turbulent boundary-layer parameters.

As input to the Carlson program, the user specifies the surface pressure distribution, an assumed airfoil shape, and the freestream flow conditions. The program then solves for the velocity potential and hence the surface slopes, $dy/dx = (v/u)_{body}$. Next, a fourth order Runge-Kutta method is used to integrate the resulting first-order ordinary differential equation to yield the surface ordinates. The airfoil ordinates thus computed are, in general, those of the "fluid" airfoil; that is, they include the boundary layer displacement thickness, δ^*. The corresponding solid airfoil is generated by subtracting the displacement thickness calculated using the Nash-Macdonald method from the fluid airfoil.

The technique outlined above can be used to design all but the leading-edge region (typically, the forward 10 to 15%) of the airfoil. The leading edge is not designed due to numerical difficulties arising from both the Cartesian computational grid and the large flow and geometric derivatives that occur there. The leading-edge contour from the assumed input airfoil shape is used to provide the initial values for integrating the body boundary condition differential equation.

Airfoil Optimization Procedure

Over the past several years, Hicks and his co-workers at NASA-Ames (ref. 7) have been developing and applying an airfoil optimization procedure. The procedure permits the user to specify an aerodynamic quantity to be minimized, referred to as the object function, (e.g., airfoil wave drag); aerodynamic or geometric constraints that must be met (e.g., t/c and/or minimum and maximum pitching moments); and parameters that may be adjusted. The parameters to be adjusted, referred to as decision variables, are usually coefficients or exponents in the equations used to describe regions of the airfoil. For example, an airfoil leading edge upper surface might be represented by

$$(y - y_o) = \sum_{n=1}^{N} a_n x^{b_n} \qquad (1)$$

where y_o is the ordinate at $x=0$. Either the a_n or b_n or combinations thereof can be the decision variables which are adjusted by the optimization procedure to minimize the design objective without violating constraints.

Airfoil optimization is accomplished by using a constrained function minimization scheme (CONMIN) developed by Vanderplaats (ref. 20) together with an inviscid transonic airfoil analysis method originated by Jameson (ref. 17). In the optimization, a solution is computed for an initial airfoil by Jameson's method. The decision variables are then individually perturbed by CONMIN and a solution computed for each perturbation. The resulting gradient information is used to compute the "search direction" which will produce the fastest reduction in the objective function. The decision variables are adjusted along this direction until either a constraint is encountered or the object function increases. At this point, a new search direction is computed and the search repeated. This iteration continues until the object function can no longer be reduced.

The calculation of search directions and the search itself requires many solutions by the Jameson program. The number of these solutions, and hence the computation costs, can be reduced by minimizing the number of decision variables. This can be accomplished by limiting the optimization to one part of the airfoil such as the leading edge. Also, the costs can be reduced by using a fast aerodynamic solution method. For this reason, the inviscid Jameson program is used in lieu of the viscous NYU code (ref. 8) in the Ames optimization procedure. The impact of neglecting viscous effects can be minimized by limiting the optimization to the leading edge region where the boundary layer is thin.

Viscous Transonic Analysis

The computer program released in 1975 by Bauer, Korn, Garabedian, and Jameson of New York University is probably the most widely used and accepted viscous, transonic airfoil-analysis method. The method was developed by combining an inviscid finite-difference 2-D full potential equation transonic program (essentially the Jameson code used in the Ames optimization procedure) with a modified Nash-Macdonald integral, compressible, turbulent boundary-layer

technique. The resulting airfoil-analysis program is applicable to flows with moderate strength shock waves (upstream Mach number less than about 1.4) and it models the viscous uncambering caused by the presence of turbulent boundary layers. The interaction of the shock wave with the boundary layer and any separation that might be present are not properly taken into account. Nevertheless, the program has proven to be an extremely useful airfoil-analysis method. The usefulness is to a large extent due to the elegant problem formulation and solution technique employed in the inviscid calculations. Specifically the Sells transformation used in the method results in a body-oriented coordinate system with very good grid resolution in the vicinity of the leading edge. The use of this coordinate system, together with the use of the full potential-equation formulation and exact boundary conditions, produces very accurate inviscid solutions over the entire airfoil. The turbulent boundary-layer calculations have been empirically adjusted to give good agreement with experimental observations.

Recently, a number of improvements have been made in the NYU program. The program originators developed a fast elliptic-equation solver and the means for including it in mixed elliptic-parabolic-hyperbolic transonic flow calculations. They also developed a wave-drag correction to take into account a spurious mass source occurring at the shock wave due to the use of a nonconservative differencing scheme. Lockheed-Georgia Company researchers added laminar (Thwaites, ref. 21) and transitional (Michel-Smith, ref. 22) boundary-layer methods both to permit the analysis of airfoils with free transition and to improve profile drag calculations.

Unified Design Procedure

The combination of the three methods previously discussed into a unified design procedure is illustrated in figure 17. The procedure was formulated to require a minimum of user prepared data card input. The unified design procedure was developed for execution on the CDC 7600 computer. The implementation of the design procedure involves the following steps:

1. User specifies flow conditions, surface design pressures, and initial

airfoil geometry. The initial geometry provides the prescribed leading edge coordinates and a starting point for the design of the aft-end. The "fluid" (equivalent) airfoil is computed using the Carlson program, the displacement surface removed, and the resulting airfoil is saved on an on-line disk file.

2. Flow conditions (e.g., M and α) are selected for the leading edge optimization phase. These may be the same conditions used in step (1) or the nose may be optimized for different flow conditions. The equations used to describe the airfoil leading edge, the object functions, and the constraints are then specified. The airfoil geometry is recovered from the disk-file and the optimization procedure then modifies the leading edge in order to minimize the object function, subject to the specified constraints. The modified airfoil is then saved on a disk-file.

3. The transonic, viscous analysis method is then employed to analyze the performance of the airfoil at selected design and off-design conditions.

4. If the predicted performance of the airfoil is not satisfactory then the program input is revised and the design phase once again initiated. This might involve repeating the entire process, or only a portion thereof. For example, the analysis might indicate that only the leading edge is unacceptable, in which case only the leading edge optimization phase would be repeated. Also the analysis might indicate that the design pressure distribution needs modifying — the entire process would then be repeated.

ROTOR SECTION DEVELOPMENT

Design Evolution

The airfoil design was initiated using the aerodynamic design criteria previously formulated for Region I (high Mach number/low-lift). Region I was selected for the initial design focus over Regions II (low-speed/high-lift) and III (hover) for several reasons. First, the Region I criteria influence the largest portion of the airfoil shape. Second, the analytical analysis methodology for predicting airfoil performance relative to the aerodynamic-performance objectives in Region I is considerably more advanced than that for Region II (see Appendix A). Lastly, Region III aerodynamic performance objectives are considerably lower in priority than those for Region I. The design conditions of $M = 0.83$, $C_\ell = 0$, and $R_N = 8.3 \times 10^6$ with laminar boundary layer transition fixed at 5% chord were chosen to be indicative of Region I performance and representative of aerodynamic-performance objective no. 8 (table I). This design condition was selected since the attainment of objective no. 8 will generally result in achieving objective no. 3.

The first task was to develop a design pressure distribution consistent with the above operating conditions, the geometric constraints and the aerodynamic design criteria for Region I. The resulting pressure distribution used for input to the Carlson design program is shown in figure 18. The initial design distribution was selected such that a symmetrical airfoil would be produced. A symmetrical airfoil, if practical, would produce zero pitching moments at zero lift and ensure the achievement of aerodynamic-performance objective no. 1. Further, if zero camber can be maintained, a higher drag-rise Mach number can be obtained. A comparison of the input pressure distribution with the design criteria illustrated in figure 7 indicates general agreement.

Also required as input to the Carlson program is a starting airfoil shape. The airfoil chosen for the starting solution is indicated in figure 19 along with its computed (NYU) pressure distribution at design conditions. The input airfoil is symmetrical and is effectively the upper-surface shape of the

FX69-H-098 airfoil reduced in thickness. A thickness-to-chord ratio of 10% was selected since it appeared that this was the maximum permissible thickness consistent with achieving an 0.81 drag-rise Mach number at zero lift (aerodynamic performance objective no. 3).

The final airfoil shape resulting from several applications of the Carlson inverse design technique is presented in figure 20 along with the computed (NYU) pressure distributions for operating conditions indicative of Region I and Region II. As can be seen, the resulting pressure distribution for $M = 0.83$ and $C_\ell = 0$ (fig. 20(b)) has a weaker shock ($M_S = 1.19$) than the original input distribution (fig. 18). Furthermore, a comparison of the resulting transonic pressure distribution with the aerodynamic criteria for Region I indicates general agreement. However, the resulting pressure distribution for the low Mach number/high-lift condition indicates a shock strength in excess of the desired level of $M_S \leq 1.4$. The solution shown in figure 20(c) is inviscid since a strong shock was expected and considerable separation would be present in a viscous calculation. The angle of attack in figure 20(c) is approximately that which would yield $C_\ell = 1.5$ in viscous flow if separation did not occur ahead of 90% chord.

The conclusion to be reached from the analysis of the section developed using the Carlson program was that forward camber, or nose droop, would have to be applied in order to reduce the shock strength at low-speed/high-lift operating conditions to acceptable levels.

Since the Carlson program cannot treat the leading-edge region, the Ames optimization program was used to modify the airfoil shape in figure 20. This modification was to achieve the target leading-edge upper-surface pressure distribution in figure 21. This distribution is consistent with the design criteria for Region II.

In the Ames program the object function selected for minimization in Region II was the airfoil drag (wave drag). The following constraints were imposed:

- o Maximum value of permissible pitching moment
- o Minimum value of permissible pitching moment
- o Maximum value of upper surface suction peak
- o Gradient aft of suction peak
- o Nose shape would have no inflexion points (constrained by y'')
- o $C_\ell = 1.5$
- o $M_S \leqq 1.4$
- o Airfoil shape to be unchanged aft of 20% chord

The equation governing the leading edge shape was indicated in a previous section (equation (1)). The decision variables that were selected for variation in this equation were: y_o, a_3, a_4, b_1, b_2, b_3, b_4. (The coefficients a_1 and a_2 are computed to maintain ordinate and slope at the airfoil match point.)

Considerable effort was expended in finding the proper combination of variables and constraints that would minimize the wave drag and at the same time produce the target pressure distribution shape in figure 21. An intermediate airfoil design resulting from application of the Ames program is presented in figure 22. This shape is of interest because it meets the Region I design criteria and does not have a lower surface leading-edge spike (fig. 22(b)). The Region II performance shown in figure 22(c) indicates substantial improvement relative to figure 20(c), but does not quite achieve the target level for shock strength. Also, the leading-edge pressure-distribution shape differs from the target shape (fig. 21). The pressure distribution indicative of hover (Region III) performance is presented in figure 22(d). As can be seen the shock for this condition ($M_S = 1.26$) is strong enough to produce considerable wave drag.

In summary, the data presented for the intermediate airfoil, using the Ames program, indicates additional leading-edge droop is required to further minimize the upper surface shock strength at Region II operating conditions and to minimize the drag for Region III operating conditions. Some deterioration in the Region I performance can be expected with increased nose droop, however, due to the increased curvature over the airfoil upper surface.

The final airfoil shape resulting from application of the Ames optimization design procedure is presented in figure 23. A list of the airfoil coordinates is included as table II. The coordinates are resolved into a mean-line and thickness distribution and are listed in table III. The airfoil surface slope distribution, mean-line, and thickness distribution are shown in figure 24.

Design Evaluation — Performance Objectives

The basic force and moment data for the new airfoil are presented in figure 25. For flow conditions where no separation is present and only weak shock waves occur, the NYU program (ref. 8) is used to compute the data. For all other conditions, empirical extrapolations of the calculated data are made using experimental results for similar airfoil sections (refs. 5 and 23). Selected pressure distributions for operating conditions representative of the various aerodynamic performance objectives are presented in figure 26 as determined from the NYU code. All data presented, unless otherwise indicated, have the boundary-layer transition locations fixed at 5% chord. In some cases where a large leading-edge peak occurred before 5% chord, the flow was allowed to transition naturally at those points.

In the following discussion the performance of the new airfoil will be evaluated relative to the target characteristics under each aerodynamic performance objective. In addition, the performance of the new airfoil and the FX69-H-098 airfoil will be compared to assist in quantifying any important improvements resulting from the new design.

Aerodynamic Performance Objective No. 1. - This objective requires *the magnitude of the section pitching-moment coefficient for the new airfoil to be less than or equal to 0.010 at a lift coefficient of zero and a Mach number of 0.30.* As indicated in figure 25(d) and summarized in figure 27, this objective was achieved. The pressure distribution for this condition is presented in figure 26(a).

Aerodynamic Performance Objective No. 2. - This objective requires *the maximum lift coefficient of the new airfoil to equal or exceed a value of 1.5 at a Mach number of 0.40.* The pressure distribution corresponding to this condition is presented in figure 26(b). A comparison of the pressure distribution for the new airfoil in figure 26(b) to the design pressure distribution in figure 13 indicates good agreement. In particular, it can be seen that the shock Mach number is approximately 1.4, which is the target value. Further, the predicted separation location on the upper surface (ref. 8) is at approximately 90% chord. Unpublished correlations of maximum lift at low speeds for airfoils with trailing-edge stall show that maximum lift is reached when separation is indicated at 80 to 90% chord using conventional turbulent boundary-layer separation criteria. Thus, it can be concluded from the pressure distribution in figure 26(b) that a maximum lift coefficient of 1.5 can probably be achieved at $M = 0.40$ with the new airfoil design.

Aerodynamic Performance Objective No. 3. - This objective requires *the drag-rise Mach number of the new airfoil be equal to or exceed 0.81 at* $C_\ell = 0$. The theoretical drag coefficient for the new airfoil is plotted versus Mach number in figure 27 at a lift coefficient of zero. As can be seen, this objective is achieved.

The pressure distribution for the new airfoil at $M = 0.81$ and $C_\ell = 0$ is presented in figure 26(e). The local Mach number preceeding the upper surface shock is 1.18 which is slightly higher than desired. The lower-surface leading-edge pressure peak, which was precipitated at this flow condition by the nose droop, is undesirable. However, the pressure peak is tolerated since the nose drop is required to meet the higher-priority $C_{\ell max}$ objective (no. 2).

Aerodynamic Performance Objective No. 4. - This objective requires *the magnitude of the pitching-moment coefficient for the new airfoil to be less than or equal to 0.015 at Mach numbers less than 0.70 for a lift coefficient of zero.* The pitching moment results are summarized in figure 27. As can be seen, the new airfoil meets the required objective.

Aerodynamic Performance Objective No. 5. - This objective requires *the drag level of the new airfoil be less than or equal to 0.0080 at a Mach number*

of 0.60, a lift coefficient of 0.60, and a Reynolds number of 6×10^6. The predicted drag coefficient results at M = 0.60 for the new airfoil are summarized in figure 28 for boundary-layer transition fixed at 5% chord and for free transition. With transition fixed at 5% chord, the predicted drag level is significantly higher than the target level. For free transition, the target drag level is achieved. The predicted transition locations were 9% chord on the upper surface and 73% chord on the lower surface. Since a laminar run of 73% chord cannot be expected in practice, it can generally be concluded that this objective cannot be met by the new airfoil at the specified Reynolds number.

The pressure distribution indicative of this aerodynamic performance objective is presented in figure 26(d). Comparison of this pressure distribution to the Region III design pressure distribution in figure 16 indicates the design criteria were generally met. The maximum upper-surface Mach number (1.21) for the new airfoil was slightly higher than the target value of 1.16. Separation of the upper-surface boundary-layer was indicated at x/c = .96. The possibility of additional pressure drag due to separation further minimizes the chances of the new airfoil to achieve the drag level of 0.0080 required by this objective.

Aerodynamic Performance Objective No. 6. - The objective requires *the section lift coefficient of the new airfoil to equal or exceed a value of 1.5 at a Mach number of 0.50 and a section drag coefficient of 0.0500.* A calculated pressure distribution for $C_\ell = 1.5$ and M = 0.50 is shown in figure 26(c). This pressure distribution is probably not representative of the real flow since the shock Mach number is very strong ($M_S = 1.70$). No doubt, considerable separation is present. Current analytical analysis methods do not properly account for separation; hence, little can be said as to whether the airfoil can support a lift coefficient of 1.5, or what the resulting drag level would be. It is conjectured, however, that the lift coefficient for the new airfoil would approach 1.5 for $C_d = .0500$ and M = .50 since little degradation in $C_{\ell_{max}}$ is noted for a similarly shaped airfoil (FX69-H-098) between M = 0.4 and M = 0.5 (ref. 23).

Aerodynamic Performance Objective No. 7. - This objective requires *the magnitude of the pitching-moment coefficient of the new airfoil be less than or equal to 0.020 at a Mach number of 0.30 and over a lift coefficient range of zero to one.* The computed pitching results for the new airfoil are given in figure 25(d) and summarized in figure 28 for the flow conditions of this performance objective. As can be seen from figure 28, the new airfoil meets the required aerodynamic performance.

Aerodynamic Performance Objective No. 8. - This objective requires *the drag coefficient of the new airfoil be less than or equal to 0.0100 at a Mach number 0.02 above the drag-rise Mach number at zero lift.* A measure of the performance of the new airfoil with respect to this objective can be obtained from figure 27. As indicated previously, the drag-rise Mach number is approximately 0.81. For transition fixed, the predicted drag level of the new airfoil at $M_D + 0.02$ (or $M = 0.83$) is approximately 0.0122 which is considerably higher than the target value of 0.0100. The target incremental drag between $M = 0.70$ (aerodynamic performance objective no. 12) and $M = 0.83$ is 30 drag counts. This compares with a drag increment of 42 drag counts for the new airfoil. With free boundary layer transition (fig. 27), the drag coefficient at $M = 0.83$ and $C_\ell = 0$ is 0.0106 which is close to the target value. Predicted boundary layer transition locations were approximately 30% and 5% chord on the upper and lower surfaces respectively.

The pressure distribution representative of this performance objective is presented in figure 26(f). A comparison with the design pressure distribution in figure 7(b) indicates general agreement with the design criteria specified for good high-speed/low-lift performance. The Mach number preceding the shock wave on the upper surface is 1.20 and is slightly higher than desired.

Aerodynamic Performance Objective No. 9. - This objective requires *the Mach number for rapid increase in pitching-moment coefficient due to compressibility, referred to as the "pitching-moment break" and indicated by a slope of $dC_m/dM = -0.25$, be equal to or greater than the drag-rise Mach number.* Inspection of figure 27 indicates the pitching moment break for

the new airfoil to occur at $M_T = 0.825$ which exceeds the drag rise Mach number of 0.81. Hence, the requirements of this performance objective are met.

Aerodynamic Performance Objective No. 10. - This objective requires *the parameter M^2C_m be maintained less than 0.01 and greater than -0.04 for all Mach numbers less than M_D and for a lift coefficient of zero.* This requirement is translated into the target pitching-moment coefficient curve presented in figure 27. From this figure, it can be seen that the pitching-moment results for the new airfoil are within the permissible limits specified by this performance objective.

Aerodynamic Performance Objective No. 11. - This objective requires *the gentlest possible stall to occur near maximum lift over a Mach number range of 0.3 and 0.4.* It is well known that the gentlest stall occurs (ref. 24) when the flow separates first at the trailing-edge and progressively moves forward. As discussed above under objective no. 2, primary emphasis in the design was placed on suppressing the leading-edge stall. Although no quantitative statement can be made concerning the type of stall, it is anticipated that a gentle stall will occur. This conjecture is supported by the gentle stall results observed on the FX69-H-098 airfoil (ref. 23) and its aerodynamic similarity to the present design.

Aerodynamic Performance Objective No. 12. - This objective requires *the section drag coefficient for the new airfoil be less than 0.0070 at Mach numbers less than 0.71 (M_D-0.10) for a lift coefficient of zero.* As shown in figure 27 for fixed transition at 5% chord, the drag is 9 to 12 counts higher for the new airfoil than the target value. For free transition ($M = 0.6$ typical), the drag level is 0.0074 (fig. 27) with the transition locations at approximately 20% and 4% chord, respectively, on the upper and lower surfaces. The lower-surface leading-edge pressure spike (i.e., fig. 26(a)) prohibits a long run of laminar flow on the lower surface at low lift coefficients.

Comparison of New Airfoil and FX69-H-098 Airfoil. - In order to quantify further the performance of the new airfoil, a comparison is made with the FX69-H-098 airfoil, which is currently in operational use. A comparison of

the pressure distributions for the new airfoil with those for the FX69-H-098 airfoil are presented in figure 29 for conditions representative of Regions I, II, and III.

In figure 29(a) comparative results are shown for a Mach number of 0.4 and lift coefficient of 1.5 (Region II). The leading-edge peak Mach number of the new airfoil ($M_\ell = 1.61$) is considerably lower than that for the FX69-H-098 airfoil ($M_\ell = 1.91$). Also, the upper-surface shock is weaker for the new airfoil. This would seem to indicate the new airfoil has a higher potential $C_{\ell_{max}}$ than the FX69-H-098 airfoil. The trailing-edge separation locations as predicted by the NYU program are approximately the same; however, it must be recognized that the boundary-layer routines in this code do not properly account for effects due to shock-wave/boundary-layer interaction.

A pressure distribution comparison indicative of Region III operating conditions for the new airfoil and the FX69-H-098 airfoil is presented in figure 29(b). As can be seen, the FX69-H-098 has very little supercritical flow (peak $M_\ell = 1.09$) whereas the new airfoil has a fairly strong shock and suction peak (peak $M_\ell = 1.21$). The new airfoil would most certainly exhibit an increase in wave drag relative to the FX69-H-098 airfoil. The trailing-edge separation locations for the two airfoils are comparable.

The comparison of pressure distribution results for the two airfoils at M=0.83 and a lift coefficient of zero (Region I) is shown in figure 29(c). The upper- and lower-surface shocks for the new airfoil are weaker than those for the FX69-H-098 airfoil. No trailing-edge separation was indicated for either airfoil. As a result of the reduced shock strengths for the new airfoil, it is expected that the drag-rise Mach number for the new airfoil will be higher relative to the FX69-H-098 airfoil.

From the above comparison, it appears that the new airfoil offers potential improvement in performance relative to the FX69-H-098 airfoil at low Mach number/high-lift conditions and at high Mach number/low-lift conditions. For conditions characteristic of hover, the new airfoil does not appear to yield the performance of the FX69-H-098 airfoil.

Design Evaluation — Geometric Constraints

The basic geometry of the new airfoil has previously been discussed. In this section the new airfoil will be analyzed relative to the specific geometric constraints listed in the rotor design objectives.

Geometric Constraint No. 1. - This constraint specifies that *the new airfoil shape must be as easy to manufacture and maintain in the field as shapes currently in use.* From figure 23 it can be seen that the new airfoil is smooth and regular with a shape resembling that of the FX69-H-098 airfoil (fig. 4). Thus, it would appear that the shape of the new airfoil would be no more difficult to manufacture than other rotor sections (such as the FX69-H-098 airfoil) currently in use.

Geometric Constraint No. 2. - This constraint requires that *the new airfoil thickness ratio be greater than or equal to 0.10.* Inspection of the airfoil coordinates in table II indicates the airfoil thickness ratio is exactly 0.10, thereby meeting the specified constraint.

Geometric Constraint No. 3. - This constraint requires that *the airfoil cut off thickness be greater than .2% chord but less than .5% chord.* The new airfoil trailing edge thickness is 0.3% chord (table II) which is within the allowable thickness range.

Geometric Constraint No. 4. - This constraint requires that *minor contour deviations, typical of manufacturing tolerances and moderate variations in leading-edge roughness should have neglible effect on aerodynamic characteristics.* Increased roughness on the airfoil has essentially the same effect as a change in Reynolds number as long as the roughness is uniform. The largest expected change would be on the ability of the airfoil to maintain a long extent of laminar flow. Without a detailed roughness analysis it is not possible to determine the quantitative effects of roughness. However, the new airfoil is not expected to be more susceptible to roughness effects than other rotor airfoils in current use.

To investigate the effect of manufacturing tolerances on the performance of the new airfoil, a bump was added to the upper-surface of the leading-edge. The bump originates at the leading-edge and extends to 10% chord. The bump was symmetrical and of sinusoidal shape. Two bump heights were investigated — .06% chord and .18% chord. The results on airfoil pressure distributions typical of Regions I and II are included in figures 30 and 31. The .06% chord bump height has hardly any effect on the airfoil performance. The .18% chord bump produces highly localized effects, but does not appear to change to any large degree the airfoil performance.

METHODOLOGY ASSESSMENT

The aerodynamic design logic as set forth in this report for the development of a new rotor airfoil persuant to the specified aerodynamic performance objectives and geometric constraints appears to be sound as evidenced by the performance predictions for the new airfoil meeting or exceeding the primary aerodynamic performance targets. However, better aerodynamic criteria are needed, particularly in Region II to define more precisely the aerodynamic conditions corresponding to $C_{\ell_{max}}$ when transonic flow is present.

The computer programs used in this design exercise form a compatible framework that can be used for rotor section design and analysis. Several deficiencies in the computer programs were highlighted, however, during the methods evaluation (Appendix A) and the rotor section development. The more important of these deficiencies are noted below and should be corrected in the future by additional research to provide a higher confidence level in the airfoil performance as predicted by these programs.

1. Additional work should be undertaken to extend the validity of the Carlson design program to include the leading-edge region in order to eliminate the specification of a leading-edge shape.
2. Develop better separation criteria and separation models for all programs to allow calculations when a significant amount of separation is present.
3. Drag calculation procedures in the NYU program are not reliable and need revision. This includes profile drag as well as wave drag.
4. The accuracy of the pitching-moment prediction in the NYU program is only fair. Research should continue to improve this portion of the program. This may require a more sophisticated boundary-layer code than currently exists in the NYU code.

The coupling of aerodynamic design criteria with a unified airfoil design and analysis procedure yields a viable approach to advanced rotor section design. The computer programs used in this effort allow the direct

translation of specified aerodynamic design criteria into airfoil geometry and the subsequent analysis of the geometry at off-design conditions to a level of confidence considerably higher than has here-to-fore existed.

The overall methodology described in this report should be extensible to rotor section designs with slightly modified operating conditions or design constraints. The aerodynamic design criteria would not hold for highly cambered airfoils such as that used on aircraft wings. If new aerodynamic design criteria were developed, however, the unified airfoil design and analysis procedure (fig. 17) can still be used with confidence.

CONCLUSIONS

A new, advanced rotor airfoil has been designed utilizing supercritical airfoil technology and theoretical transonic design and analysis methods. The airfoil was designed to meet stringent geometric design constraints and numerous weighted aerodynamic performance objectives covering the complete spectrum of rotor operating conditions.

Some of the more important conclusions of this design effort are described below.

1. The overall design and analysis methodology, as described in this report, can be assessed as adequate for the purpose of designing a rotor section to meet the specified aerodynamic performance objectives and geometric constraints. The methodology is extensible to the design of rotor sections with operating conditions not considerably different from those considered in this exercise.

2. Considerable compromising of the rotor design was required to deal with the closely related, often conflicting requirements of the design criteria.

3. All of the target low pitching-moment characteristics were achieved by the new airfoil design even though nose-droop was required from high-lift considerations.

4. The new rotor section is predicted to achieve a maximum lift coefficient of 1.5 at 0.4 freestream Mach number.

5. The predicted zero-lift drag-rise Mach number of the new airfoil is 0.81 at $R_N = 8.1 \times 10^6$. This matches the target value. In general the various target drag levels cannot be achieved unless the rotor operating environment will permit moderate-to-substantial regions of laminar flow to exist on the airfoil.

6. When compared with the FX69-H-098 advanced rotor airfoil, the performance of the new design is predicted to be superior at low-speed/high-lift and high-speed/low-lift operating conditions. For typical hover conditions (moderate Mach number/moderate lift) the performance of the new airfoil is not expected to match that of the FX69-H-098 airfoil.

APPENDIX A

EVALUATION OF DESIGN/ANALYSIS METHODS

In this section, the Carlson (ref.6) and the NYU (ref. 8) codes will be evaluated as to their predictive accuracy. In particular, their strong points and weaknesses will be identified. The Ames optimization procedure (ref. 7) is not evaluated *per se* since the predictive accuracy of this method is directly keyed to the accuracy of the analysis method coupled in the program (Jameson code (ref. 17)). The Jameson code is essentially an inviscid version of the NYU code and its evaluation is implicit in the evaluation of the inviscid portion of the NYU program.

Carlson Design Method

In figure 32, the correlation of the actual and predicted coordinates for the NACA 0012 airfoil using the Carlson airfoil design method is presented. The input pressure distribution was computed for inviscid, transonic conditions using the NYU analysis method. As can be seen, the agreement between the predicted solution and the actual airfoil is excellent.

A second correlation of the Carlson program is presented in figure 33. This example uses as input the experimental pressure distribution for the Lockheed-Georgia Co. LG4-612 airfoil as obtained in the Lockheed Compressible Flow Facility. This airfoil at the conditions shown has a fairly strong shock wave. Further, the high aft loading of the airfoil results in a substantial boundary-layer growth over the rear of the airfoil. Inspection of the correlation of the actual airfoil with the calculated solid airfoil (fluid airfoil minus boundary-layer displacement thickness) shows good agreement back to about 70% of the airfoil chord. The disagreement over the remainder of the airfoil can be attributed to the inadequacy of the boundary-layer routines to cope with the extensive pressure gradients present for this case. It will also be noted that separation was indicated to occur near the trailing-edge on the upper-surface, and no provision for this is included in the program.

The above example is considered to be an extreme case. For rotor sections which are not aft-loaded and have mild trailing-edge pressure recoveries, the Carlson program should be expected to yield good results.

NYU Analysis Method

The NYU viscous transonic airfoil analysis method will be evaluated relative to experimental data obtained on four airfoils of different design concept:

- o NACA 0012 airfoil
- o NACA 64A010 airfoil
- o NASA 11% symmetrical supercritical airfoil
- o FX69-H-098 airfoil

The correlations were accomplished for each airfoil at three flow conditions: (1) conditions approaching low-speed maximum-lift, (2) hover ($M = 0.6$, $C_{\ell} = 0.6$), and (3) zero-lift drag-rise.

In figure 34, the results from the NYU airfoil analysis program are compared with experimental data for the NACA 0012 airfoil from reference 25. The pressure-distribution comparison for figure 34(a) is good despite a small amount of trailing-edge separation. The NYU program does not properly account for separation; hence, the large discrepancy in drag is not surprising. The correlation for the hover condition presented in figure 34(b) also indicates good agreement. The precise transition location was not known for any of the experimental tests in reference 25, thus introducing unknowns into the drag comparisons. The correlation of pitching-moment coefficient for both conditions is only fair. The discrepancy is due to inaccuracies in both the pressure recovery and loading over the last 20% to 30% of the airfoil. Again, inadequate modeling of viscous effects over the trailing-edge region of the airfoil is responsible for this discrepancy. The zero-lift, high Mach number comparison in figure 34(c) indicates a level shift between the theory and experiment. This level shift could be due to an inadequacy in the theory or due to errors in the experimental data (i.e., wall interference effects).

Data from reference 26 are compared to results from the NYU program for the NACA 64A010 airfoil in figure 35. In general, the pressure distribution correlations are very good. Differences shown in figure 35(a) arise due to the presence of separation near the airfoil trailing edge. All experimental data were obtained with natural transition. The discrepancy near the shock wave in figure 35(c) is due to the laminar shock-wave/boundary-layer interaction that occurred experimentally; whereas, the theory approximates a turbulent interaction. The disagreement in pitching-moment is comparable to that evidenced for the NACA 0012; both are considerably over predicted.

The correlation of experimental data for the 11% symmetrical airfoil with results from the NYU program is given in figure 36. The pressure distribution correlation is generally good over most of the airfoil with the exception being near the trailing-edge. A shift in the shock location is also noted in figure 36(c). The theory appears to underpredict the drag and the level of nose-up pitching-moment for conditions in figures 36(a) and 36(b). However, at zero-lift conditions the NYU program appears to predict the drag level quite well over a wide Mach number range as indicated in figure 37.

The correlation of experimental data from references 23 and 27 for the FX69-H-098 airfoil with the results from the NYU code are presented in figures 38 and 39 respectively. The agreement between theory and experiment shown in figures 38(a) and 38(b), representative of low-speed/high-lift and hover conditions, is similar to that shown previously for the other airfoils. However, the comparison in figure 38(c) for the high Mach number/low-lift condition representation of Region 1 is poor. A similar comparison to that of figure 38(c) is presented in figure 39 using the data of reference 27. As can be seen, the agreement is good. The results in figure 38(c) and 39 are included to point out that poor correlation is not always the inadequacy of the theory, but can be due to extraneous effects on the experimental data such as wind-tunnel wall effects, which is probably the case in figure 38(c).

REFERENCES

1. Davenport, F. J.; and Front, J. V.: Airfoil Sections for Helicopter Rotors — A Reconsideration. Proceedings of the Twenty-Second Annual National Forum. American Helicopter Society, Inc. May 11, 1966, Washington, D. C.

2. Blackwell, James A. Jr.: Aerodynamic Characteristics of an 11-Percent-Thick Symmetrical Supercritical Airfoil at Mach Numbers Between 0.30 and 0.85. NASA TM X-1831, July 1969.

3. Wortmann, F. X.: The Quest for High-Lift. AIAA Paper 74-1018, 1974.

4. Liebeck, R. H.: A Class of Airfoils Designed for High Lift in Incompressible Flow. *Journal of Aircraft*, Vol. 10, No. 10, 1973.

5. Sloof, J. W.; Wortmann, F. X.; and Duhon, J. M.: The Development of Transonic Airfoils for Helicopters. Preprint 901, 31st Annual National Forum, American Helicopter Society, May 1975.

6. Carlson, L. A.: Transonic Airfoil Design Using Cartesian Coordinates. NASA CR-2578, December 1975.

7. Vanderplaats, Garret N.; Hicks, Raymond N.; and Murman, Earll M.: Application of Numerical Optimization Techniques to Airfoil Design. NASA SP-347, 1975.

8. Bauer, F.; Garabedian, P.; Korn, D.; and Jameson, A.: Supercritical Wing Sections II. *Lecture Notes in Economics and Mathematical Systems*, Vol. 108, Springer-Verlag, New York, 1975.

9. Dadone, Leo U.; and Fukushima, Toshiyuki: A Review of Design Objectives for Advanced Helicopter Rotor Airfoils. Paper presented at American Helicopter Society Symposium on Helicopter Aerodynamic Efficiency, American Helicopter Society (Hartford, CT) March 1975.

10. Paglino, Vincent M.; and Clark, David R.: A Study of the Potential Benefits of Advanced Airfoils for Helicopter Applications. Paper presented at American Helicopter Society Symposium on Helicopter Aerodynamics Efficiency, American Helicopter Society (Hartford, CT) March 1975.

11. Pearcey, H. H.: The Aerodynamic Design of Section Shapes for Swept Wings. Proceedings of 2nd International Congress of Aeronautical Sciences, Zurich, 1960.

12. McNally, William D.: Fortran Program for Calculating Compressible Laminar and Turbulent Boundary Layers in Arbitrary Pressure Gradients. NASA TN D-5681, May 1970.

13. Stratford, B. S.: The Turbulent Boundary Layer at Separation. N.G.T.E. Note No. NT.238, June 1956.

14. Horner, S. F.: Fluid-Dynamic Drag. 1965.

15. Lindsey, W. F.; and Johnston, P. J.: Some Observations on Maximum Pressure Rise Across Shocks Without Boundary-Layer Separation on Airfoils at Transonic Speeds. NACA TN 3820, November 1956.

16. Wortmann, F. X.: Design of Airfoils with High Lift at Low and Medium Subsonic Mach Numbers. Conference paper presented at AGARD Specialist's Meeting on the Fluid Dynamics of Aircraft Stalling. Lisbon, 1972.

17. Jameson, A.: Iterative Solution of Transonic Flows Over Airfoils and Wings. Comm. Pure Applied Mach, Vol. 27, 1974.

18. Bauer, F.; Garabedian, P.; and Korn, D.: Supercritical Wing Sections. *Lecture Notes in Economics and Mathematical Systems*, Vol. 66, Springer-Verlag, New York, 1972.

19. Steger, J. L.; and Klineberg, J. M.: A Finite-Difference Method for Transonic Airfoil Design. AIAA Paper 72-679, 1972.

20. Vanderplaats, Garret N.: CONMIN — A Fortran Program for Constrained Function Minimization. NASA TM X-62282, 1973.

21. Thwaites, B.: Approximate Calculation of the Laminar Boundary Layer. *Aero Quarterly*, Vol. 1, p. 245, 1949.

22. Cebeci, T.; Mosinskis, G. J.; and Smith, A. M. O.: Calculation of Viscous Drag of Two-Dimensional and Axisymmetric Bodies in Incompressible Flows. AIAA Paper 72-1, 1972.

23. Kemp, Larry D.: An Analytical Study for the Design of Advanced Rotor Airfoils. NASA CR-112297, March 29, 1973.

24. Prouty, R. W.: A State-of-the-Art Survey of Two-Dimensional Airfoil Data. American Helicopter Society Symposium on Helicopter Aerodynamic Efficiency. March, 1975.

25. Gregory, N.; and Wilby, P. G.: NPL 9615 and NACA 0012, A Comparison of Aerodynamic Data. ARC C.P. No. 1261, 1973.

26. Stivers, Louis S. Jr.: Effects of Subsonic Mach Number on the Forces and Pressure Distributions on Four NACA 64A-Series Airfoil Sections at Angles of Attack as High as 28°. NACA TN 3162, March 1954.

27. Noonan, Kevin W.; and Bingham, Gene J.: Two Dimensional Aerodynamic Characteristics of Several Rotorcraft at Mach Numbers from 0.35 to 0.90. NASA TM X-73990, January 1977.

TABLE I. AERODYNAMIC PERFORMANCE OBJECTIVES

		FIRST PRIORITY	SECOND PRIORITY	THIRD PRIORITY
REGION I	M	(3) $M_D \geq 0.81$ @ • $C_\ell = 0$		(9) $M_T \geq M_D$
	C_d		(8) $C_d \leq 0.0100$ @ • $M = M_D + 0.02$ • $C_\ell = 0$	(12) $C_d \leq 0.0070$ @ • $M \leq M_D - 0.10$ • $C_\ell = 0$
	C_m	(4) $\lvert C_m \rvert \leq 0.015$ @ • $M \leq 0.70$ • $C_\ell = 0$		(10) $0.01 \geq M^2 C_m \geq -0.04$ @ • $M \leq M_D$ • $C_\ell = 0$
REGION II	C_ℓ	(2) $C_\ell \geq 1.5$ @ • $M = 0.40$ • $C_{\ell_\alpha} = 0$	(6) $C_\ell \geq 1.5$ @ • $M = 0.50$ • $C_d = 0.0500$	
	C_m	(1) $\lvert C_m \rvert \leq 0.010$ @ • $M = 0.30$ • $C_\ell = 0$	(7) $\lvert C_m \rvert \leq 0.020$ @ • $M = 0.30$ • $0 \leq C_\ell \leq 1.0$	(11) GENTLEST POSSIBLE STALL @ • $0.30 \leq M \leq 0.40$
REGION III	C_d		(5) $C_d \leq 0.0080$ @ • $M = 0.60$ • $C_\ell = 0.60$	

TABLE II. — DESIGN COORDINATES OF ROTOR AIRFOIL

X/C	Y/C	
	UPPER SURFACE	LOWER SURFACE
.00000	.00000	.00000
.00106	.00529	-.00411
.00433	.01115	-.00729
.00972	.01724	-.01001
.01722	.02349	-.01267
.02678	.02973	-.01525
.03844	.03594	-.01773
.05206	.04164	-.02010
.06767	.04668	-.02238
.08428	.05079	-.02444
.09928	.05369	-.02605
.12942	.05782	-.02881
.15972	.06037	-.03107
.19018	.06187	-.03292
.22077	.06266	-.03445
.25148	.06298	-.03569
.28231	.06294	-.03667
.32000	.06246	-.03753
.35000	.06181	-.03797
.37500	.06111	-.03817
.40000	.06026	-.03823
.42500	.05926	-.03813
.45000	.05813	-.03791
.47500	.05684	-.03753
.50000	.05543	-.03703
.52500	.05388	-.03638
.55000	.05219	-.03561
.57500	.05037	-.03470
.60000	.04842	-.03366
.62500	.04634	-.03250
.65000	.04415	-.03122
.67500	.04183	-.02981
.70000	.03938	-.02828
.72500	.03682	-.02664
.75000	.03415	-.02489
.77500	.03136	-.02302
.80000	.02846	-.02104
.82500	.02545	-.01895
.85000	.02234	-.01676
.87500	.01911	-.01446
.90000	.01579	-.01206
.92500	.01236	-.00957
.95000	.00884	-.00697
.97500	.00521	-.00428
1.00000	.00150	-.00150

TABLE III. — CAMBER AND THICKNESS DISTRIBUTION OF THE ROTOR AIRFOIL

X/C	Y_c/C	Y_t/C
.00000	.00000	.00000
.00106	.00059	.00470
.00433	.00193	.00922
.00972	.00362	.01362
.01722	.00541	.01808
.02678	.00724	.02249
.03844	.00910	.02683
.05206	.01077	.03087
.06767	.01215	.03453
.08428	.01317	.03761
.09928	.01382	.03987
.12942	.01451	.04331
.15972	.01465	.04572
.19018	.01447	.04739
.22077	.01411	.04856
.25148	.01365	.04933
.28231	.01314	.04980
.32000	.01247	.05000
.35000	.01192	.04989
.37500	.01147	.04964
.40000	.01102	.04924
.42500	.01057	.04869
.45000	.01011	.04802
.47500	.00966	.04719
.50000	.00920	.04623
.52500	.00875	.04513
.55000	.00829	.04390
.57500	.00783	.04254
.60000	.00738	.04104
.62500	.00692	.03942
.65000	.00647	.03768
.67500	.00601	.03582
.70000	.00555	.03383
.72500	.00509	.03173
.75000	.00463	.02952
.77500	.00417	.02719
.80000	.00371	.02475
.82500	.00325	.02220
.85000	.00279	.01955
.87500	.00233	.01678
.90000	.00187	.01392
.92500	.00140	.01097
.95000	.00094	.00791
.97500	.00046	.00474
1.00000	.00000	.00150

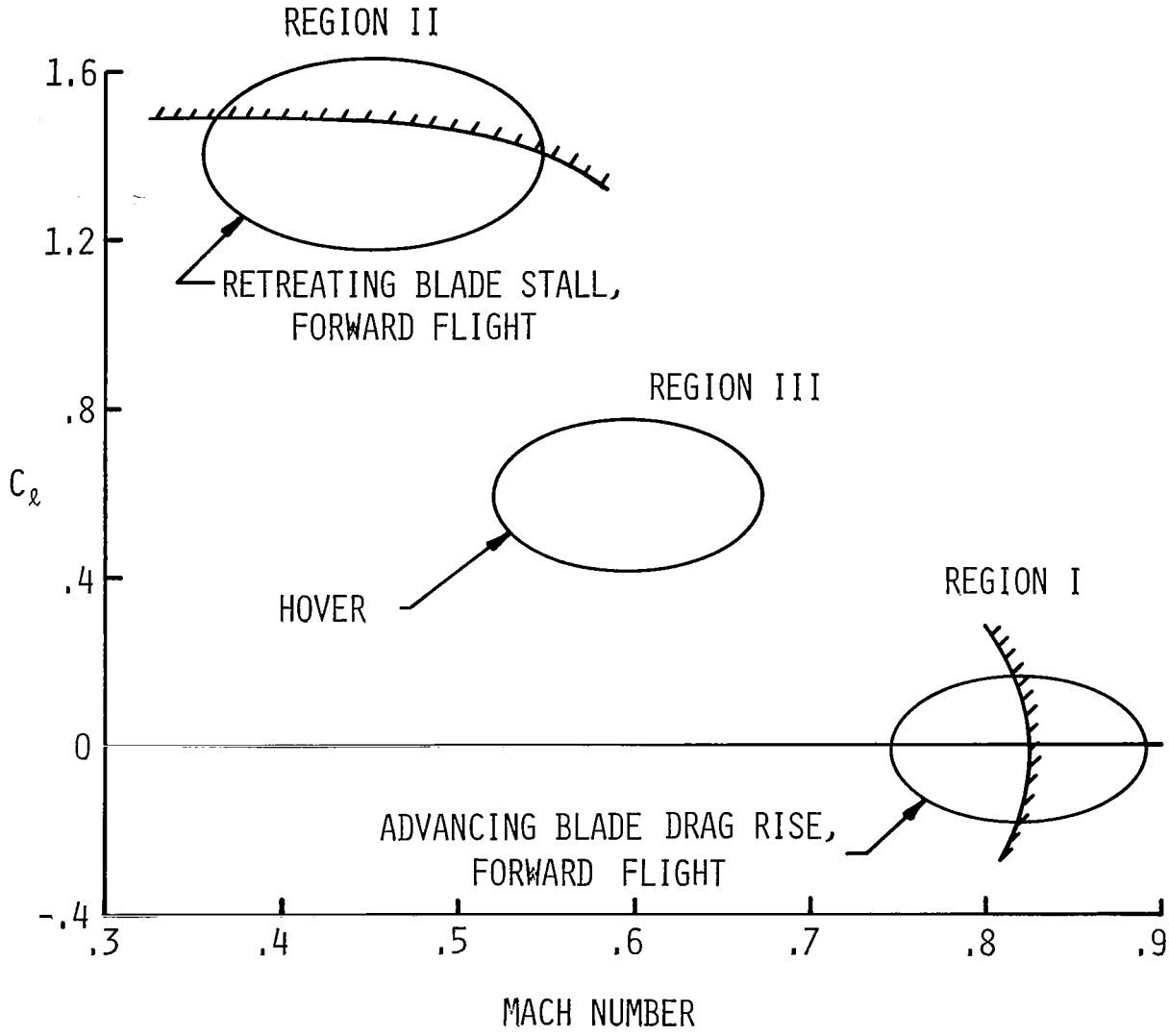

Figure 1. Operating conditions for helicopter rotor section.

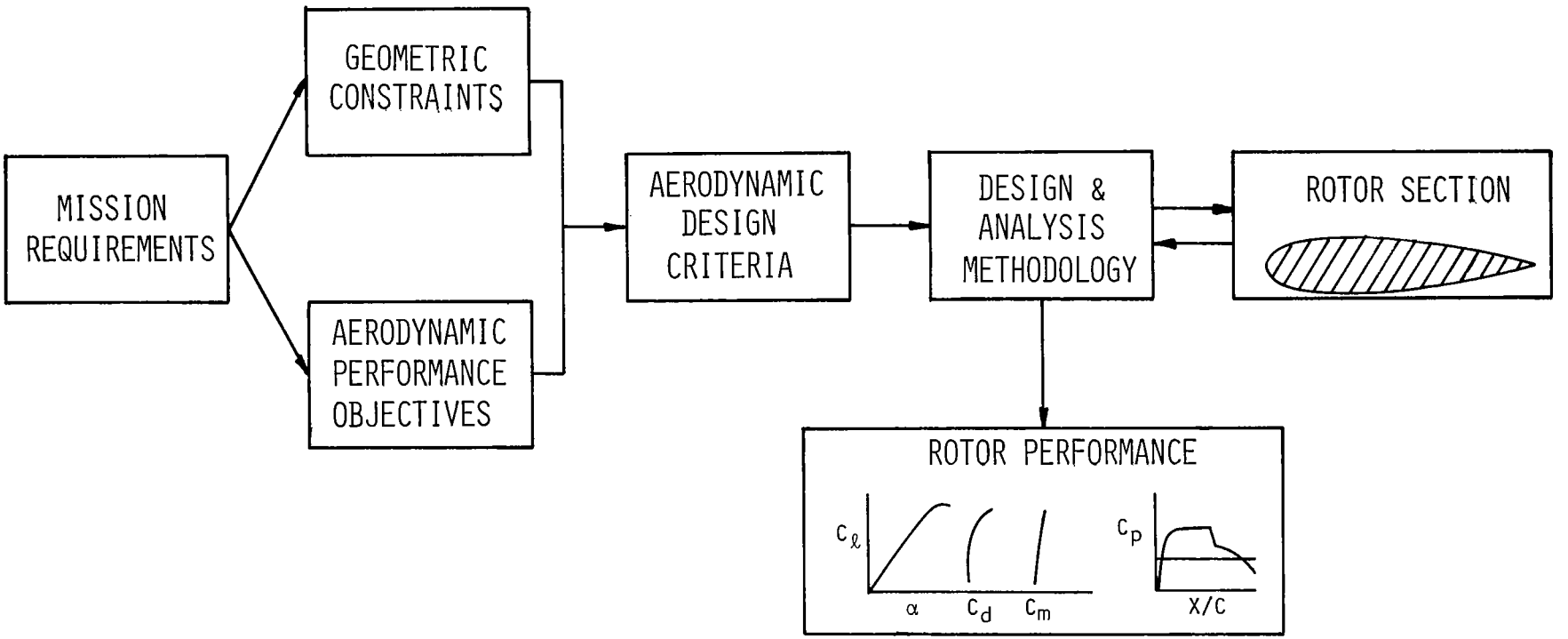

Figure 2. - Rotor section design process.

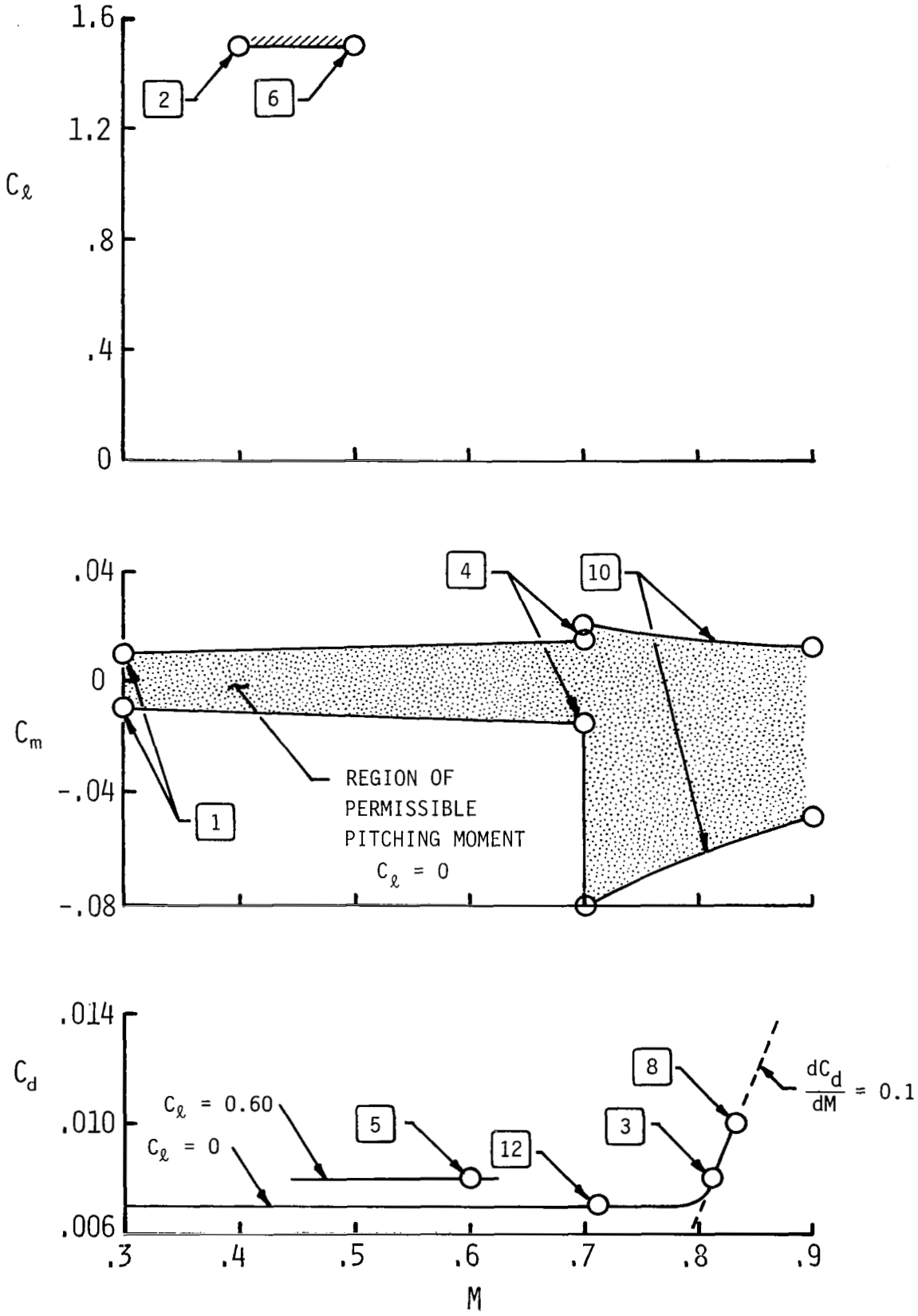

Figure 3. Illustration of aerodynamic performance objectives.

NACA 0010 AIRFOIL

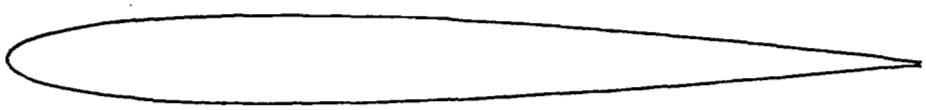

NACA 64A010 AIRFOIL

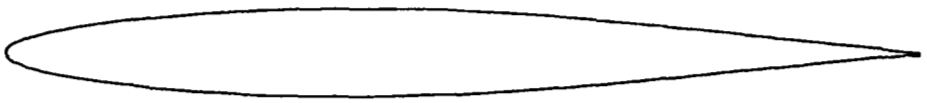

NASA 11% SYMMETRICAL SUPERCRITICAL AIRFOIL

FX 69-H-098

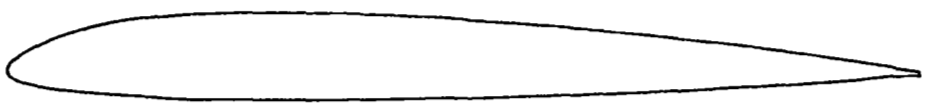

Figure 4. - Sketch of various airfoil shapes applicable to rotor sections.

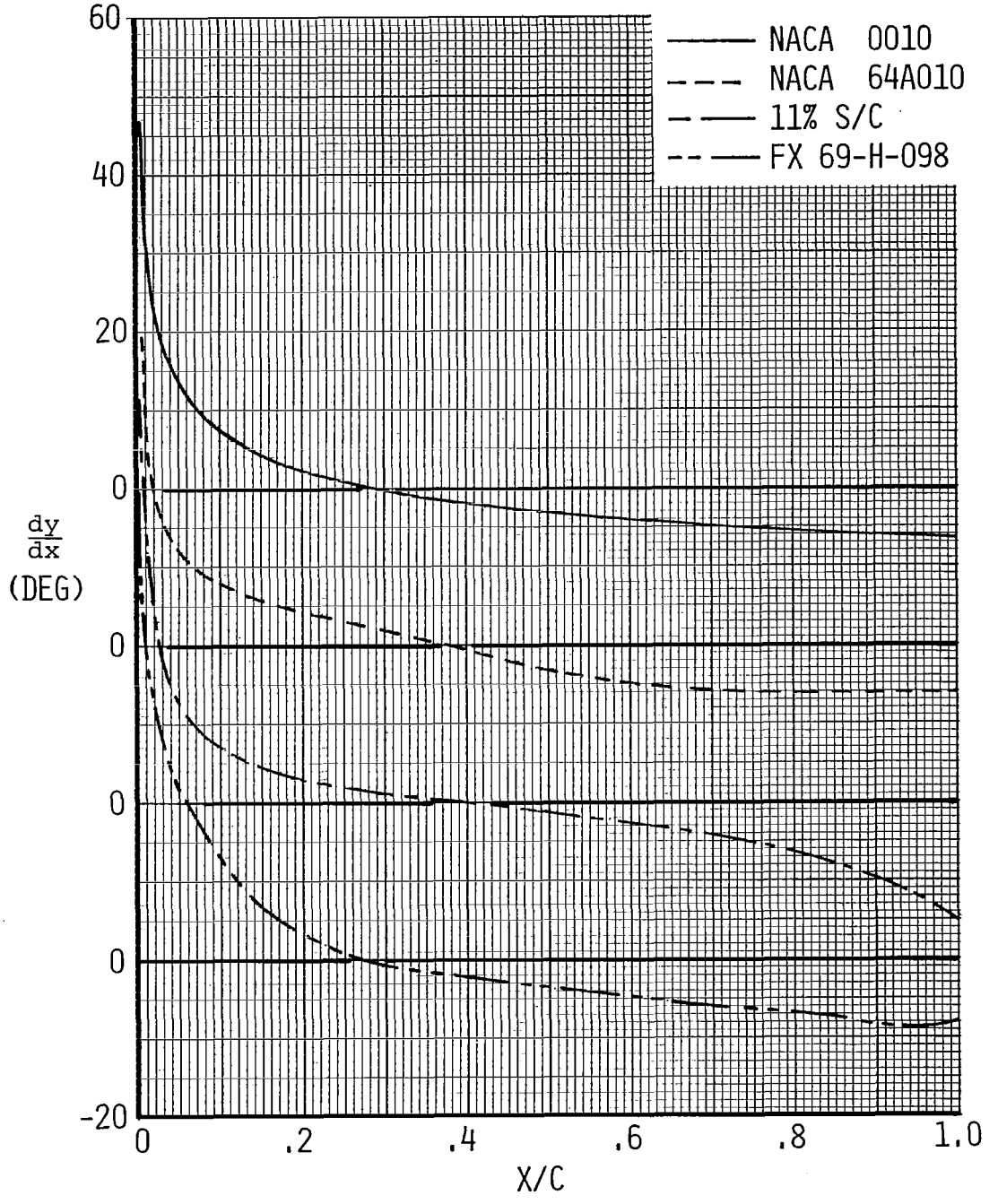

Figure 5. - Comparison of slope diagrams for various airfoil shapes applicable to rotor sections. (Upper surface only.)

	AIRFOIL	α	C_m	C_d
———	0010	0	0	.0123
– – – –	64A010	0	0	.0114
——	11% S/C	0	0	.0098
——	FX69-H-098	-1.24	-.045	.0138

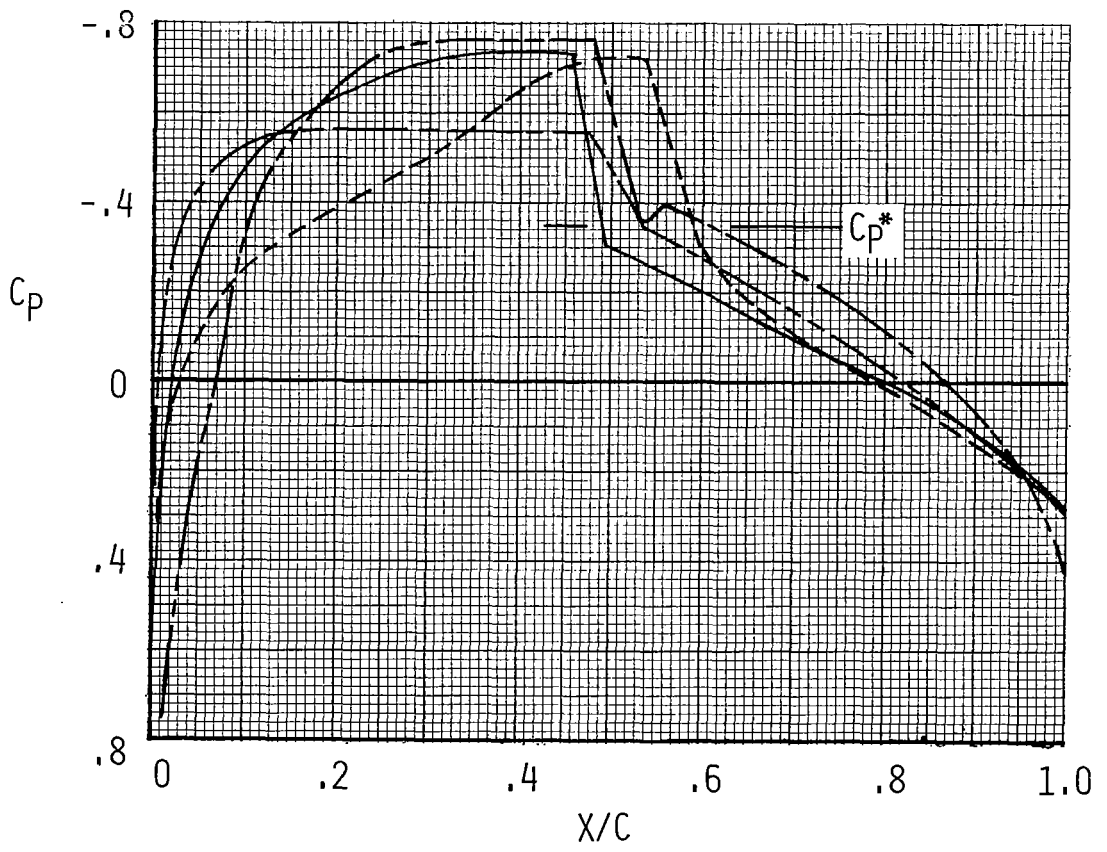

Figure 6. - Comparison of Region I theoretical performance characteristics for four airfoil concepts. $C_\ell = 0$; $M = 0.83$; $R_N = 8.3 \times 10^6$; $[X_T/C] \cong .05$. (Upper surface only.)

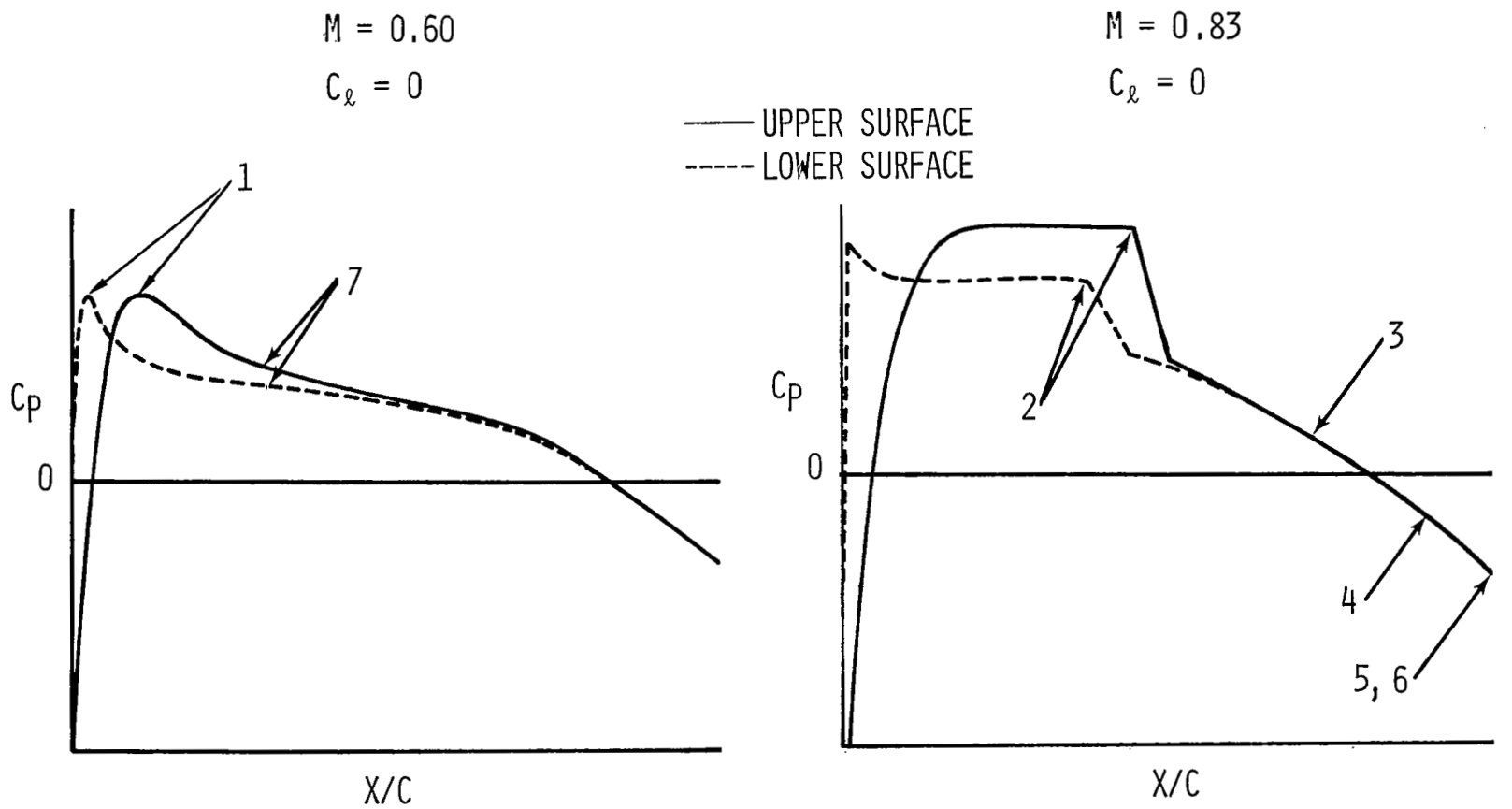

a. Subcritical design pressure distribution.

b. Transonic design pressure distribution.

Figure 7. - Aerodynamic design criteria for Region I.

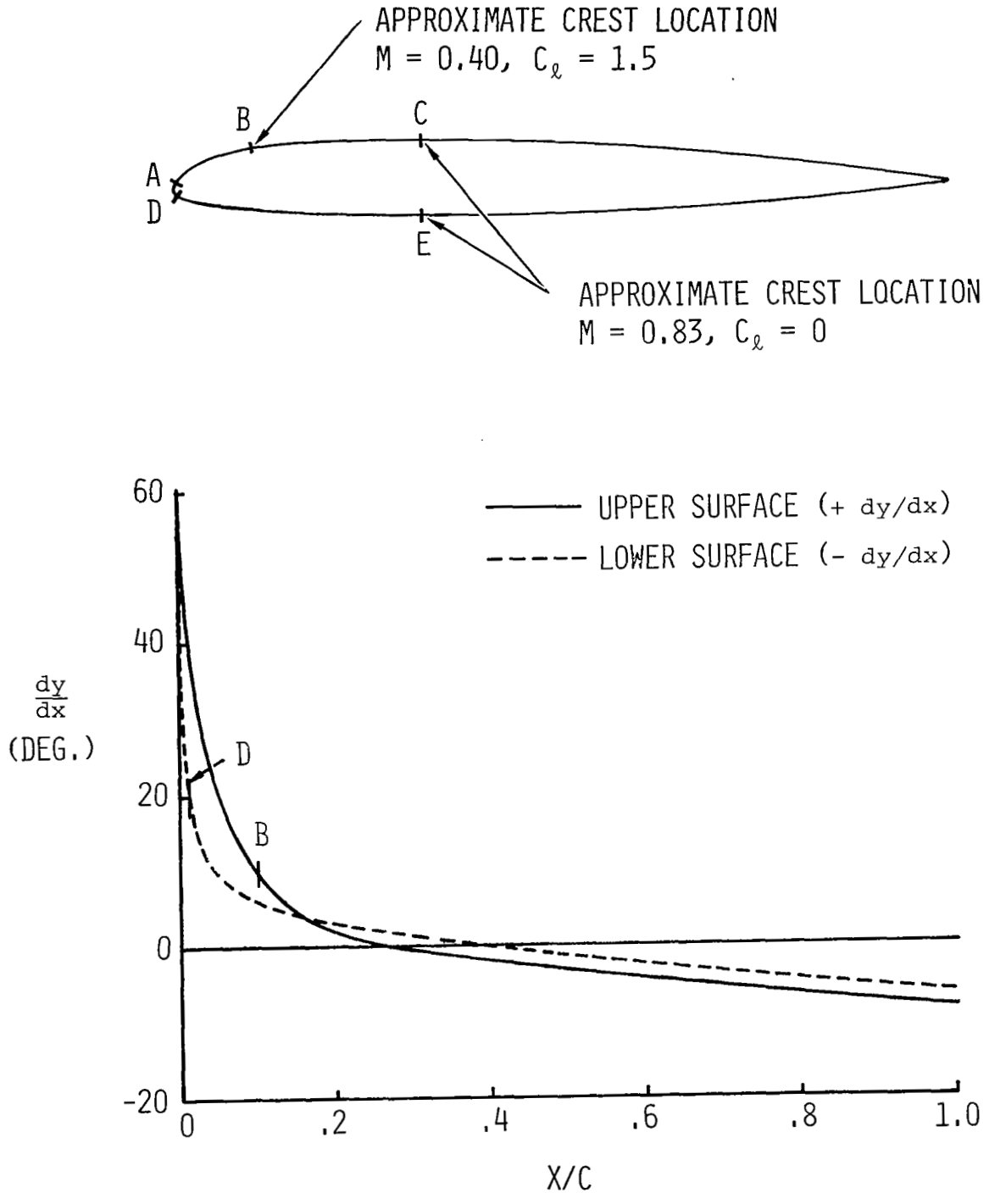

Figure 8. Geometric illustration of design criteria.

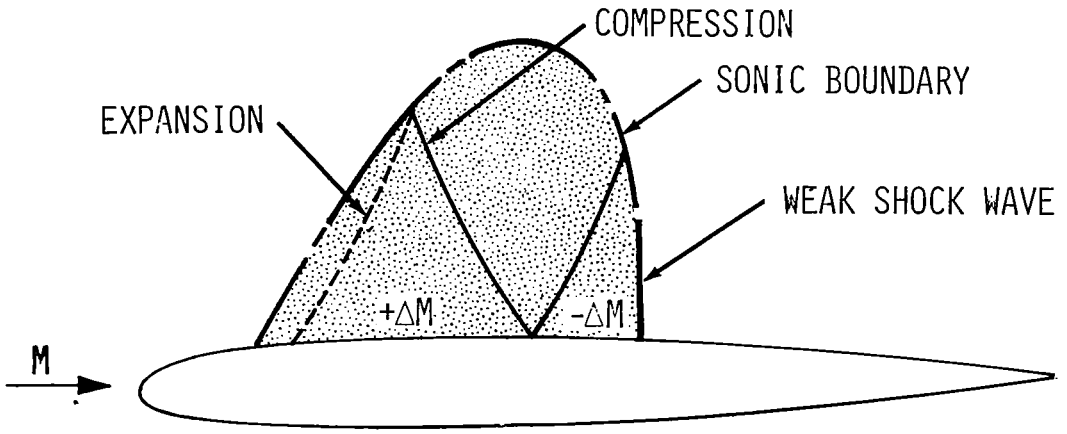

Figure 9. - Schematic illustration of supercritical flow phenomena for Region I.

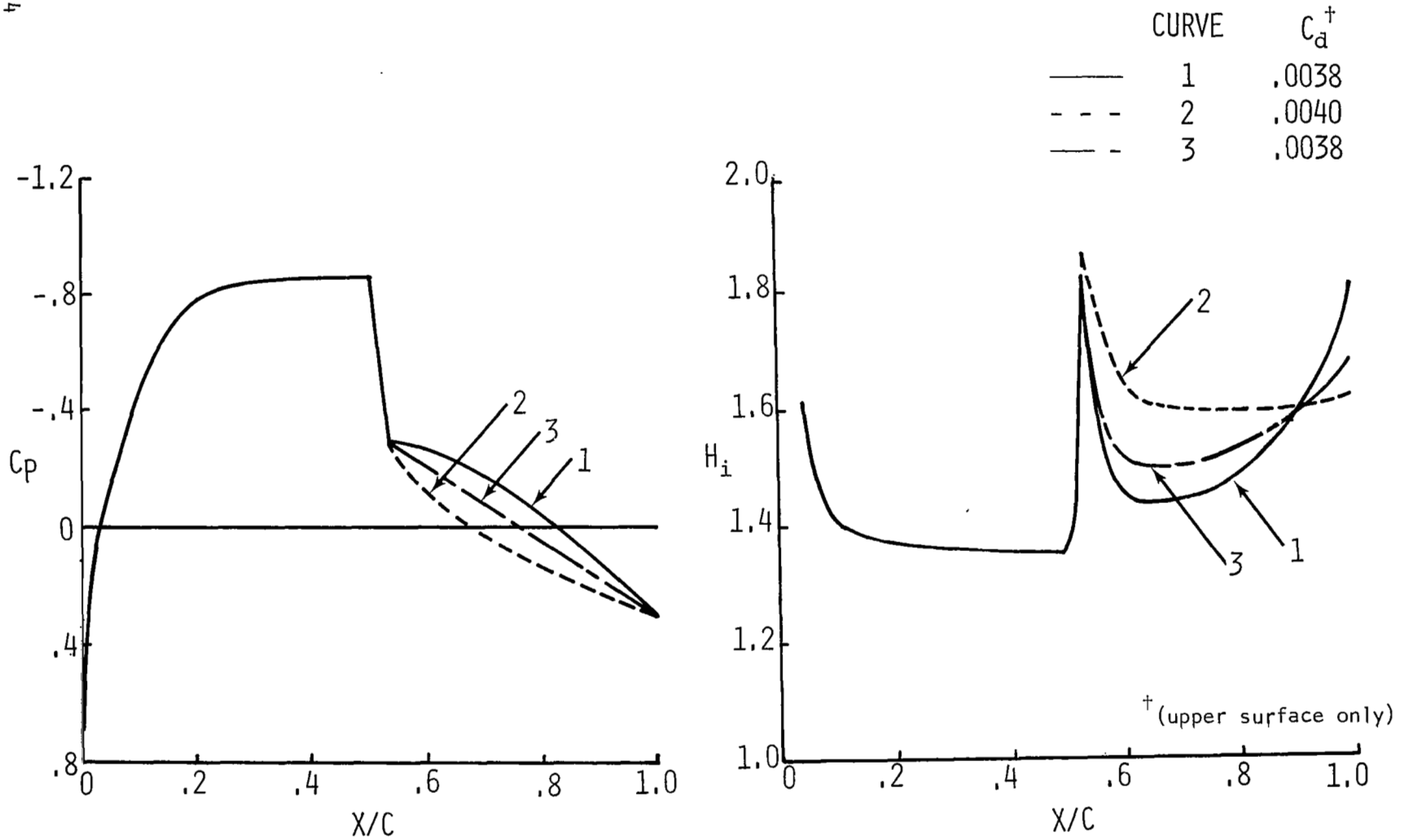

Figure 10. - Effect of pressure distribution shape over the rear of the airfoil on airfoil performance in Region I. M = 0.83, $R_N = 8.3 \times 10^6$, $[X_T/C] = .05$.

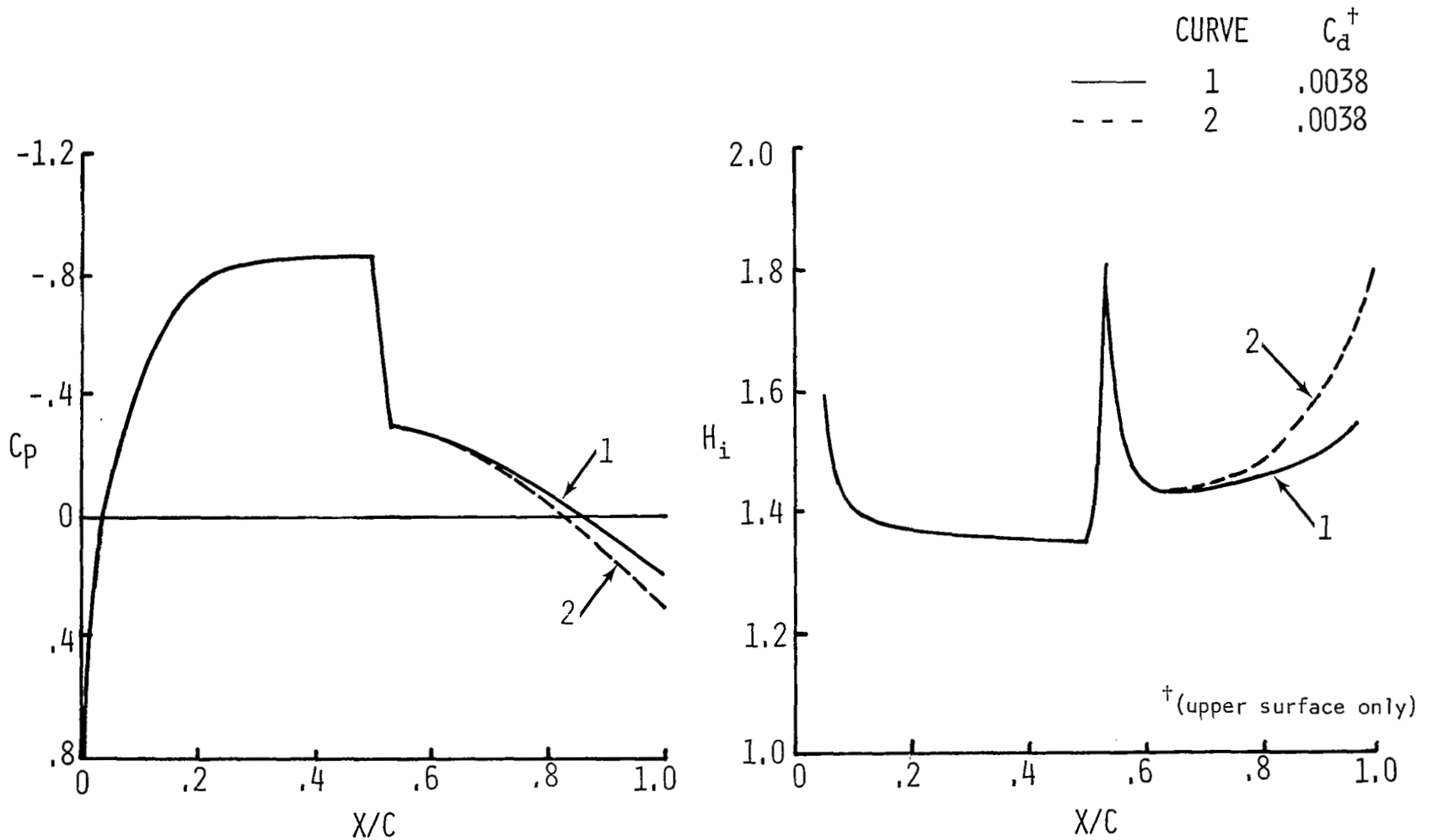

Figure 11. - Effect of trailing-edge pressure level on airfoil performance in Region I. $M = 0.83$, $R_N = 8.3 \times 10^6$, $[X_T/C] = .05$.

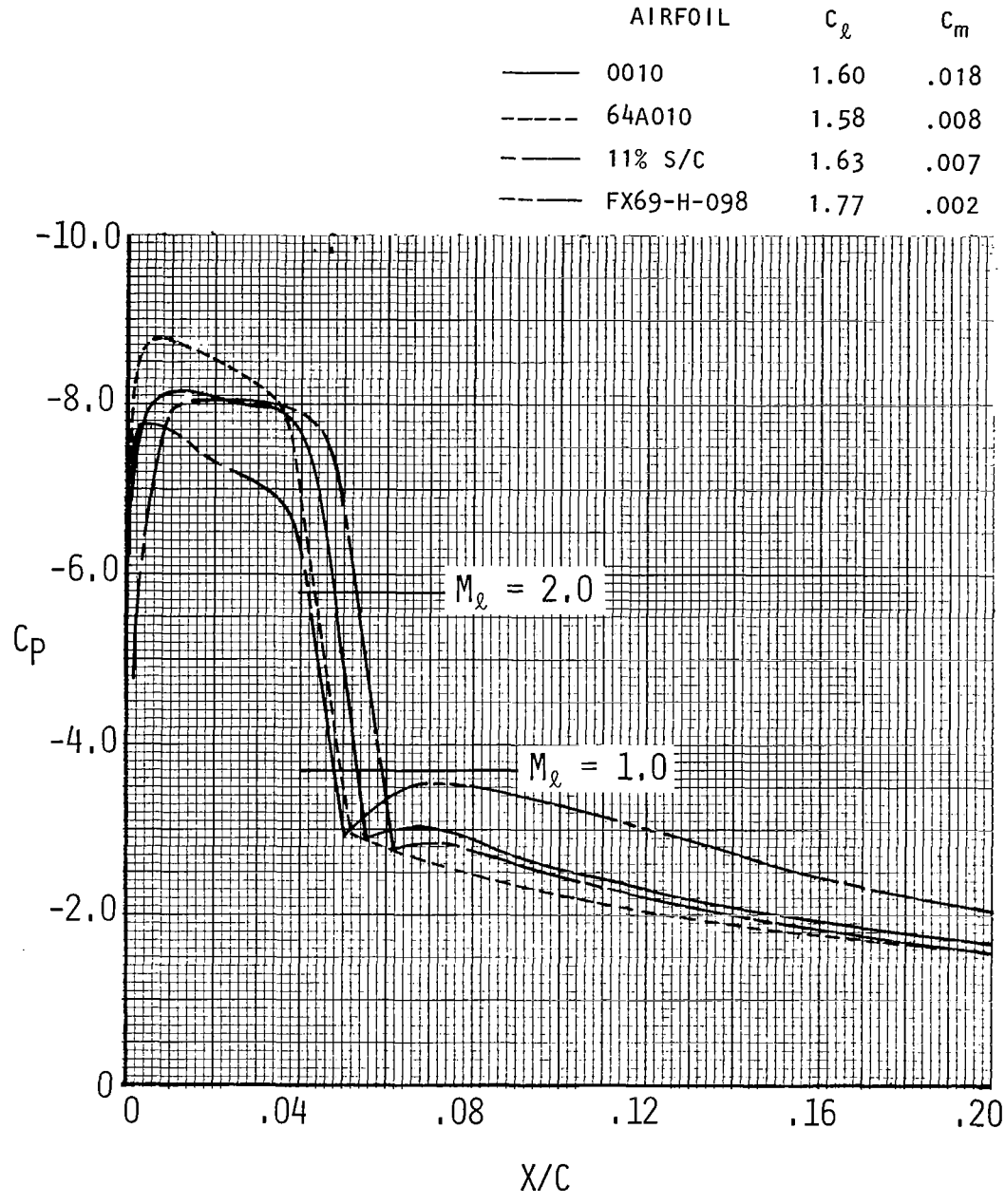

a. $0 \geq X/C \geq 0.2$

Figure 12. - Comparison of Region II theoretical performance for four airfoil concepts. $M = 0.40$, $\alpha = 12°$, inviscid, upper surface only.

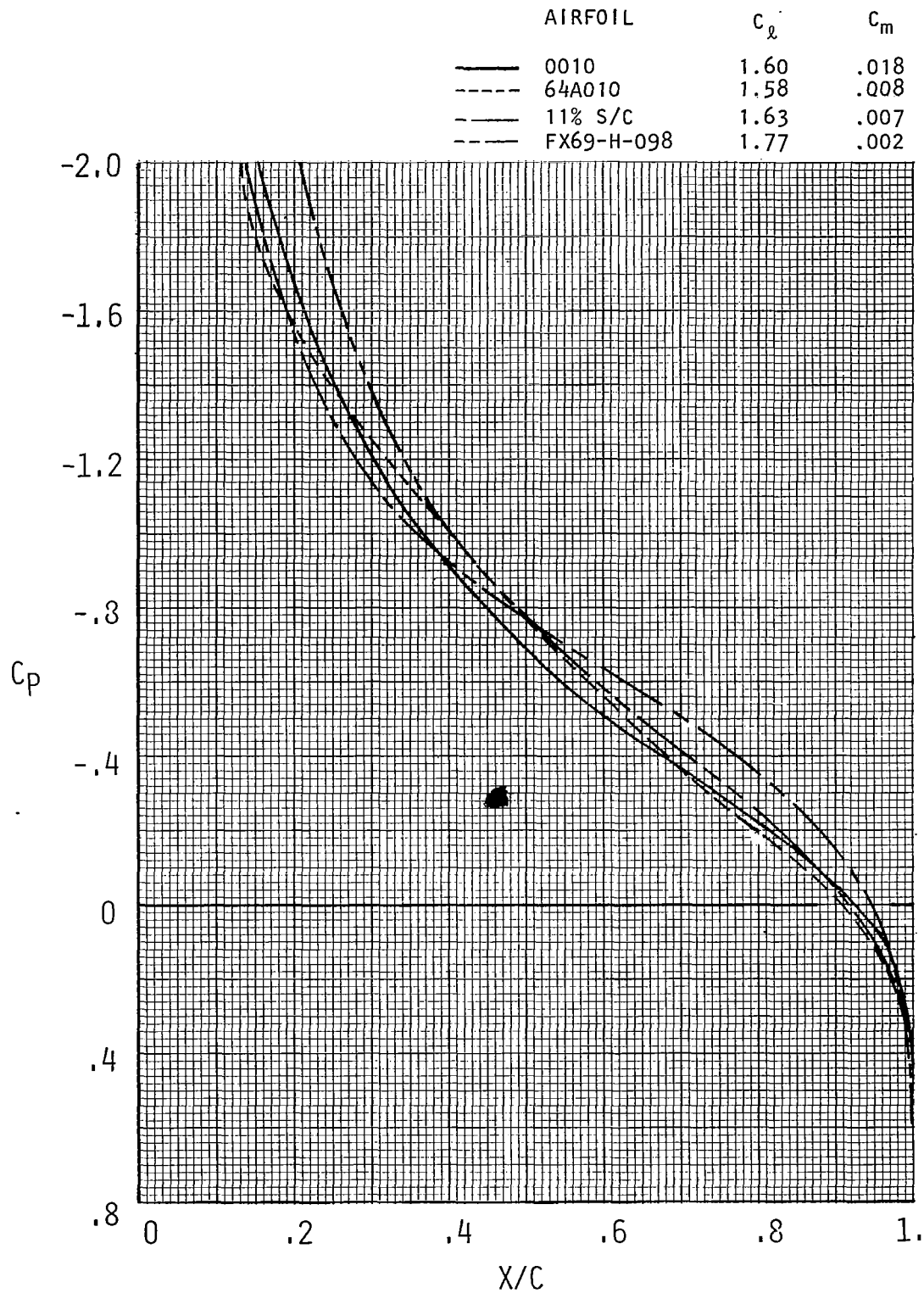

b. X/C $\geq$ 0.2

Figure 12. - Concluded.

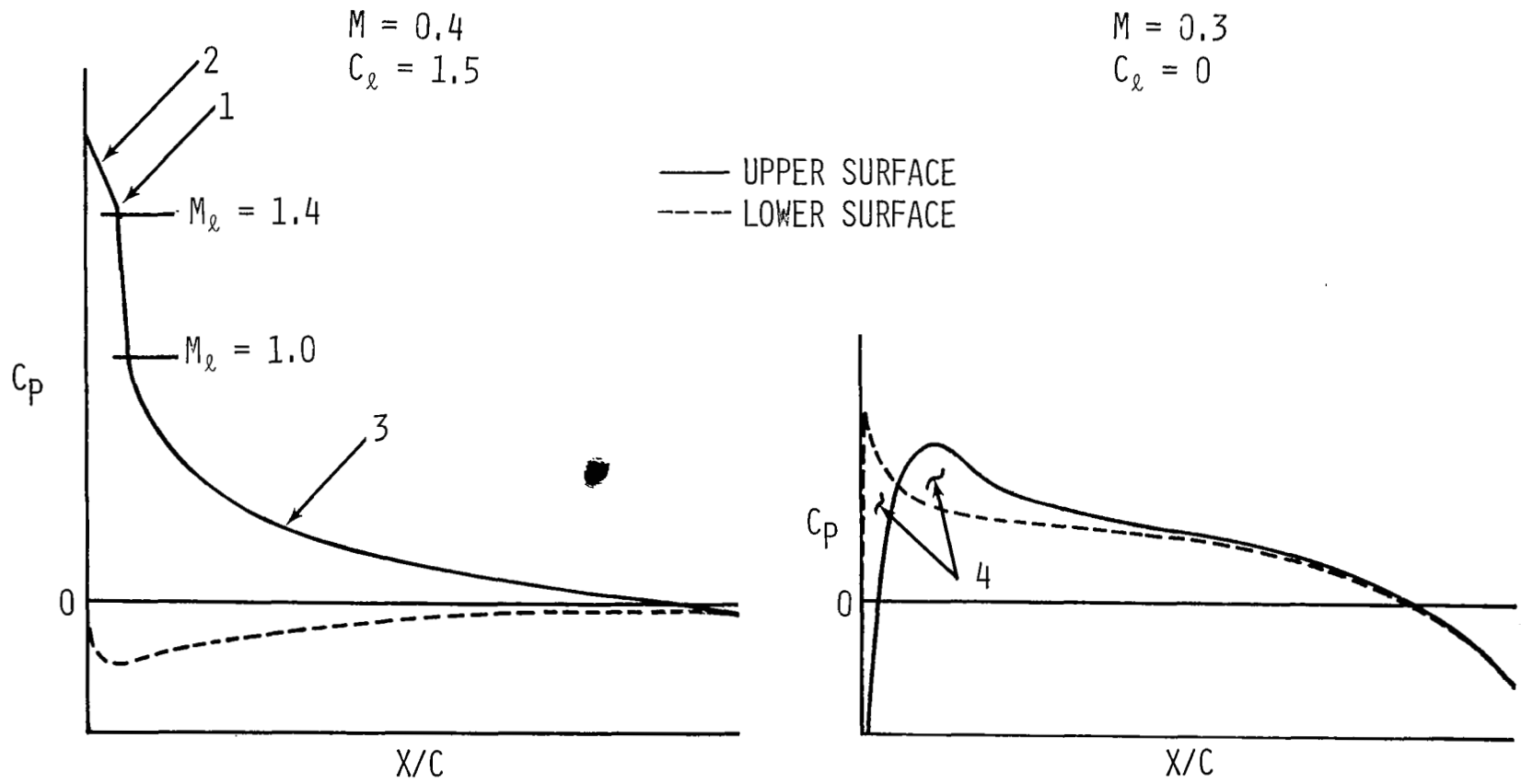

a. High lift design pressure distribution.

b. Zero lift design pressure distribution.

Figure 13. - Aerodynamic criteria for Region II.

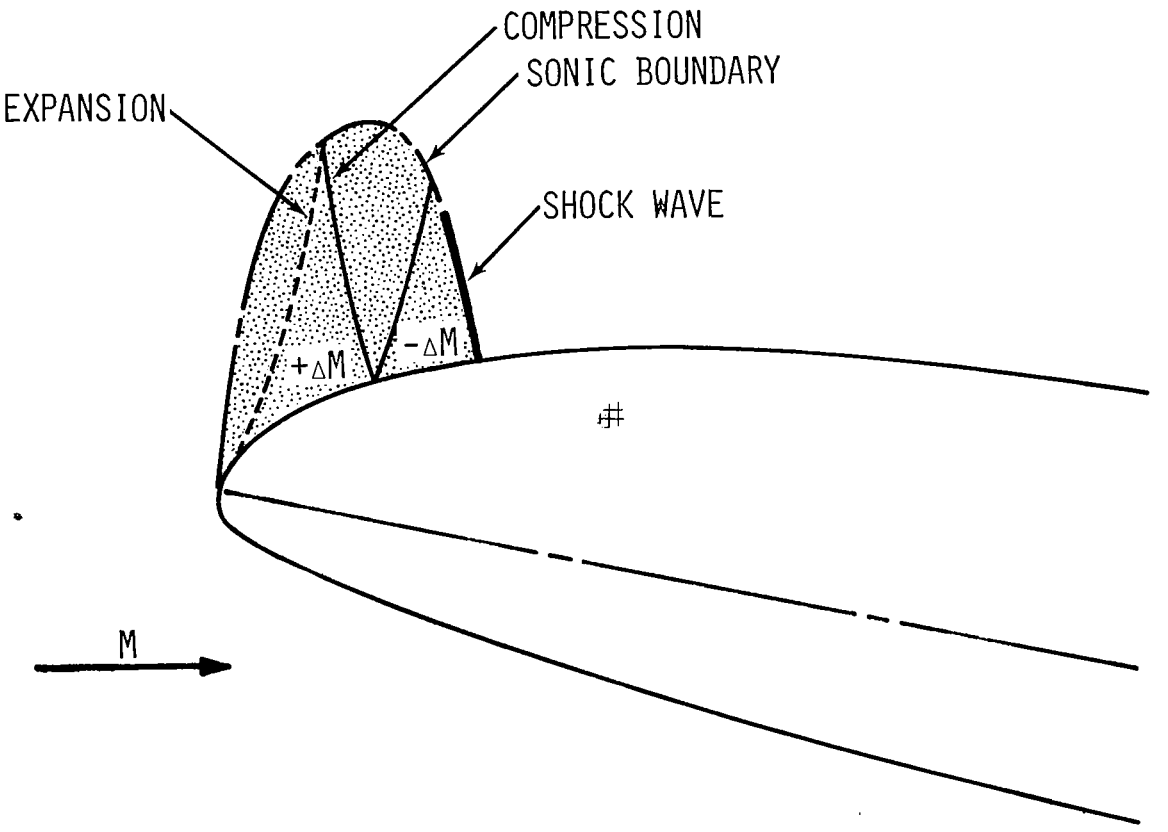

Figure 14. - Schematic illustration of supercritical flow phenomena for Region II.

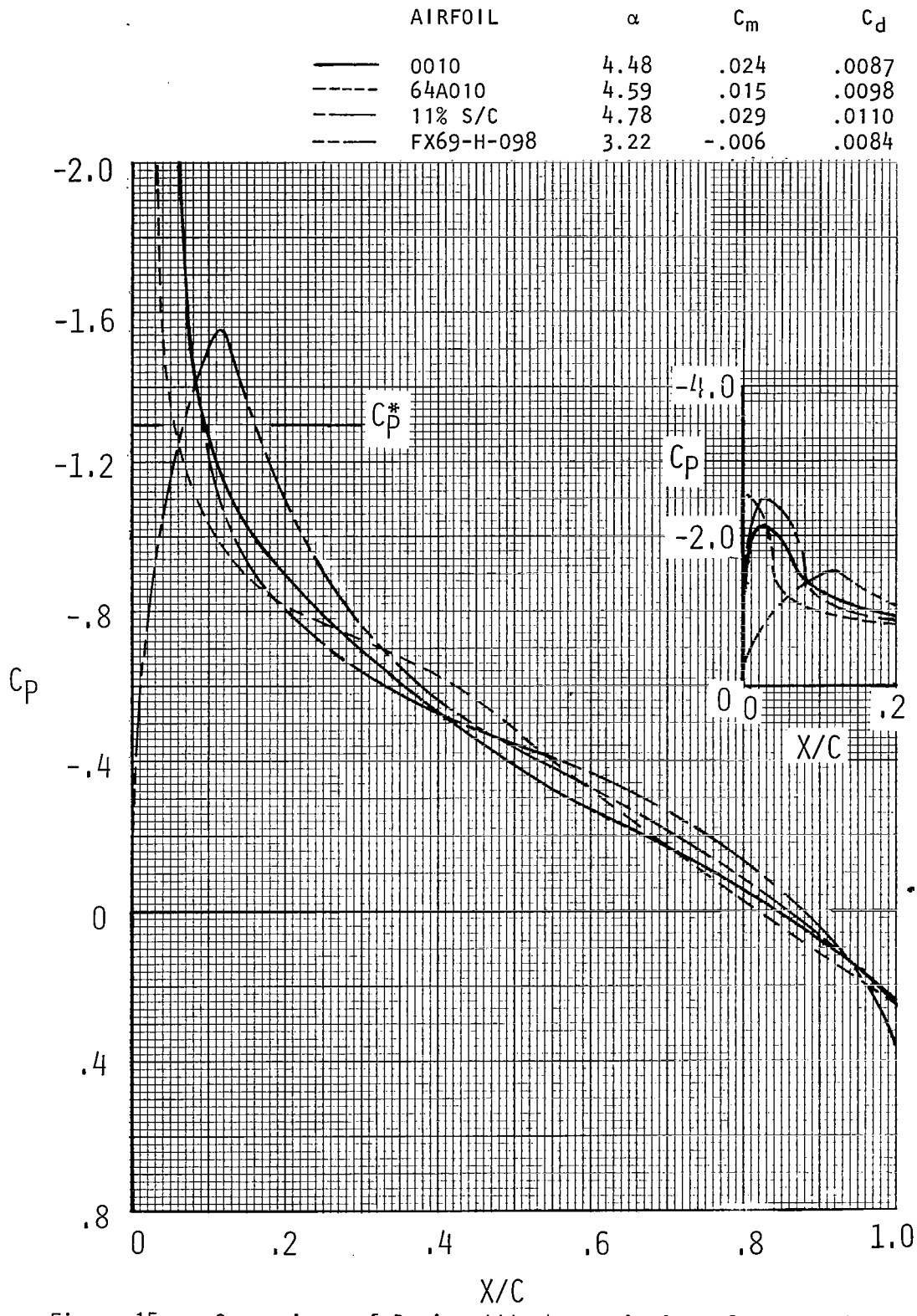

Figure 15. - Comparison of Region III theoretical performance for four airfoil concepts. $M = 0.60$, $C_\ell = .60$, $R_N = 6 \times 10^6$, $[X_T/C] = .05$. (Upper surface only).

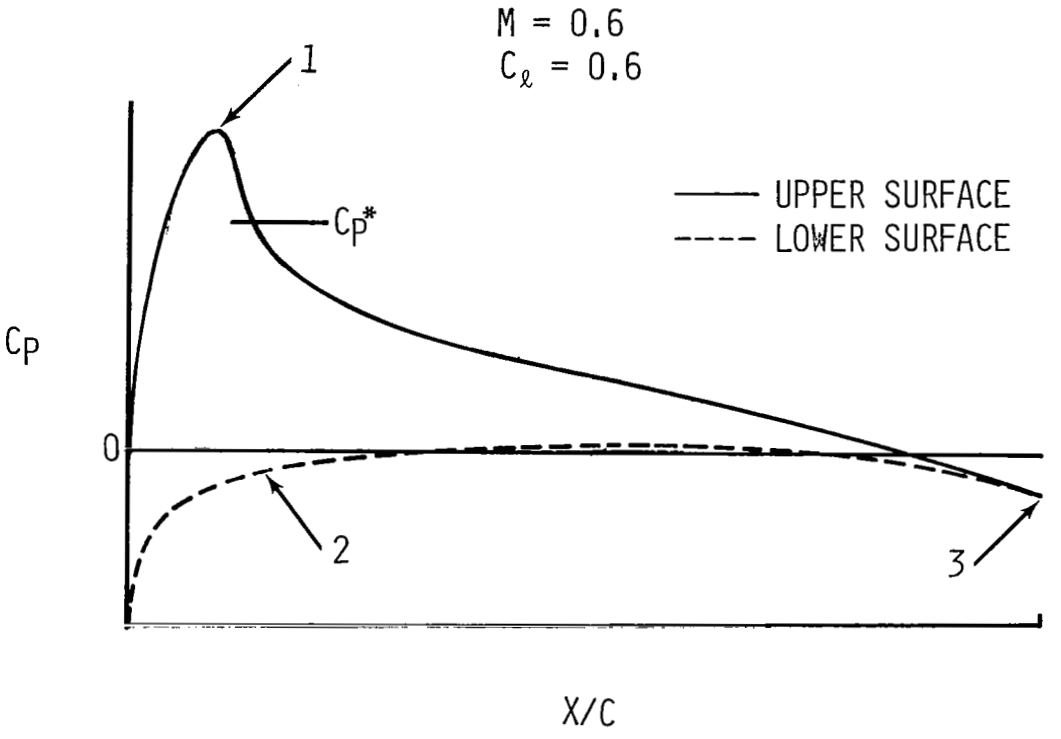

Figure 16. - Aerodynamic criteria for Region III.

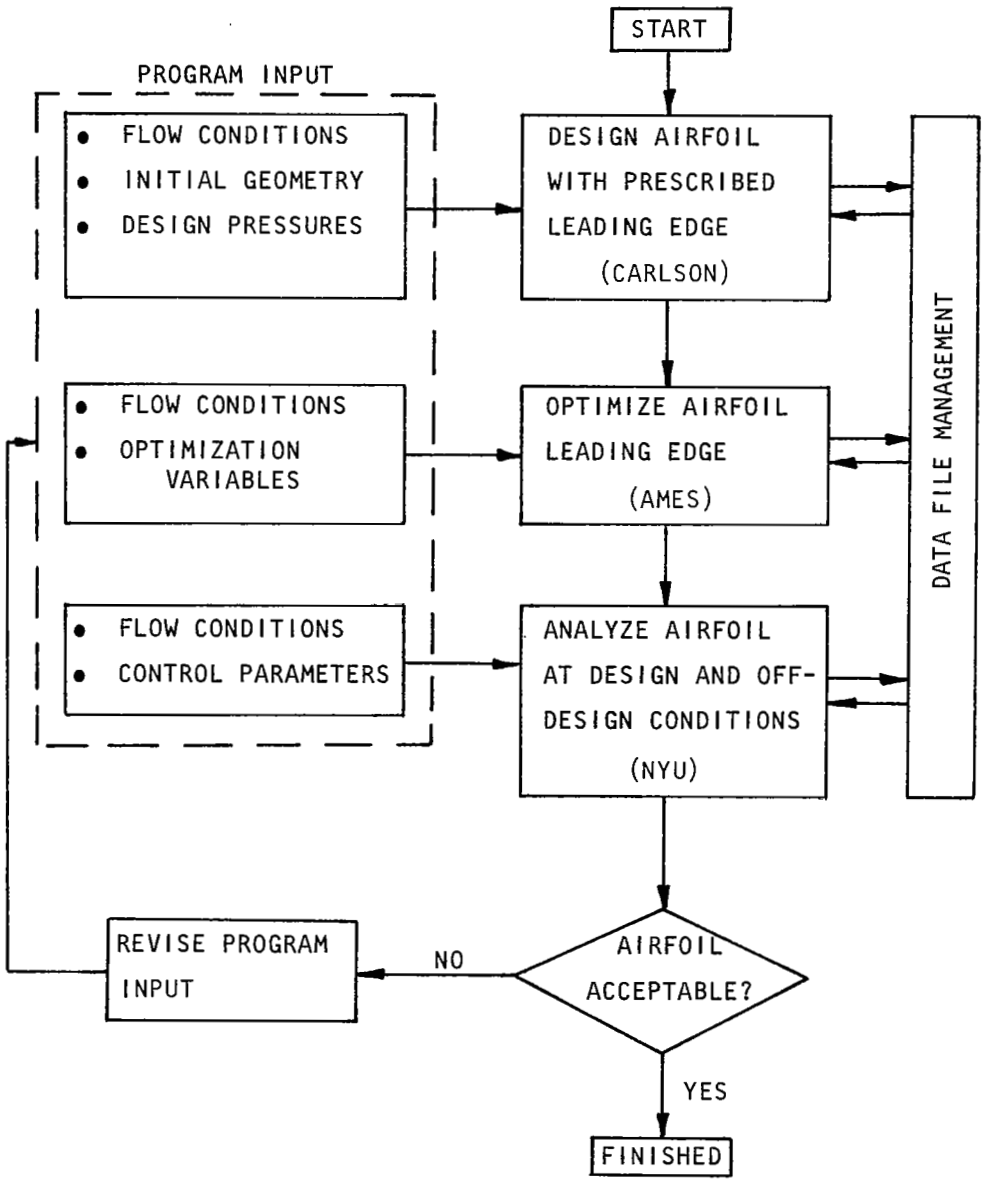

Figure 17. - Unified airfoil design and analysis procedure.

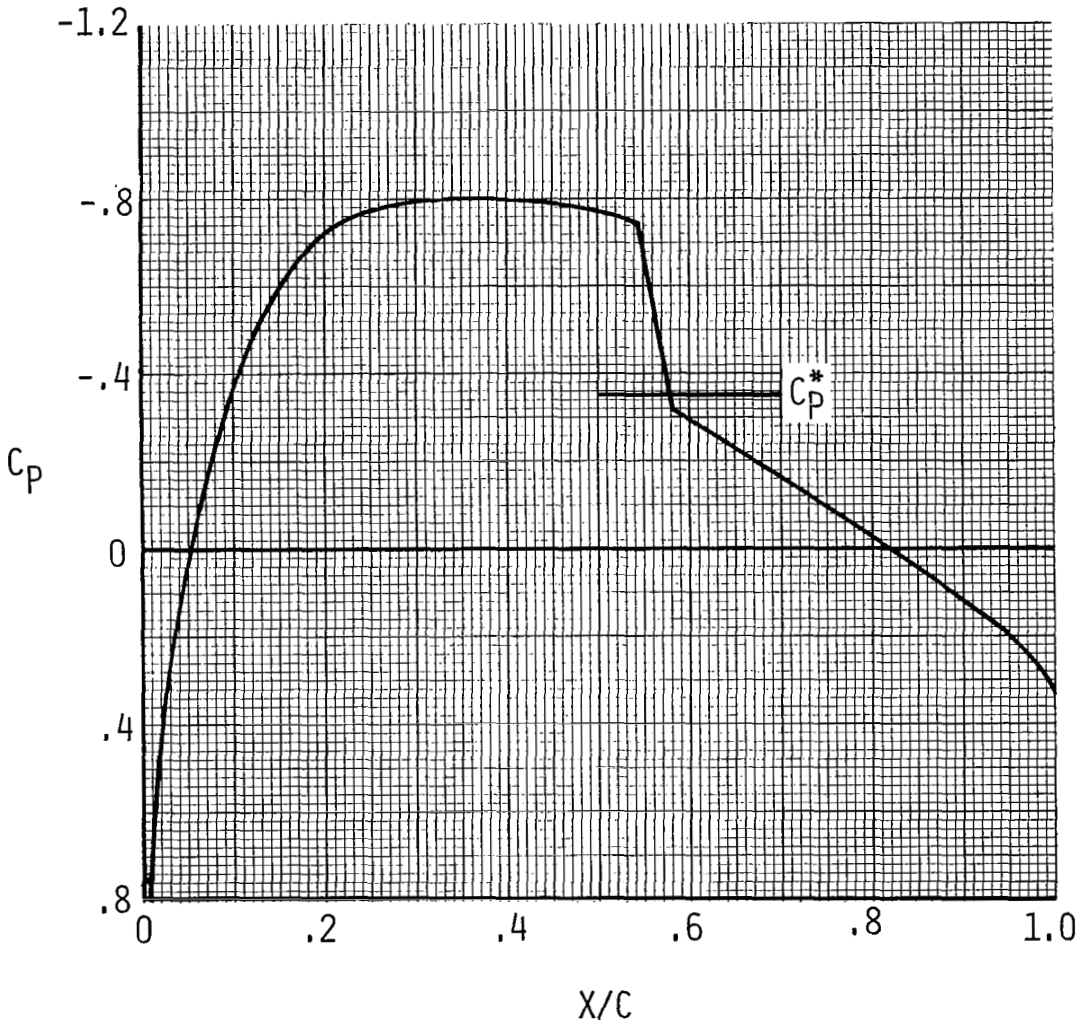

Figure 18 . - Initial input design pressure distribution (Region 1) for Carlson program. $M = 0.83$, $C_\ell = 0$, $R_N = 8.3 \times 10^6$, $[X_T/C] = .05$.

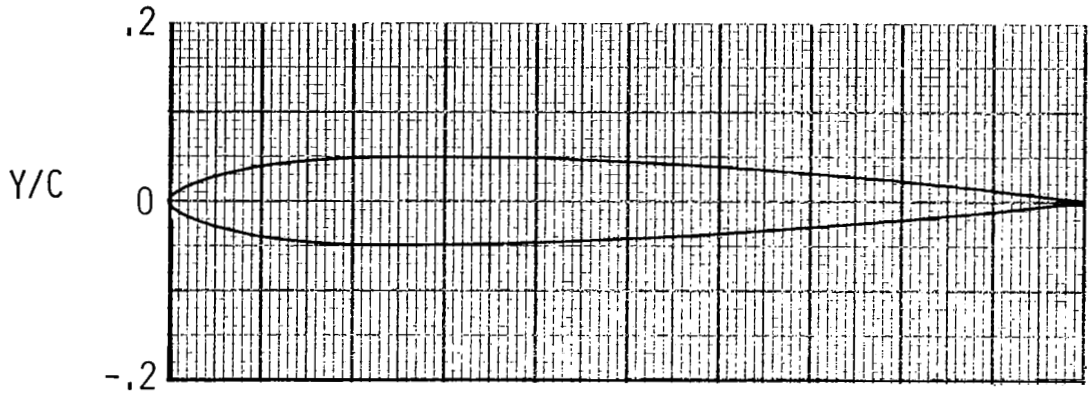

a. Airfoil shape.

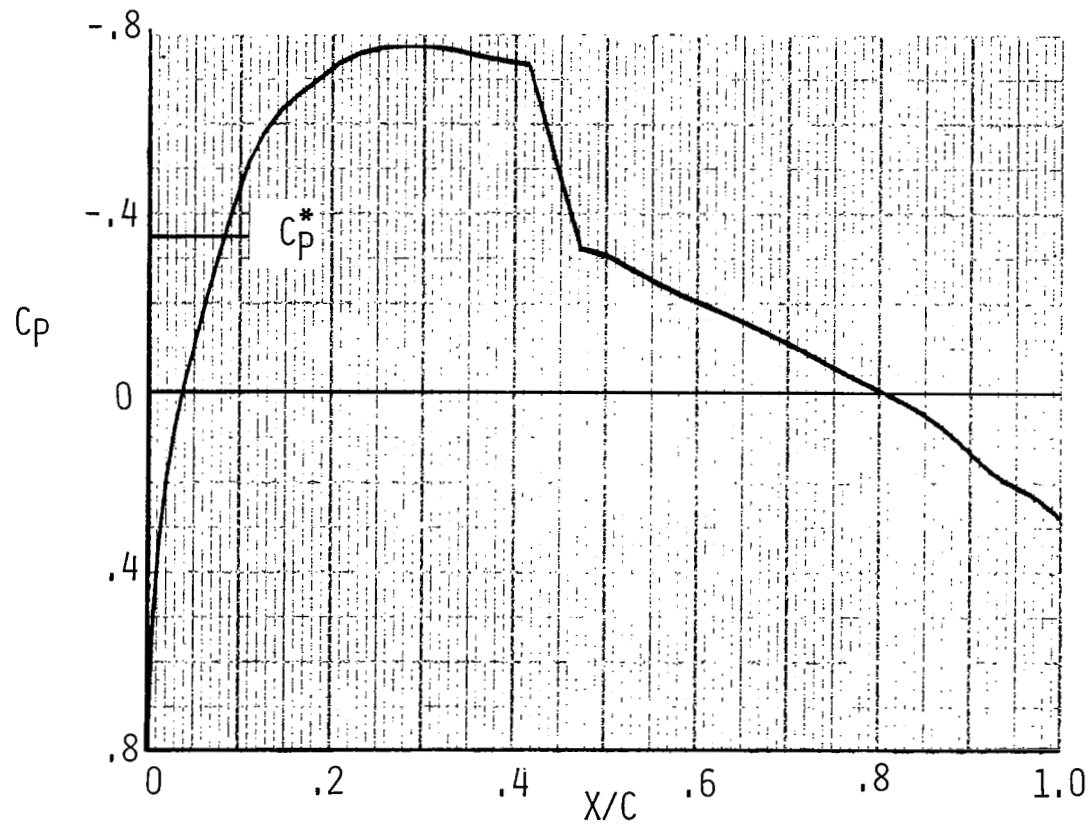

b. Pressure distribution. $M = 0.83$, $C_\ell = 0$, $R_N = 8.3 \times 10^6$, $[X_T/C] = .05$.

Figure 19. - Initial input airfoil shape to the Carlson program and a transonic pressure distribution typical of its Region I performance.

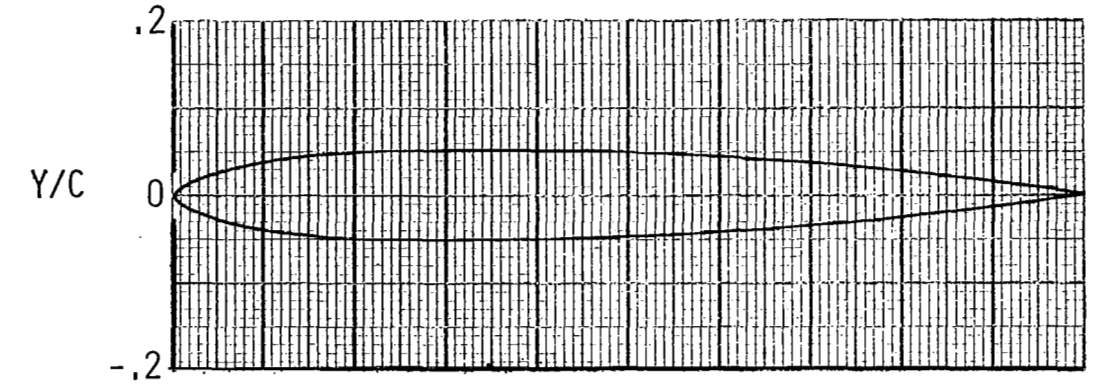

a. Airfoil shape.

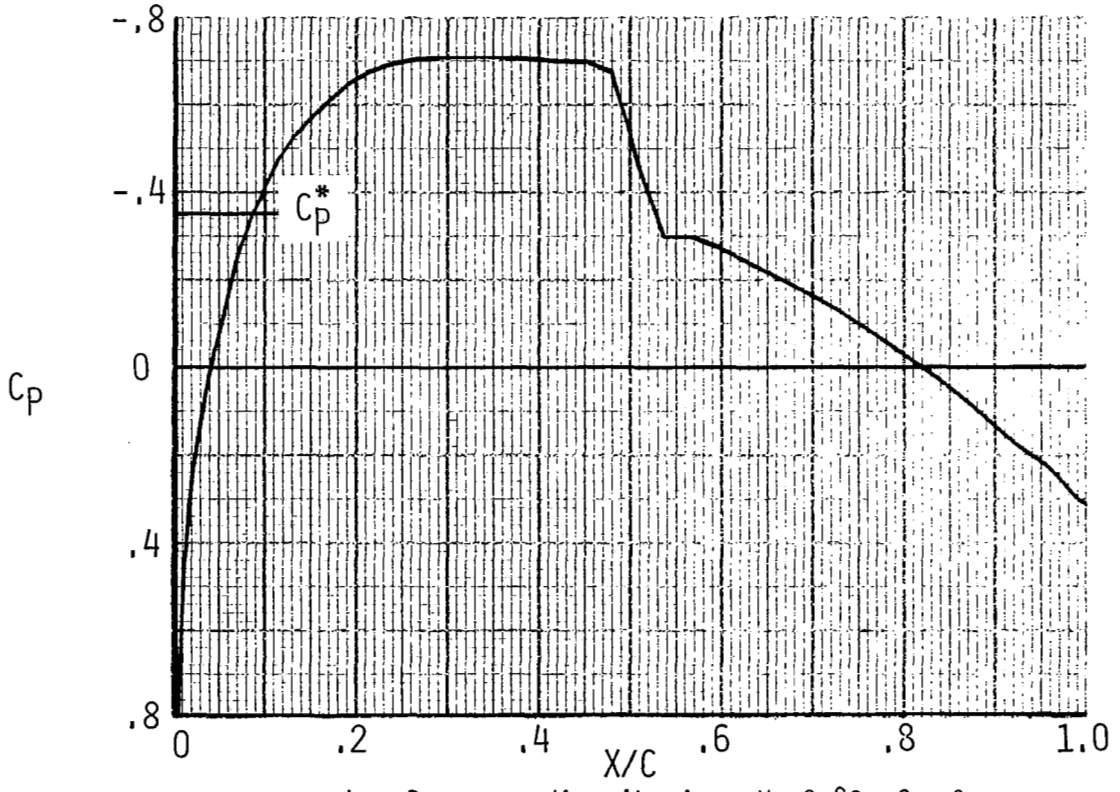

b. Pressure distribution. $M = 0.83$,. $C_\ell = 0$, $R_N = 8.3 \times 10^6$, $[X_T/C] = .05$.

Figure 20. - Final airfoil shape resulting from application of Carlson program and pressure distributions typical of the performance in Regions I and II.

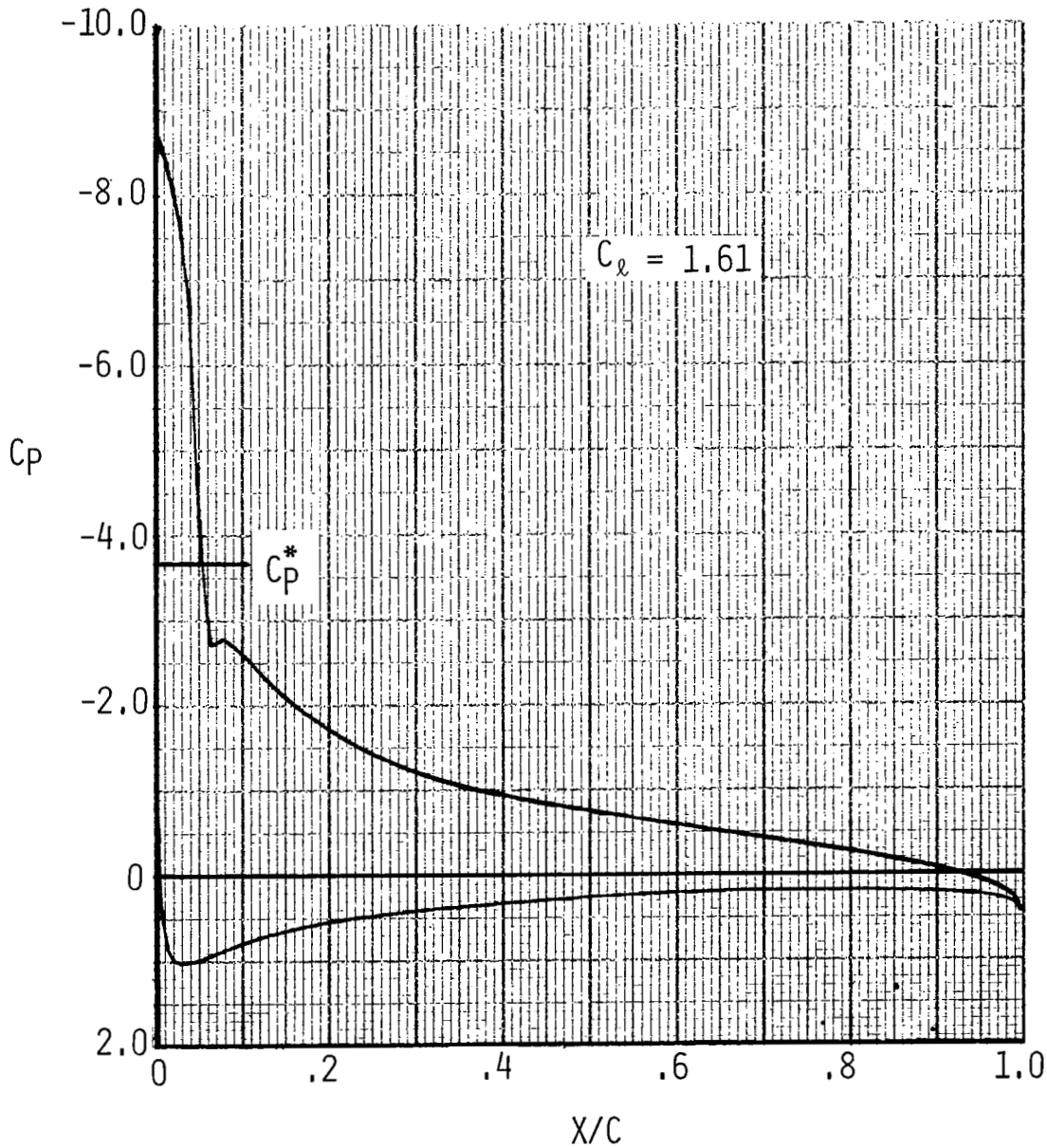

c. Pressure distribution. $M = 0.40$, $\alpha = 12°$, inviscid.

Figure 20. - Concluded.

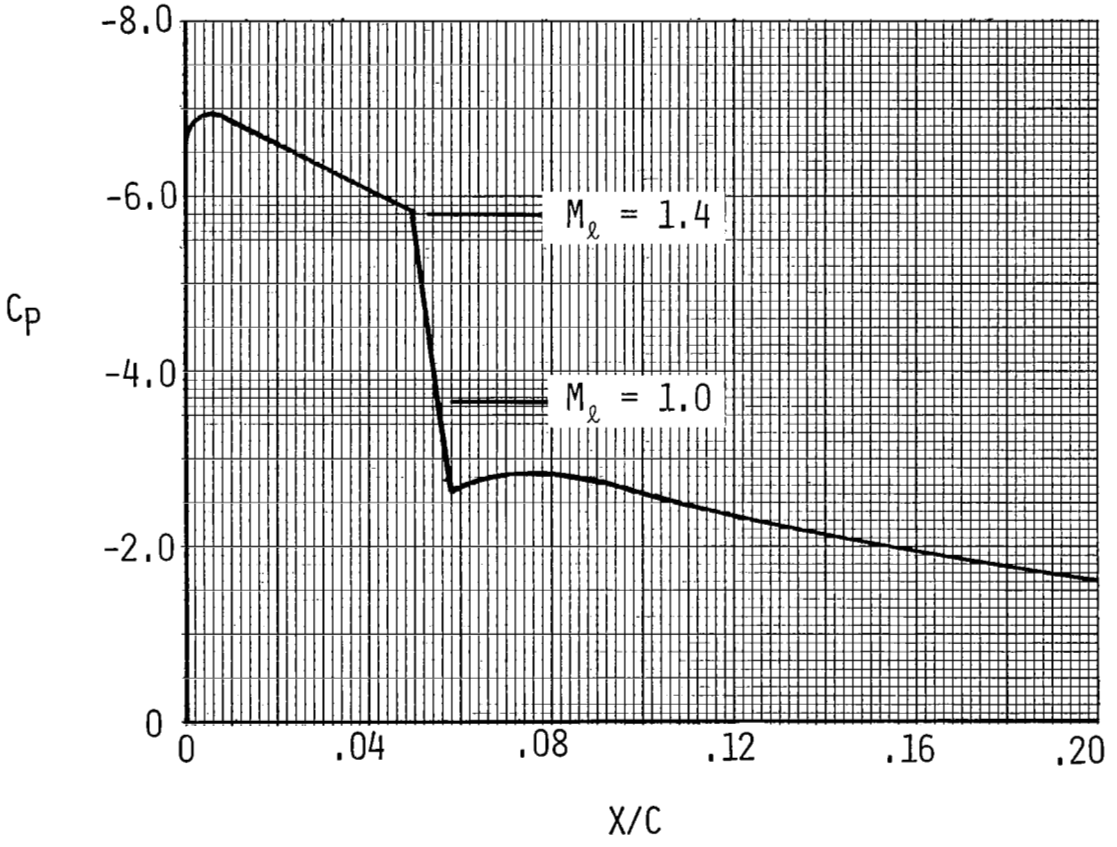

Figure 21. - Target leading-edge, upper-surface distribution for Region II. $M = 0.40$, $C_\ell = 1.5$, $R_N = 4 \times 10^6$, $[X_T/C] = 0$.

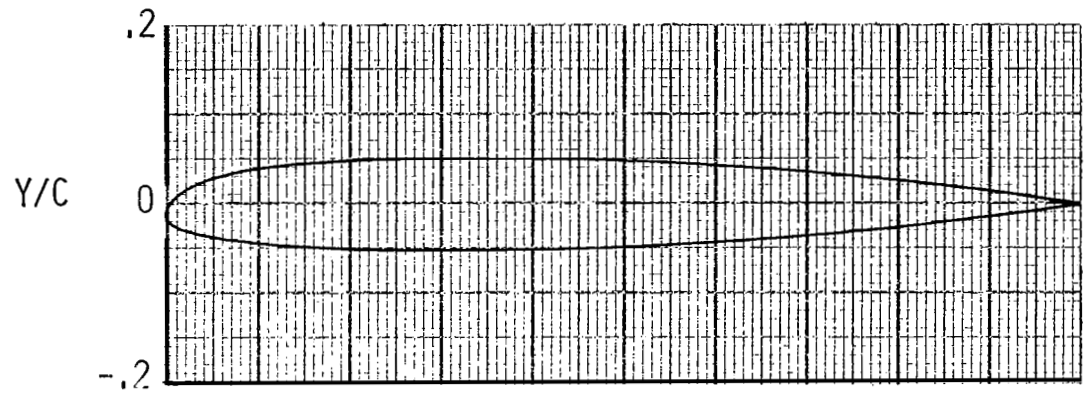

a. Airfoil shape

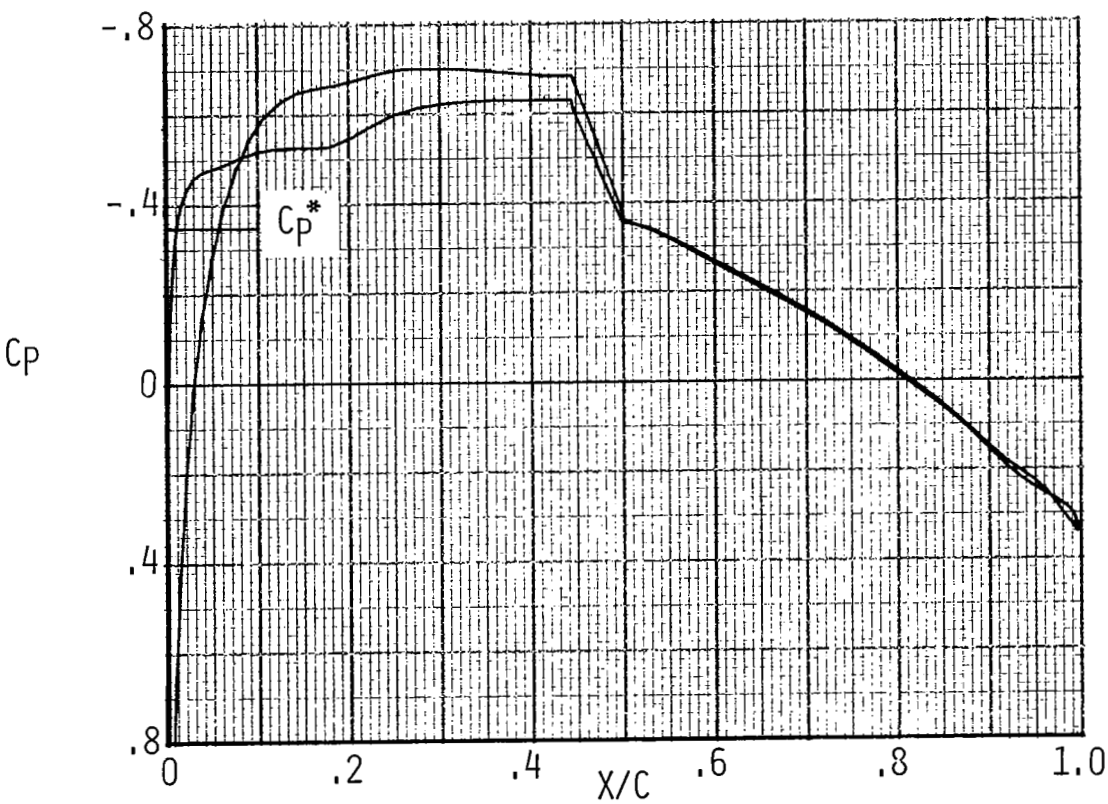

b. Pressure distribution. $M = 0.83$, $C_\ell = 0$, $R_N = 8.3 \times 10^6$, $[X_T/C] = .05$.

Figure 22. - Intermediate airfoil shape resulting from application of Ames program and pressure distribution typical of the performance in Regions I, II and III.

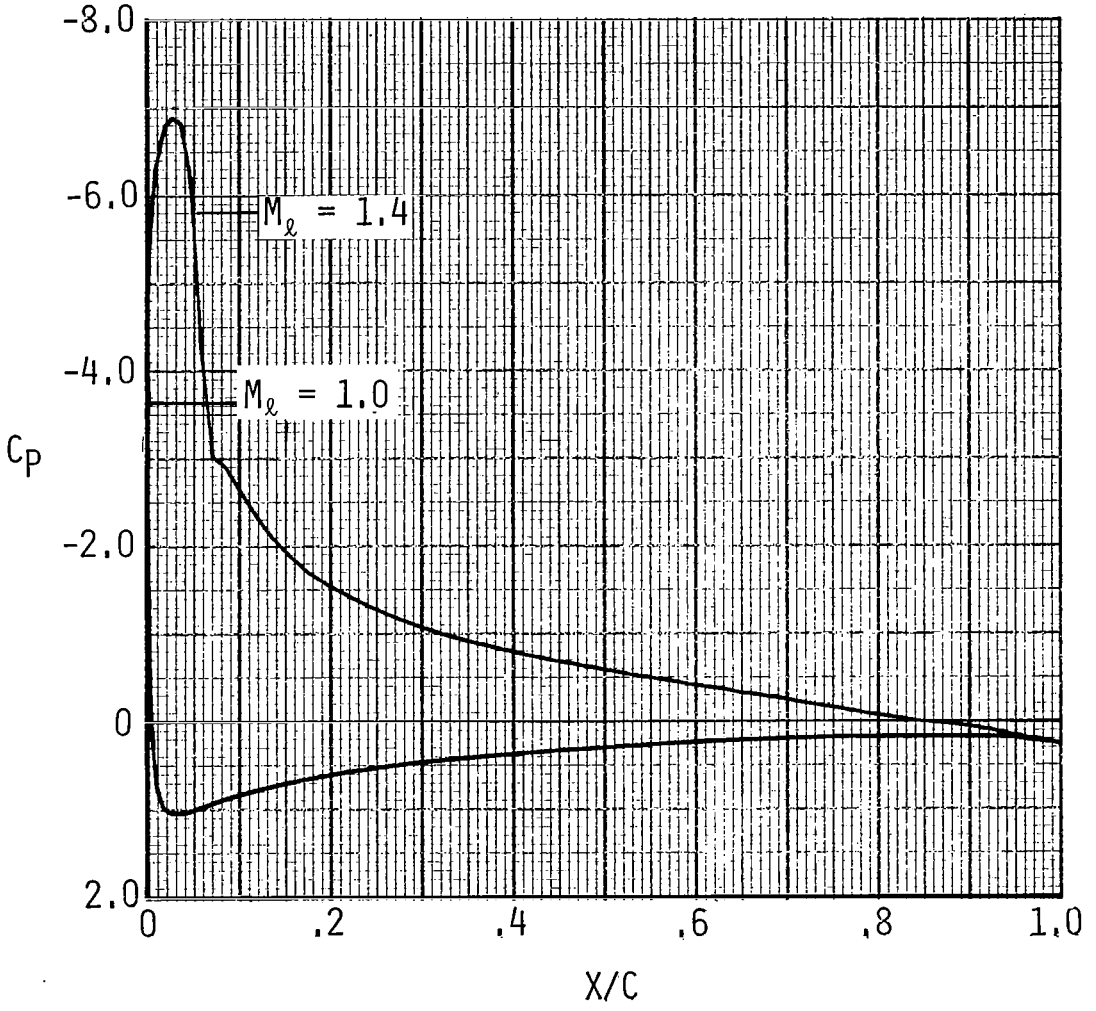

c. Pressure distribution. $M = 0.40$, $C_\ell = 1.5$, $R_N = 4 \times 10^6$, $[X_T/C] = .05$.

Figure 22. - Continued.

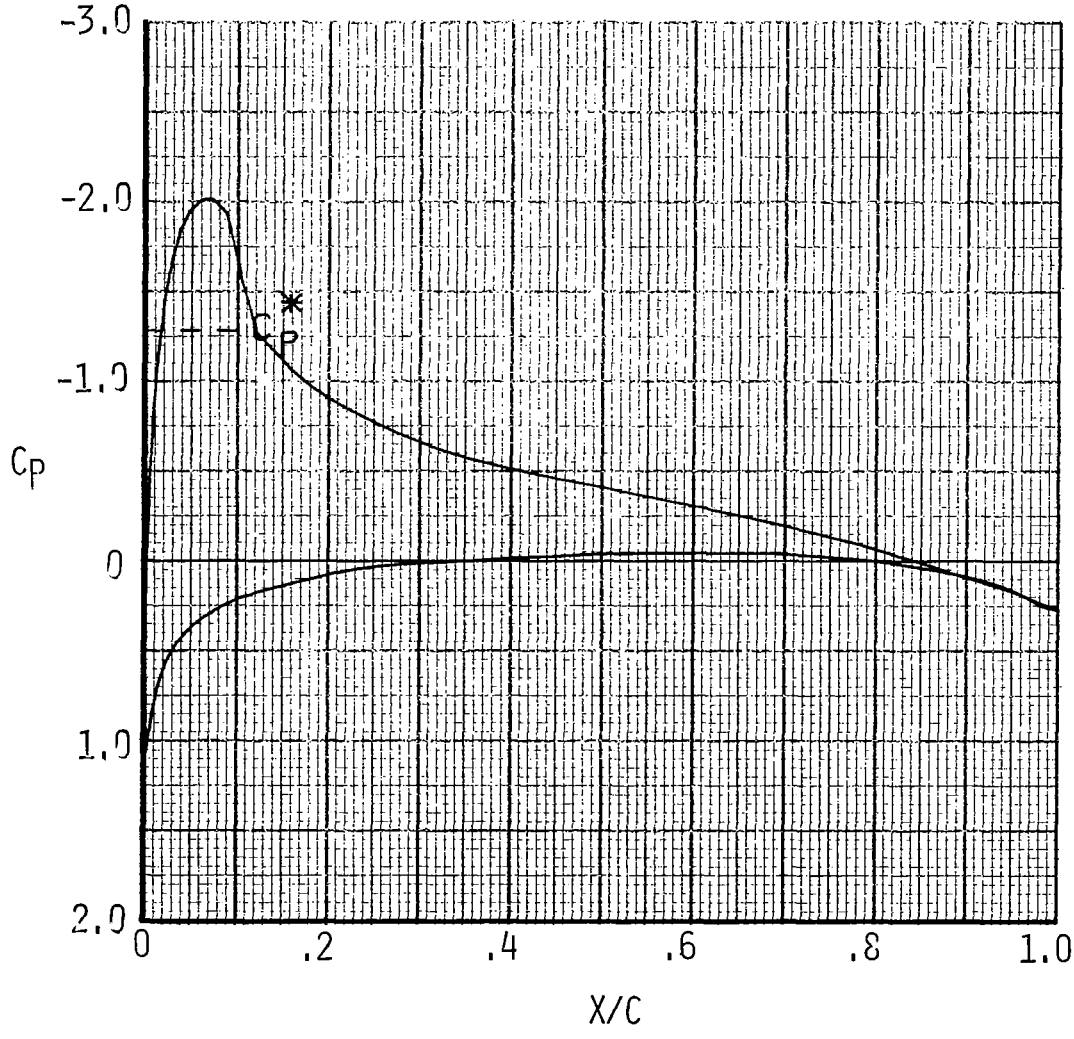

d. Pressure distribution. $M = 0.60$, $C_\ell = 0.60$, $R_N = 6 \times 10^6$, $[X_T/C] = .05$.

Figure 22. - Concluded.

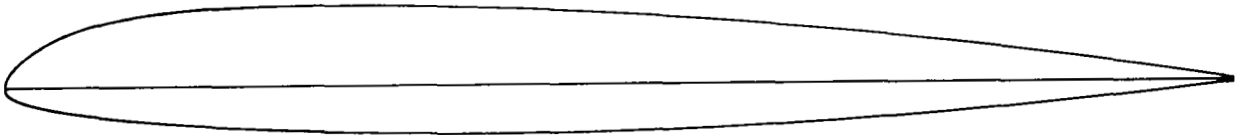

Figure 23. - Sketch of rotor airfoil.

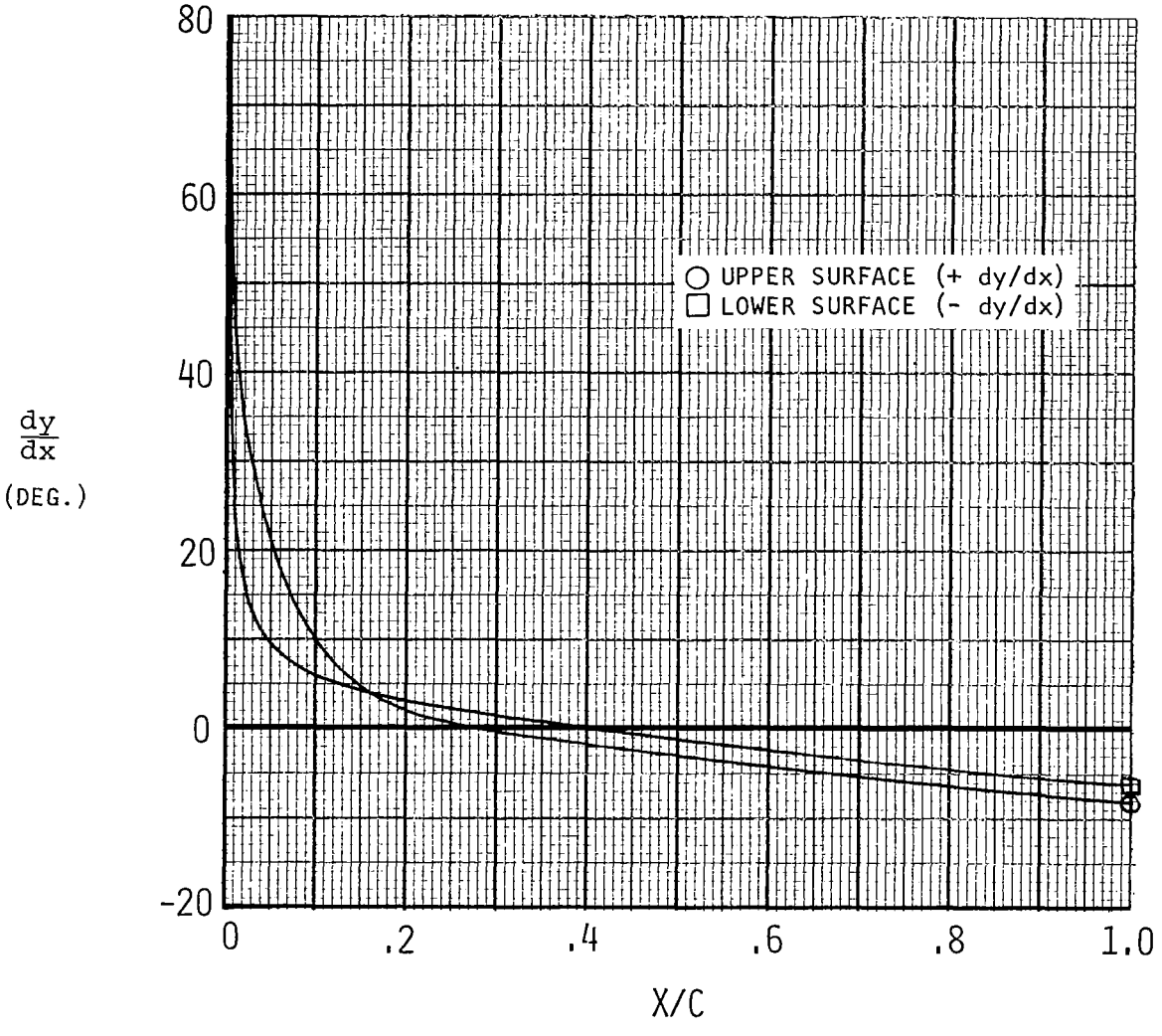

(a) Surface slope distribution.

Figure 24. - Rotor airfoil geometry.

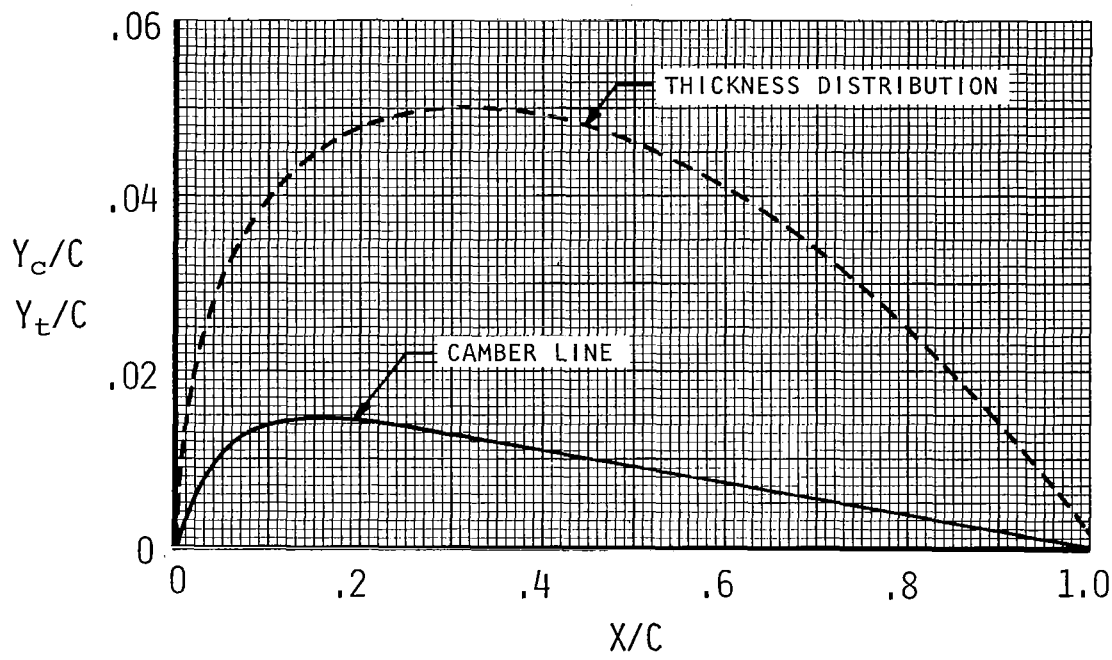

(b) Camber and thickness distribution.

Figure 24. - Continued.

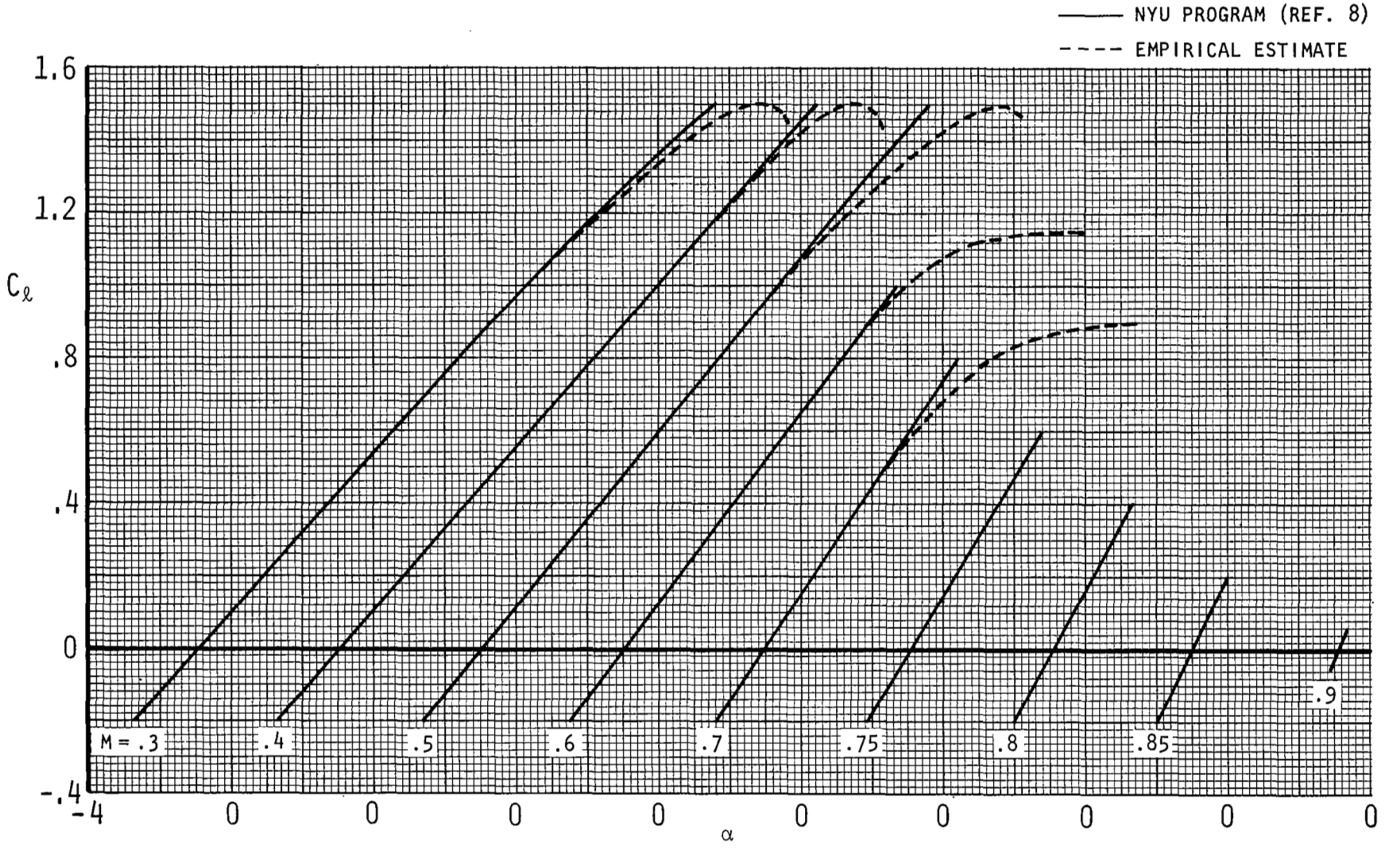

(a) Lift coefficients

Figure 25. - Predicted aerodynamic characteristics of the rotor airfoil. $R_N = M \times 10^7$, $[X_T/C] = .05$.

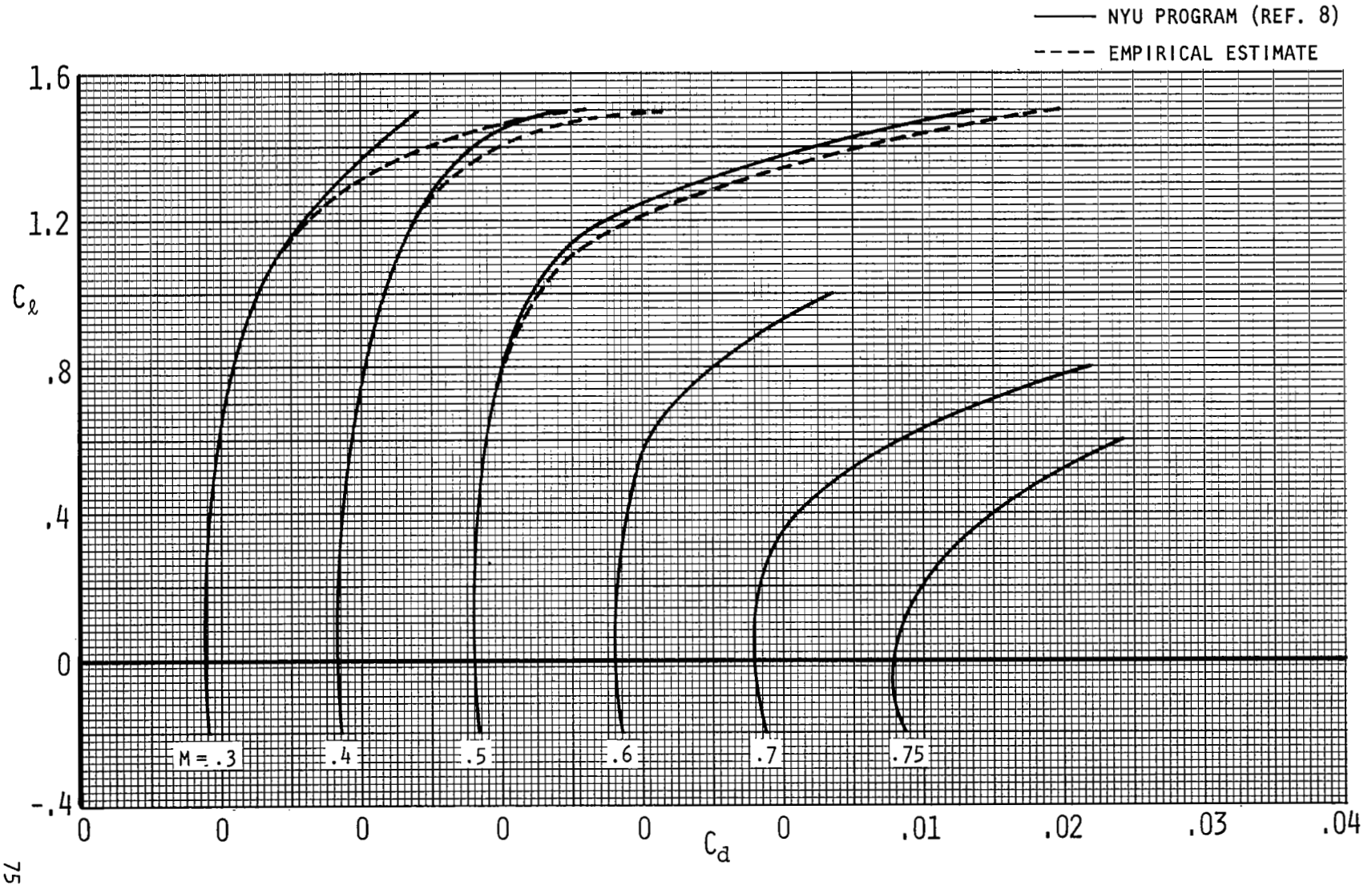

(b) Drag coefficients, M = 0.3 to 0.75

Figure 25. - Continued.

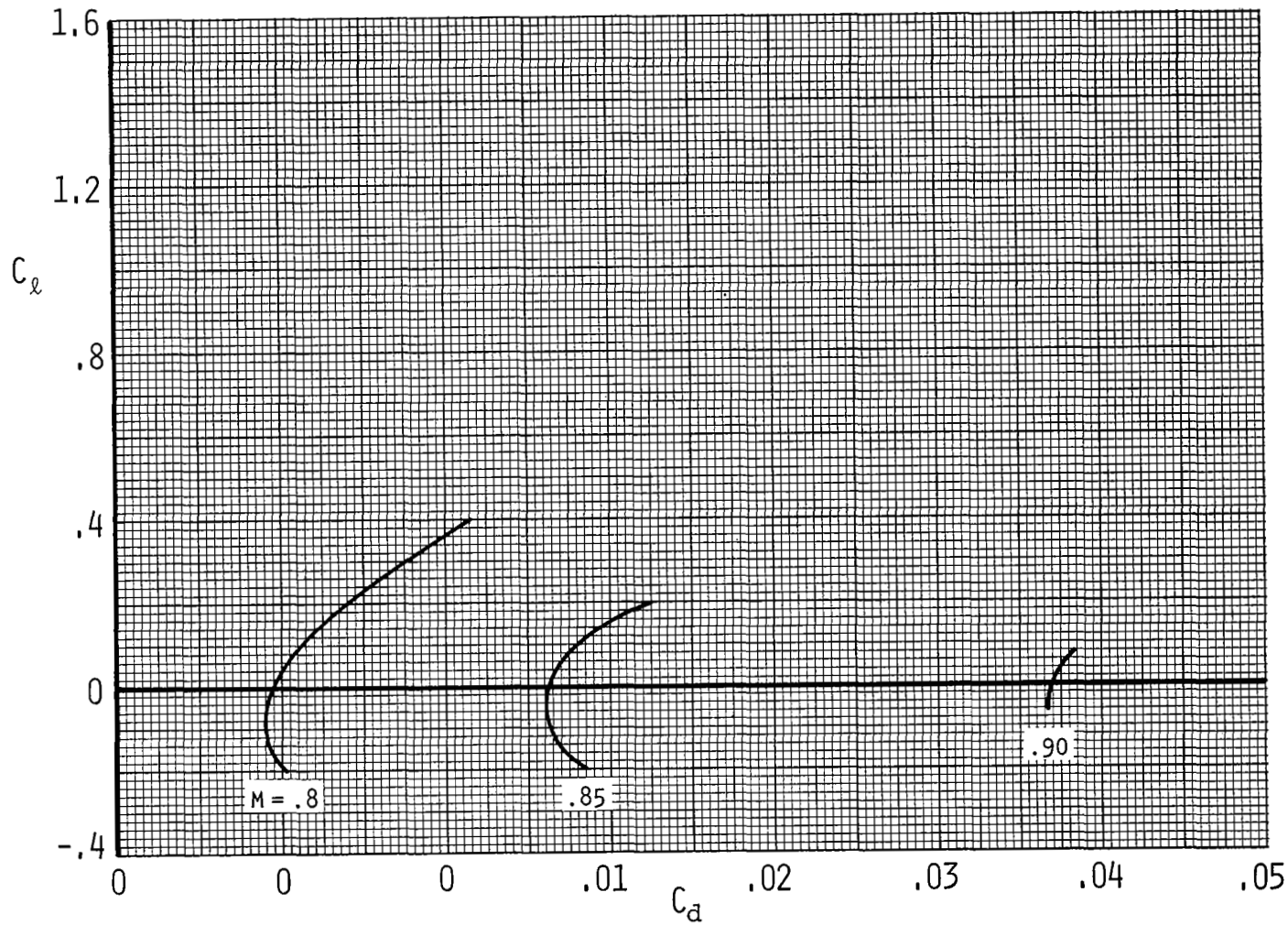

(c) Drag coefficients, M = 0.80 to 0.90

Figure 25. - Continued.

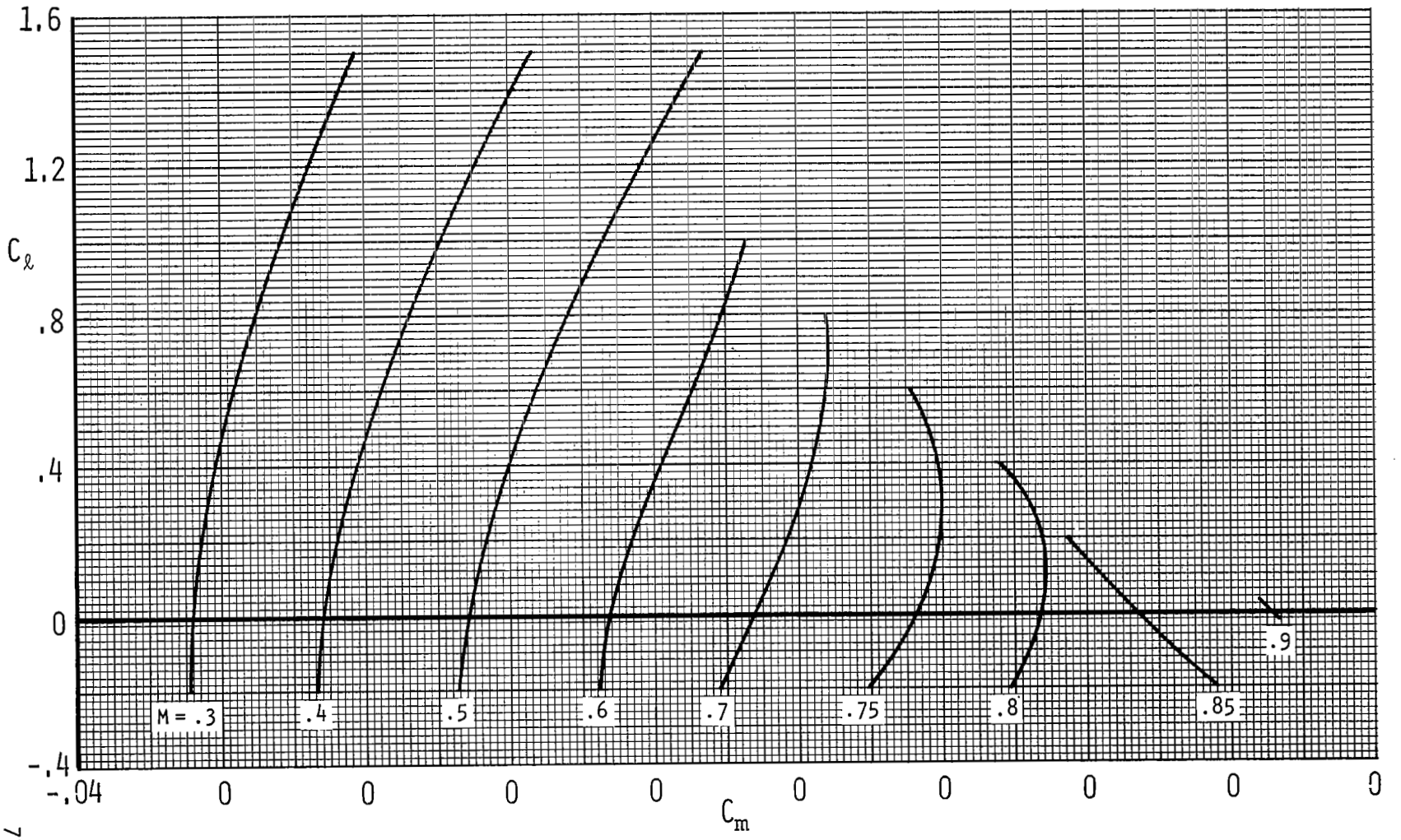

(d) Pitching-moment coefficients

Figure 25. - Concluded.

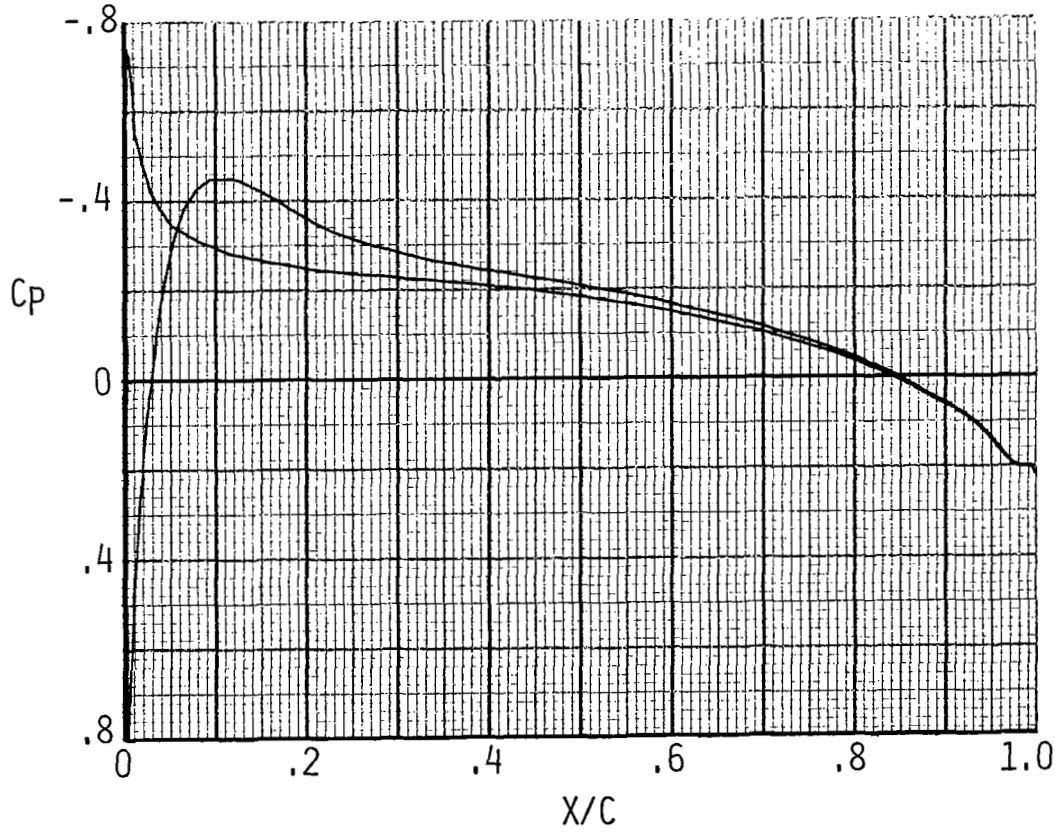

a. $M = 0.30$, $C_\ell = 0$, $R_N = 3 \times 10^6$

Figure 26. - Airfoil pressure distributions. $[X_T/C] = .05$

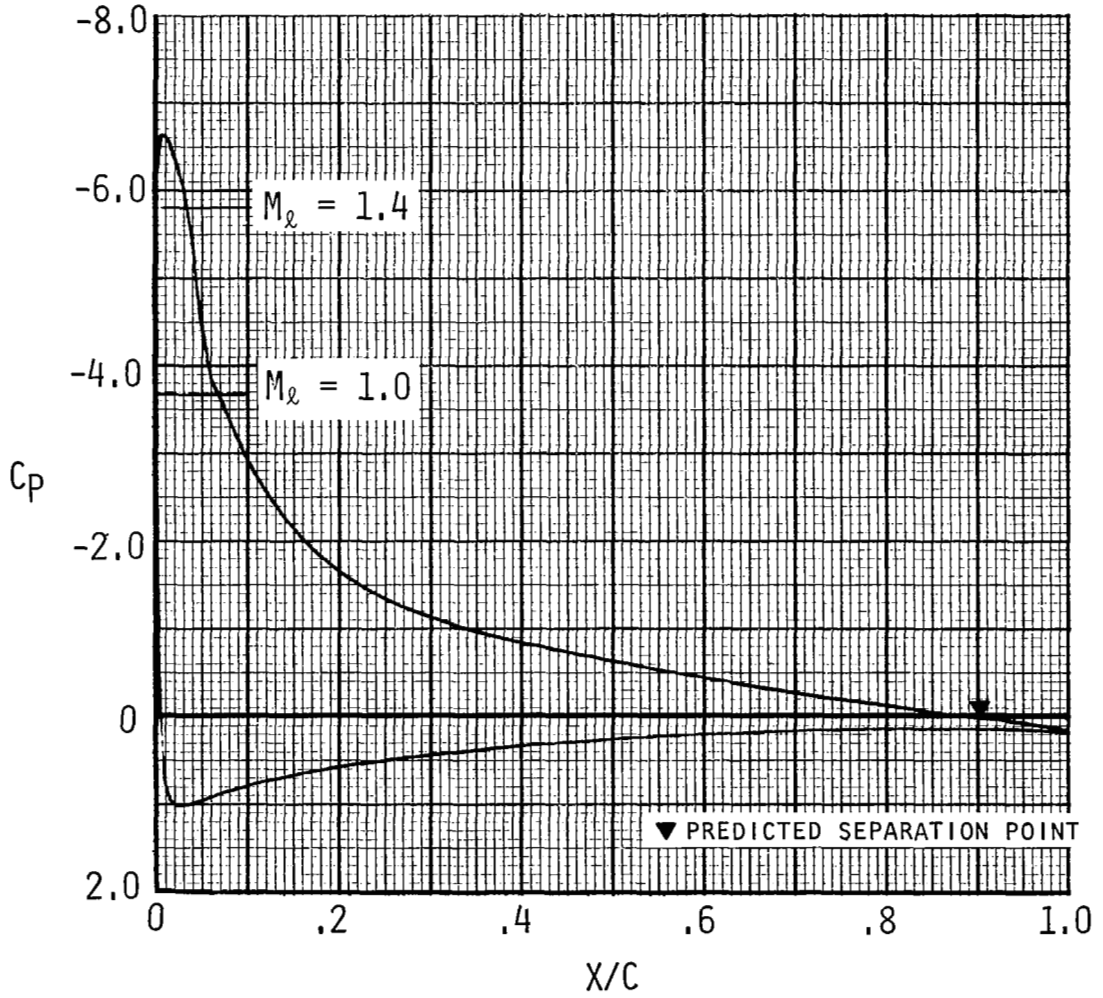

b. $M = 0.40$, $C_\ell = 1.5$, $R_N = 4 \times 10^6$

Figure 26. - Continued.

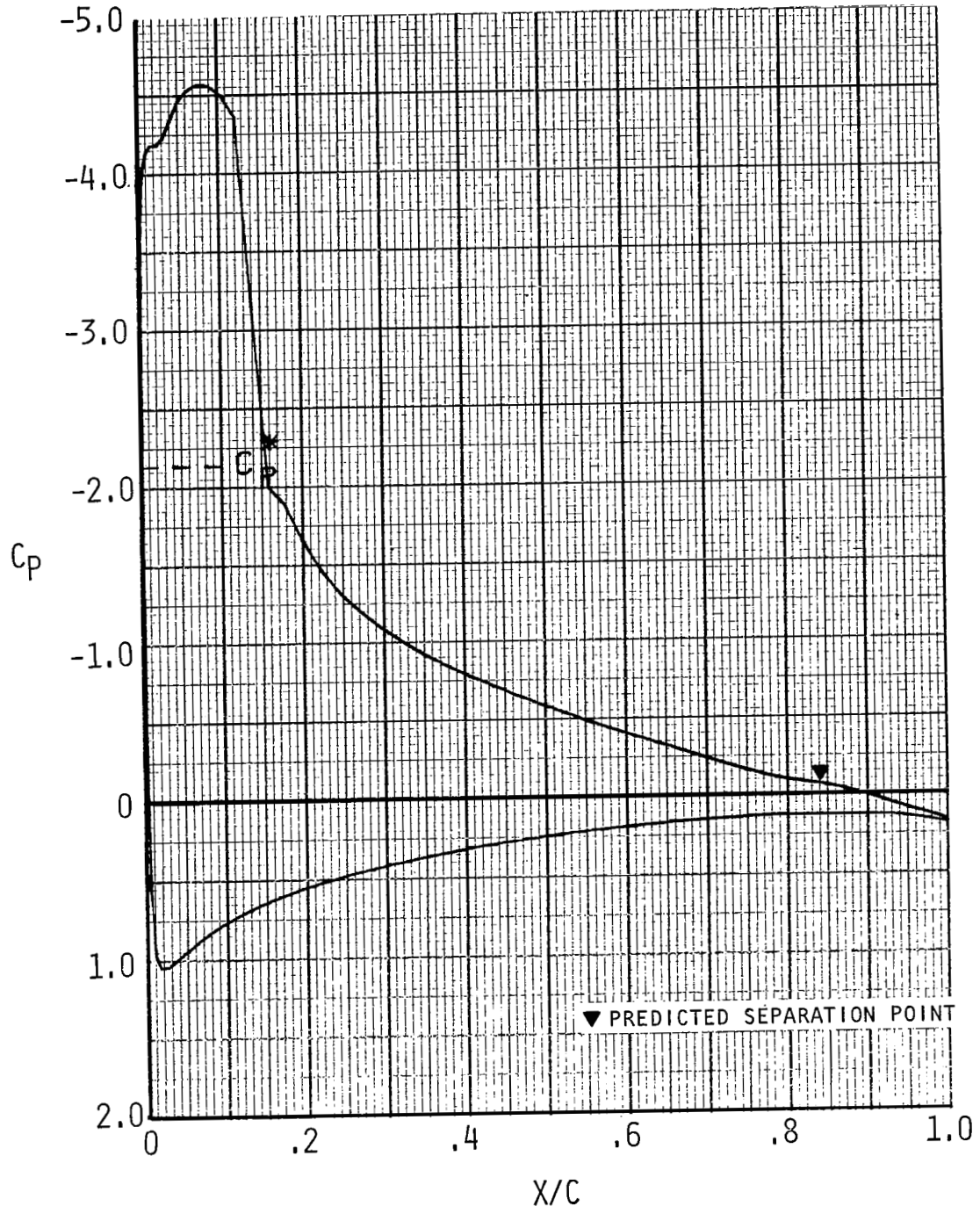

c. $M = 0.50$, $C_\ell = 1.5$, $R_N = 5 \times 10^6$

Figure 26. - Continued.

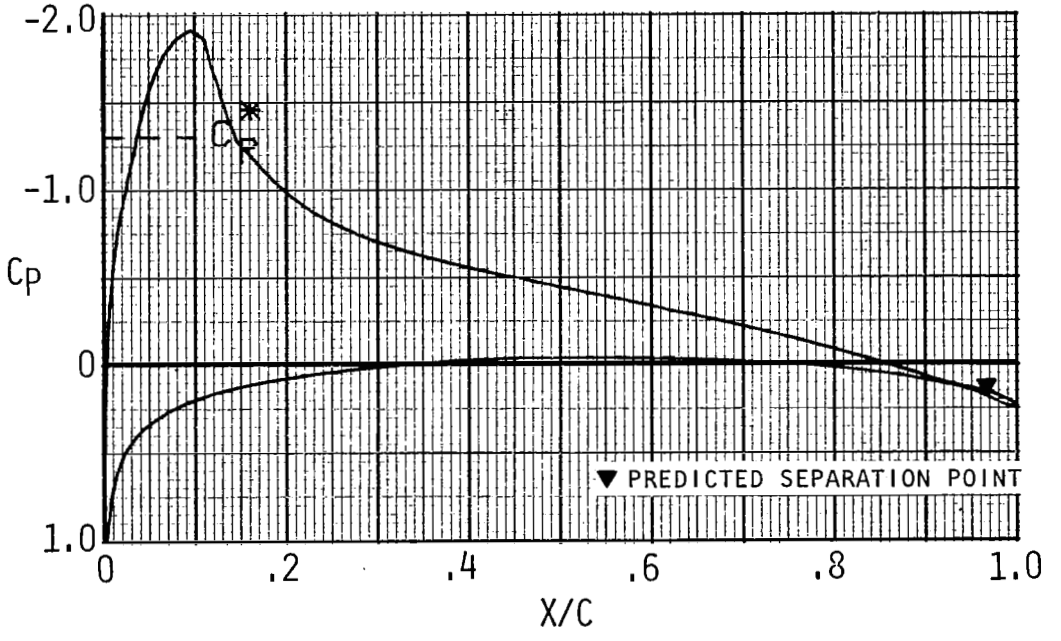

d. $M = 0.60$, $C_\ell = 0.6$, $R_N = 6 \times 10^6$

Figure 26. - Continued.

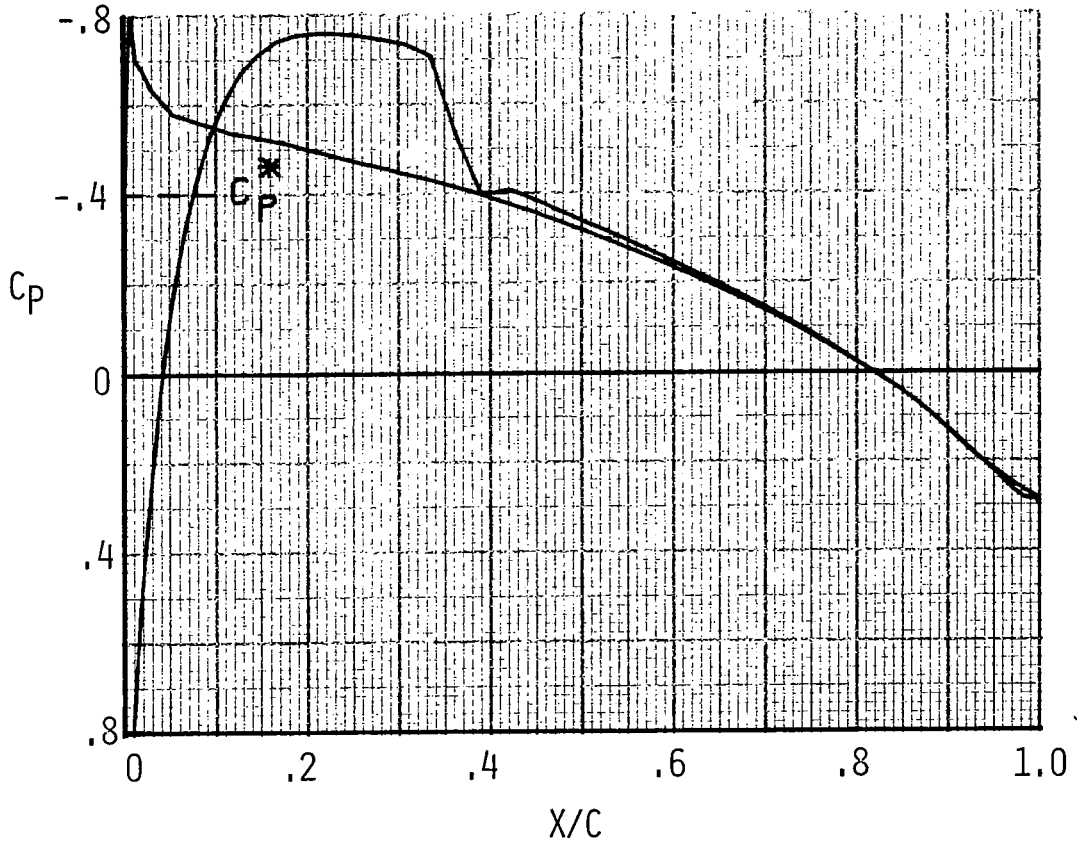

e. $M = 0.81$, $C_\ell = 0$, $R_N = 8.1 \times 10^6$

Figure 26. - Continued.

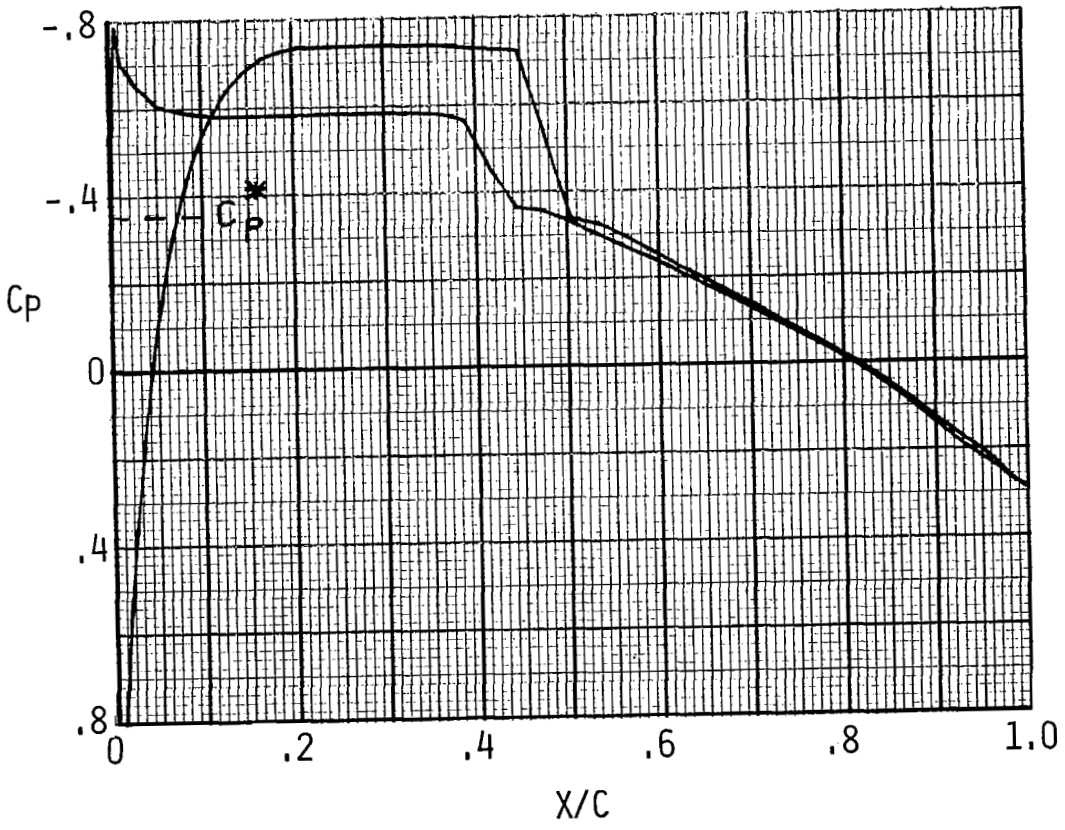

f. $M = 0.83$, $C_\ell = 0$, $R_N = 8.3 \times 10^6$

Figure 26. - Concluded.

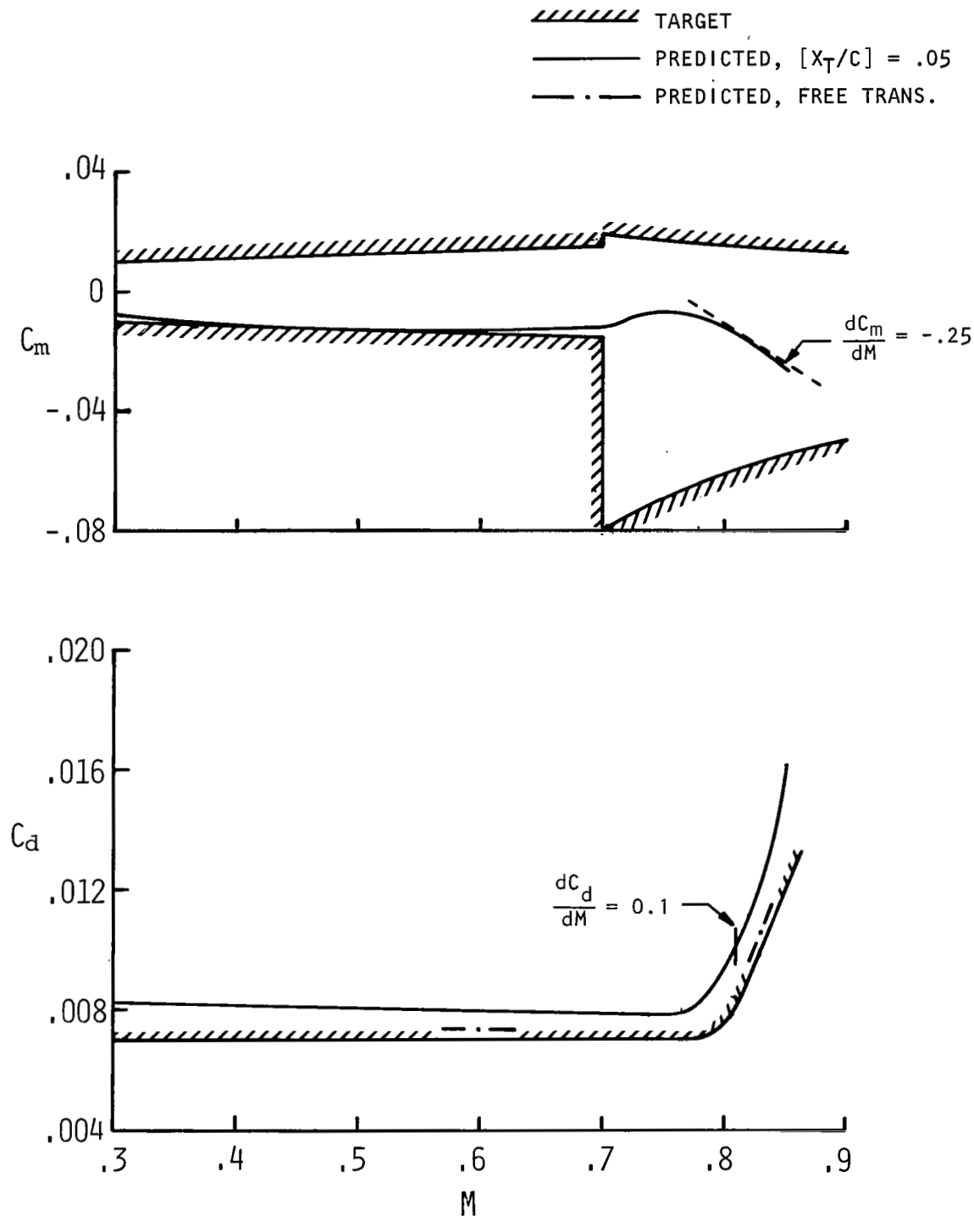

Figure 27. - Comparison of target and predicted force data for $C_\ell = 0$, $R_N = M \times 10^7$.

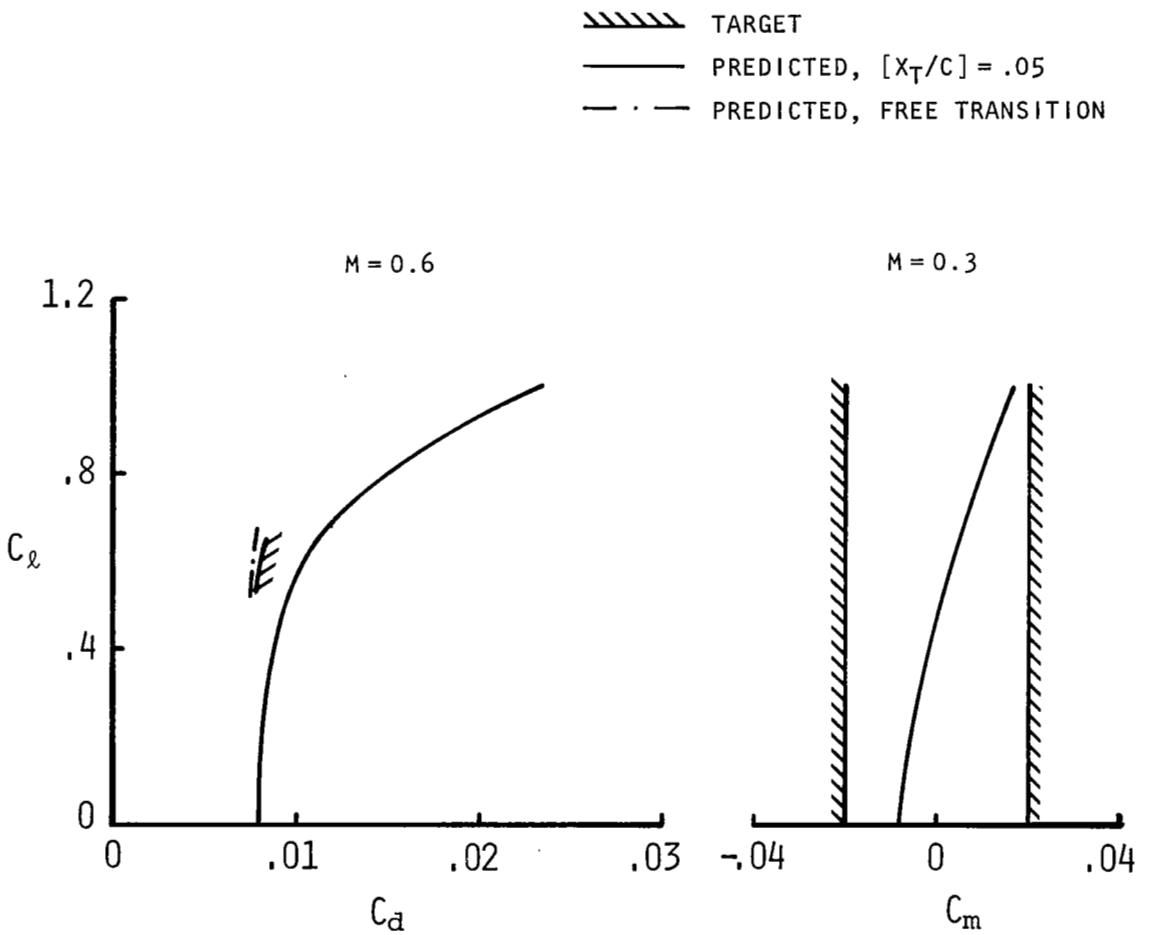

Figure 28. - Comparison of target and predicted force and moment characteristics. $R_N = M \times 10^7$.

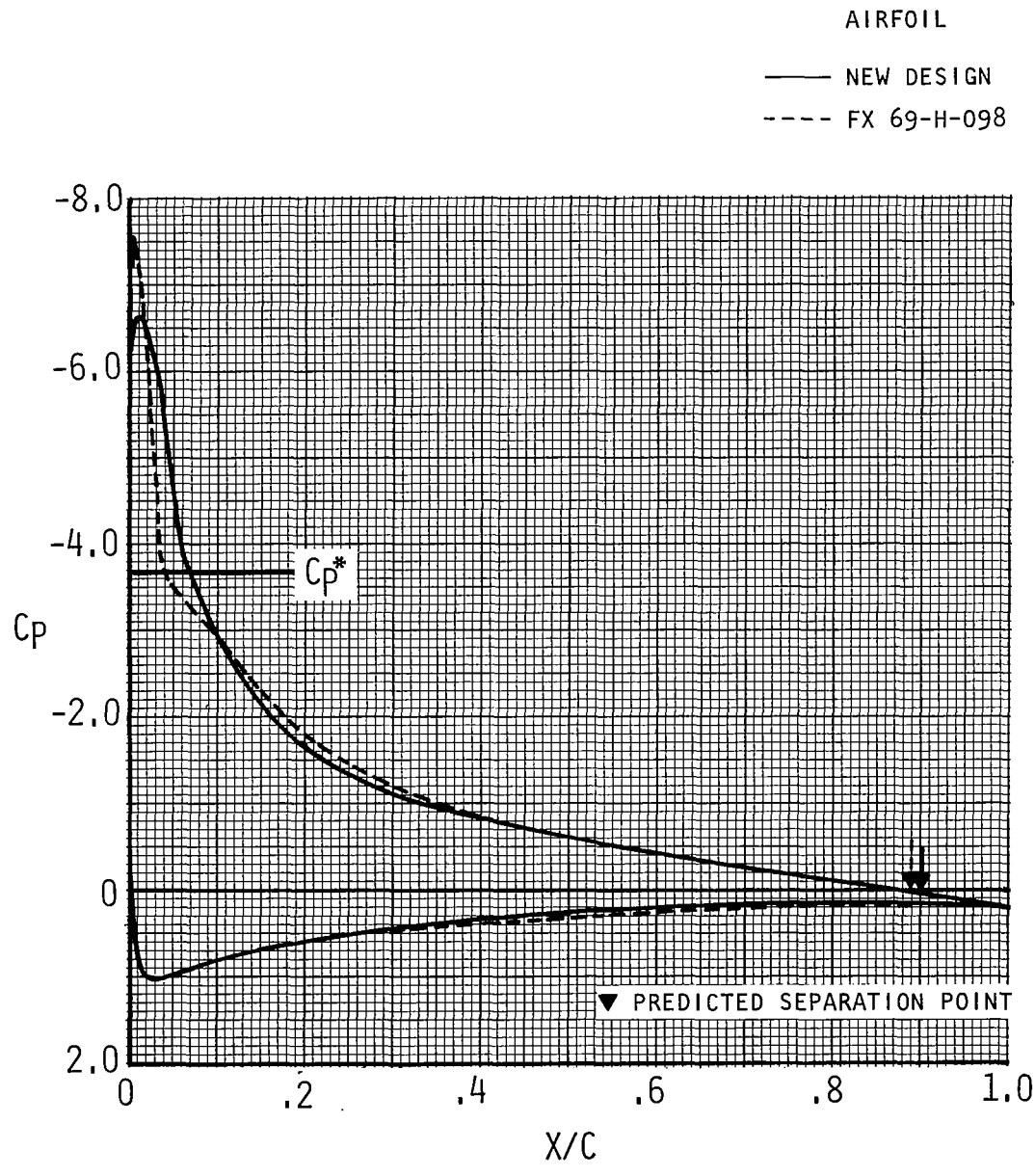

a. $M = 0.40$, $C_\ell = 1.5$, $R_N = 4 \times 10^6$

Figure 29. - Comparison of pressure distributions for new airfoil with those for the FX69-H-098 airfoil for Regions I, II and III. $[X_T/C] = .05$

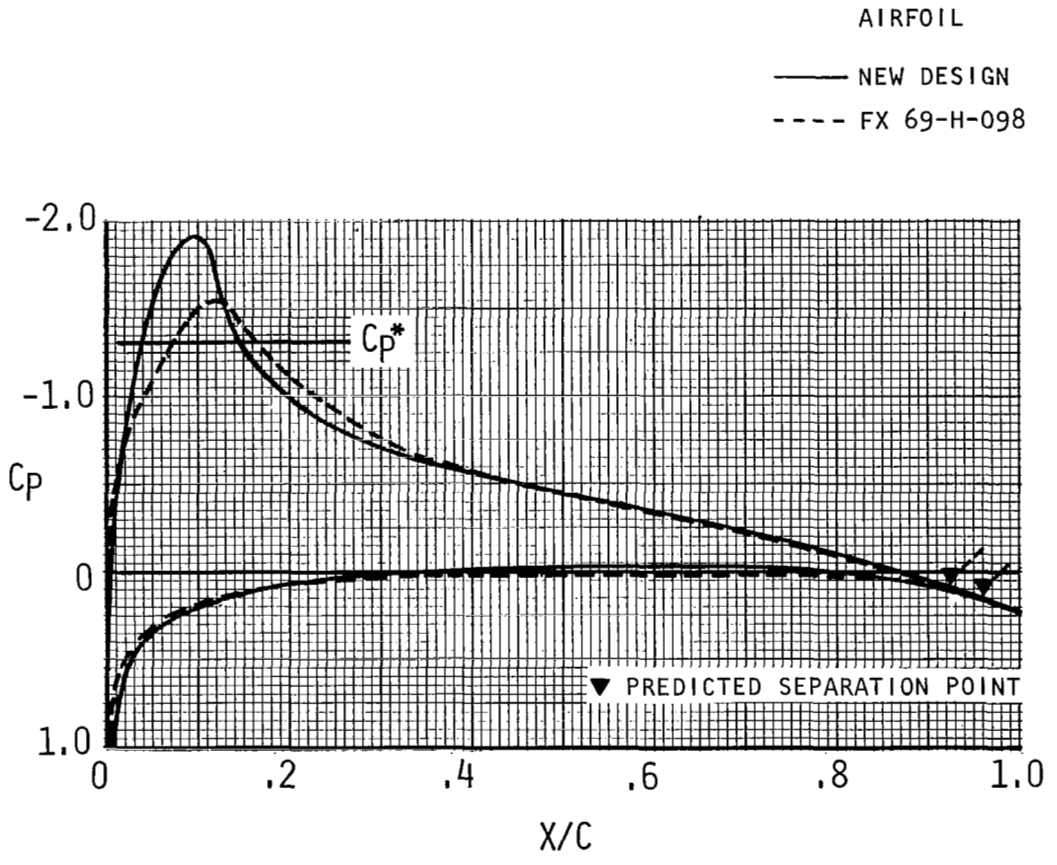

b. $M = 0.60$, $C_\ell = 0.60$, $R_N = 6 \times 10^6$

Figure 29. - Continued.

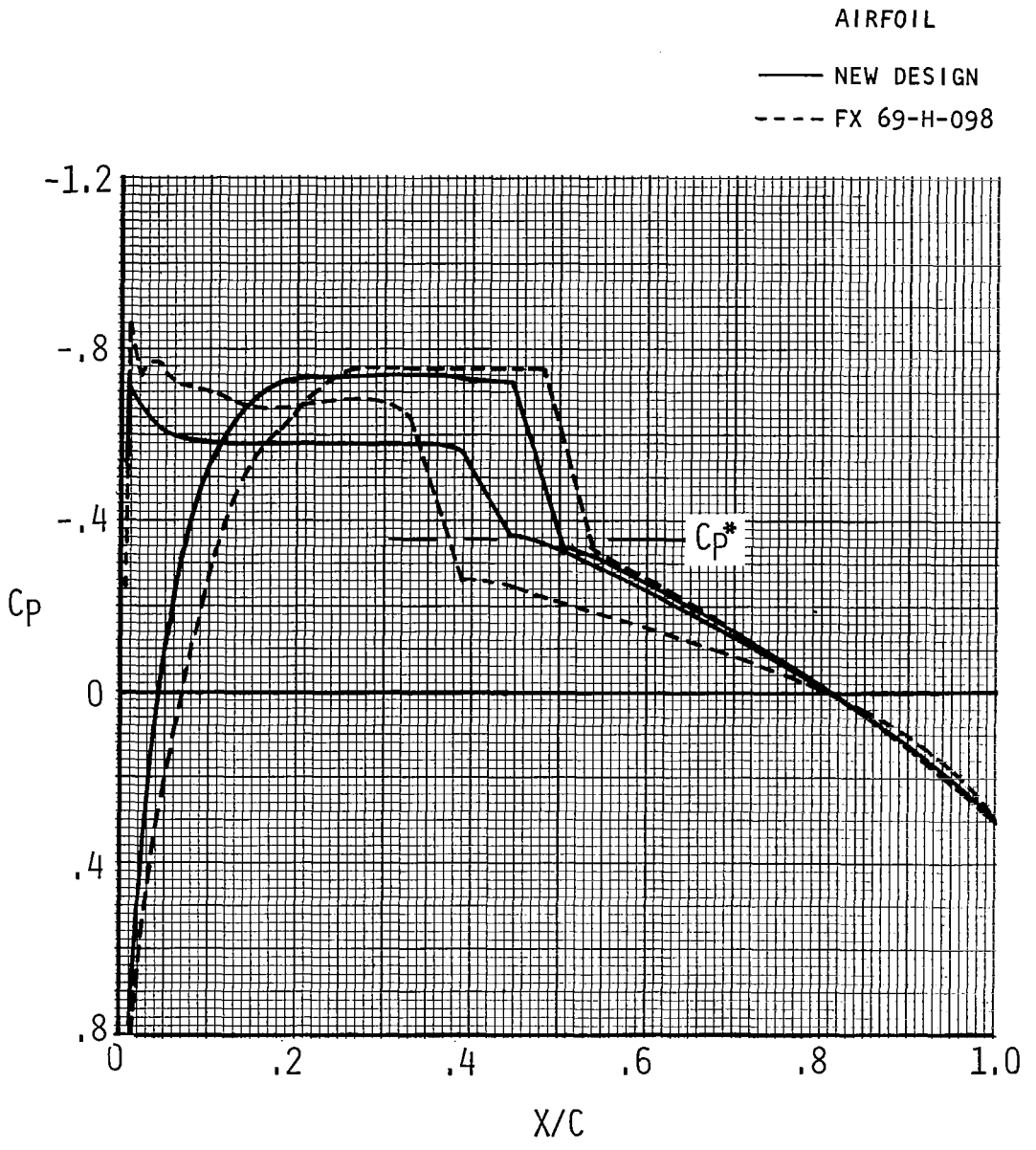

c. $M = 0.83$, $C_\ell = 0.$, $R_N = 8.3 \times 10^6$

Figure 29. - Concluded.

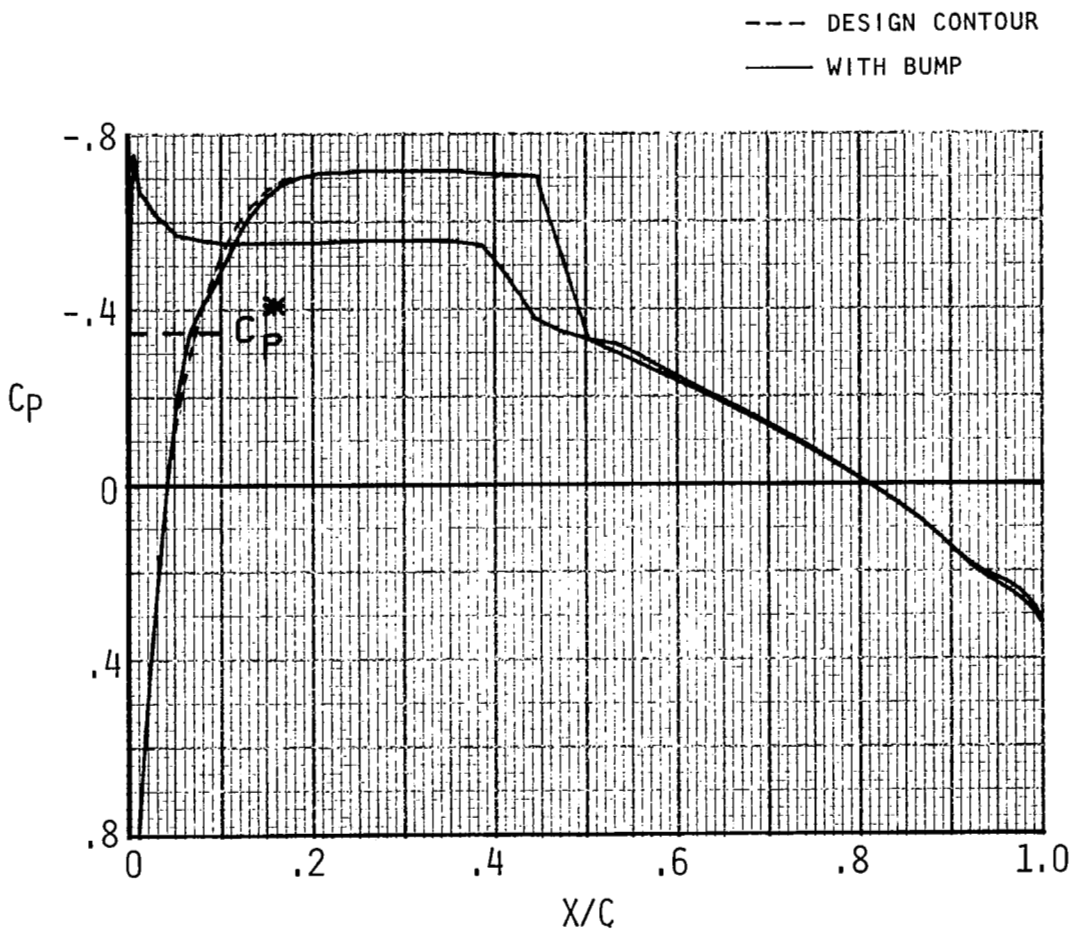

a. Bump height - 0.06% chord.

Figure 30. - Effect of upper surface leading-edge contour deviation at $M = 0.83$, $C_\ell = 0.$, $R_N = 8.3 \times 10^6$, $[X_T/C] = .05$.

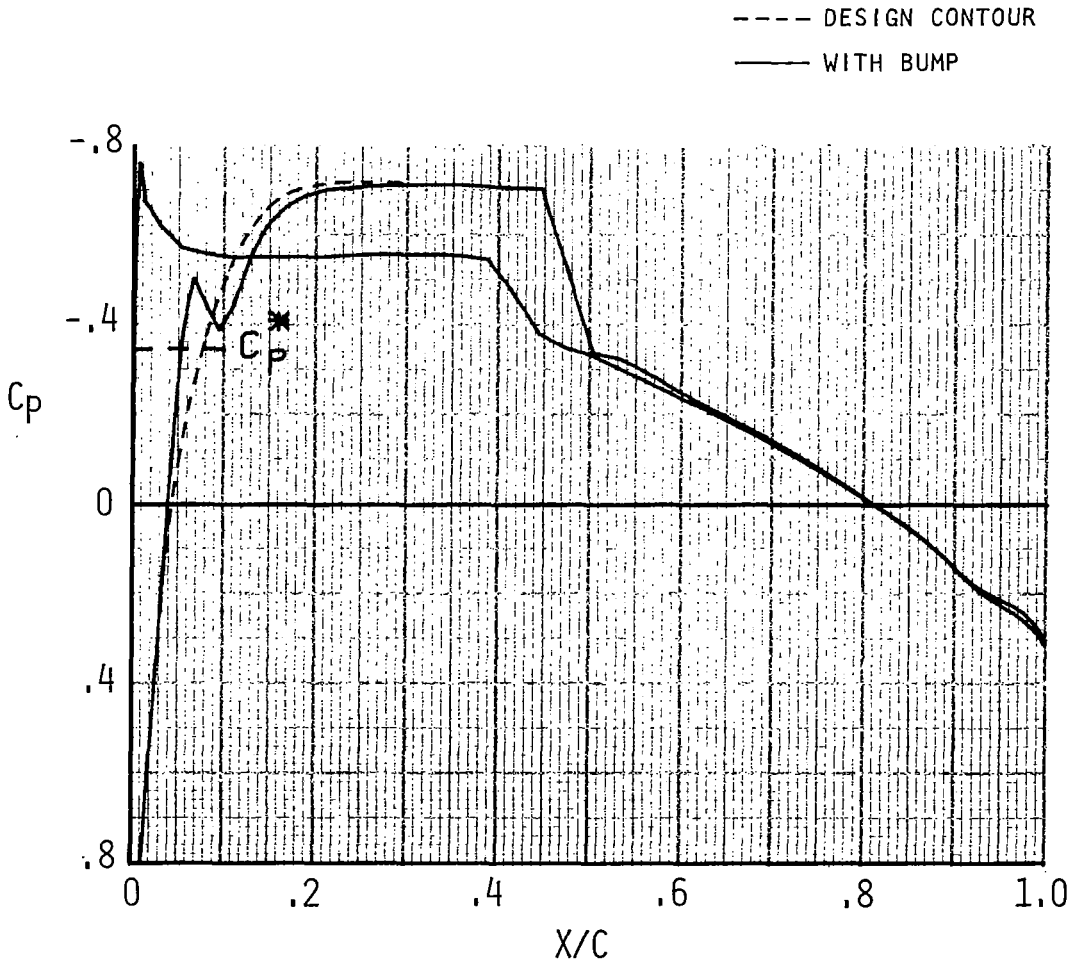

b. Bump height - 0.18% chord.

Figure 30. - Concluded.

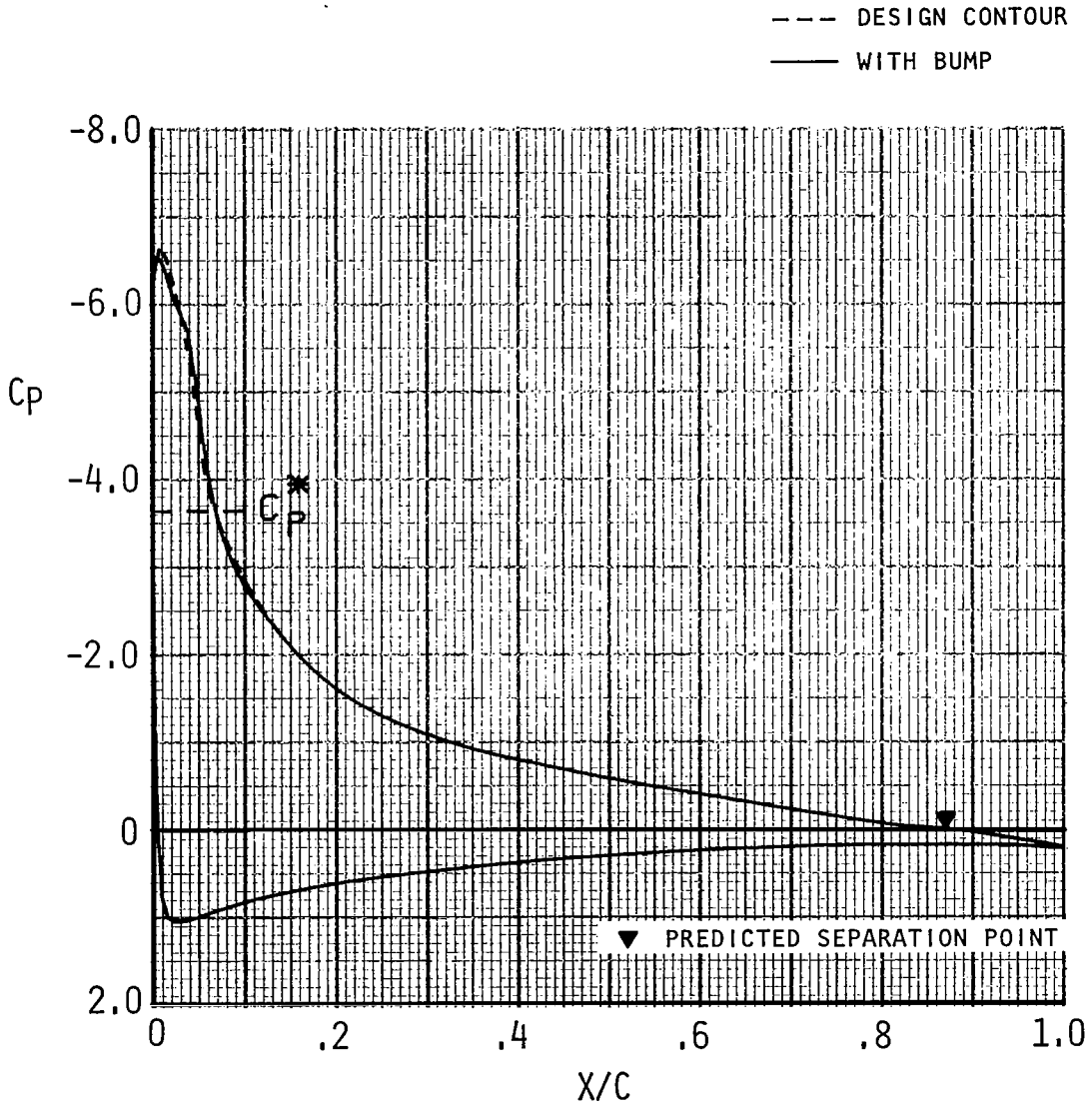

a. Bump height - 0.06% chord.

Figure 31. - Effect of upper surface leading-edge contour deviation at $M = 0.40$, $C_\ell = 1.5$, $R_N = 4 \times 10^6$, $[X_T/C] = .05$.

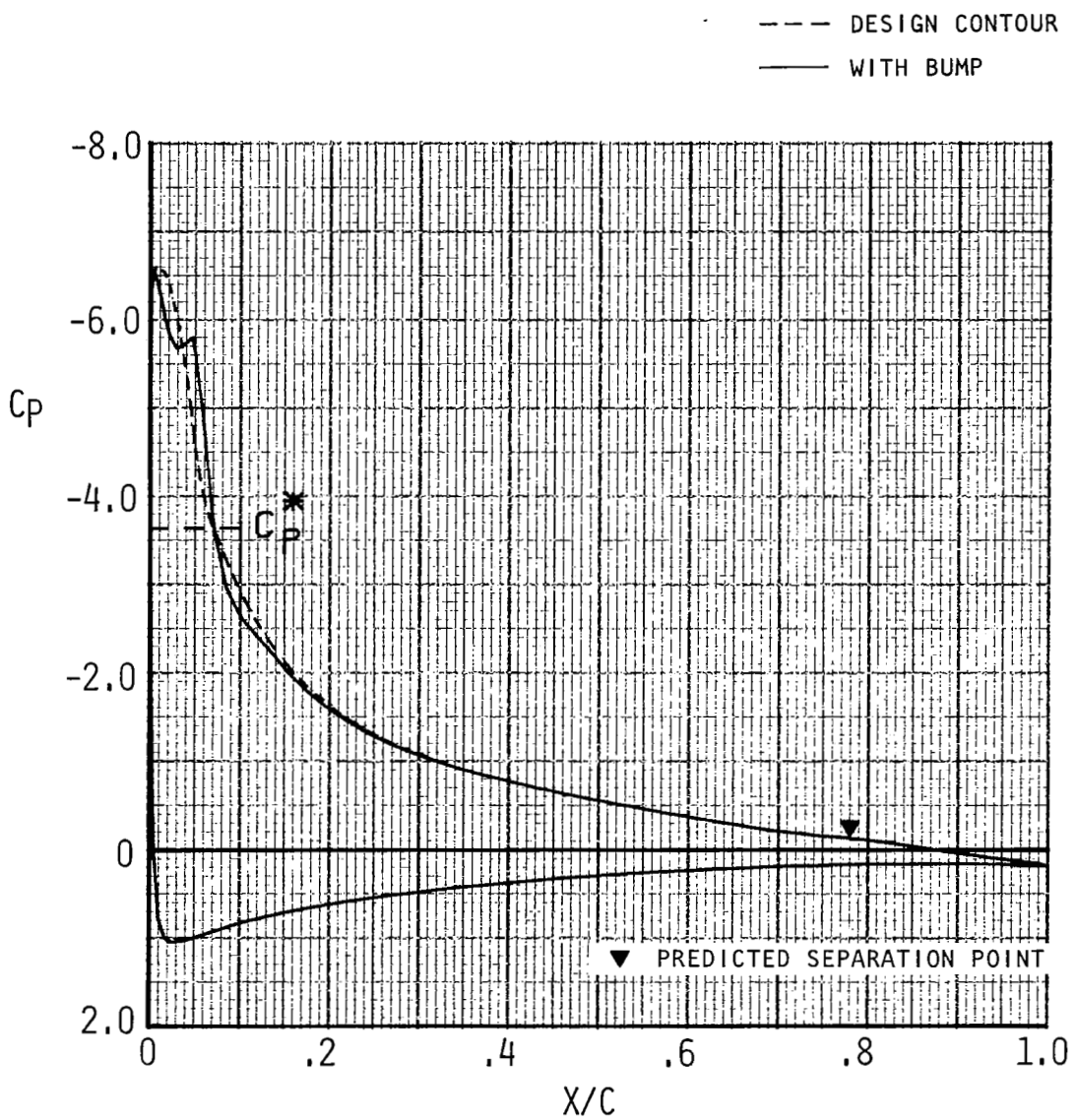

b. Bump height - 0.18% chord.

Figure 31. - Concluded.

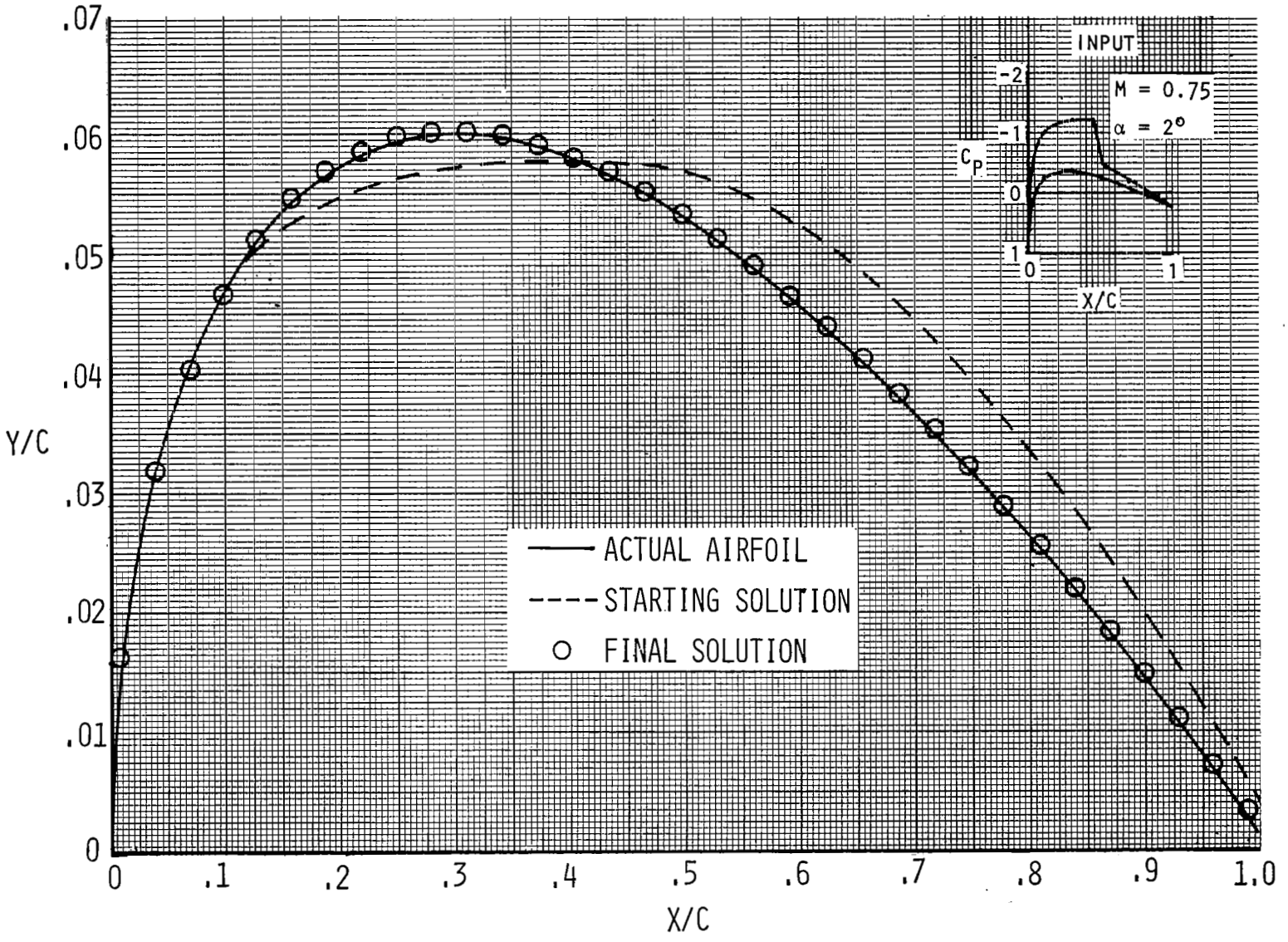

Figure 32. - Correlation of actual and predicted coordinates for the NACA 0012 airfoil using the Carlson airfoil design method.

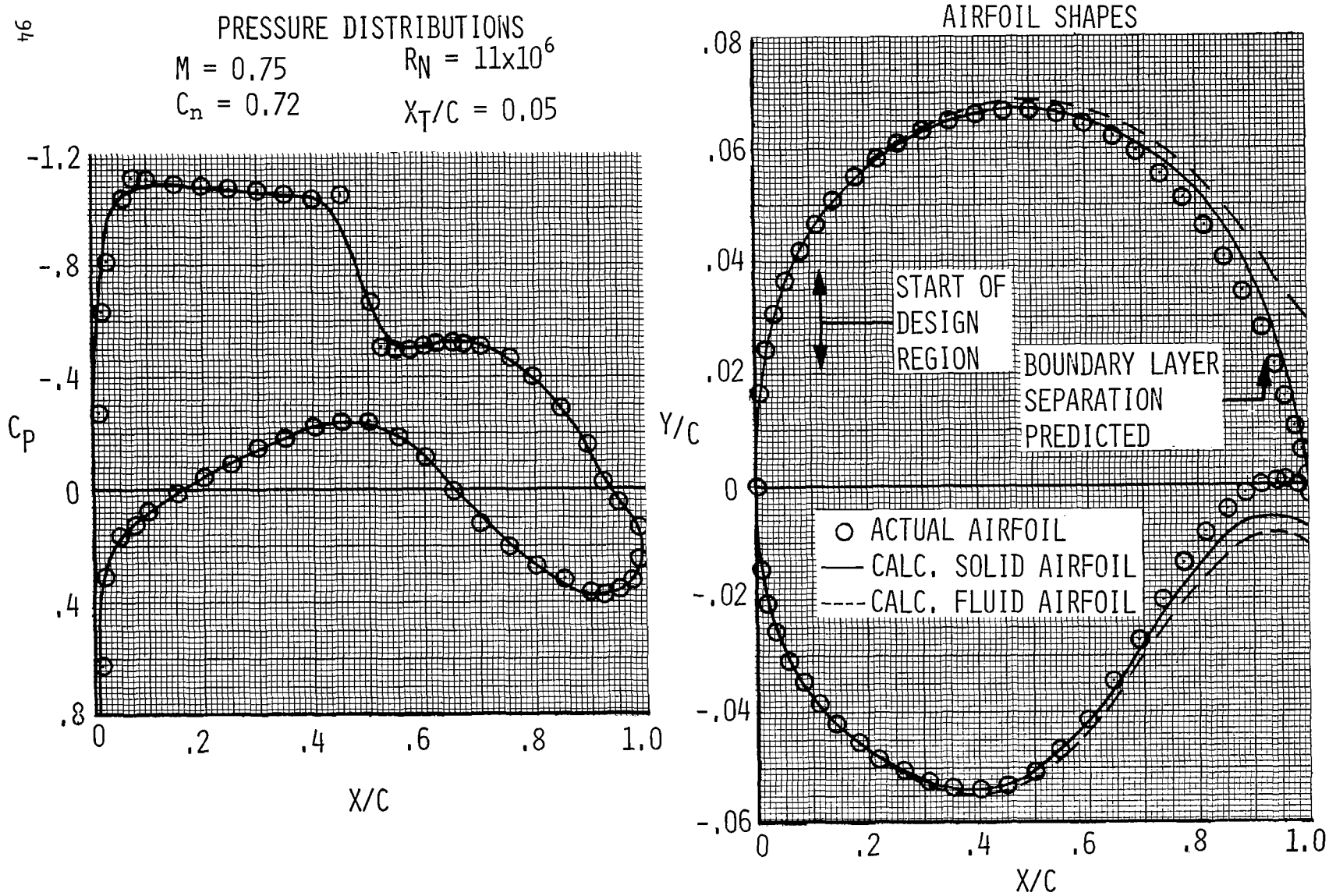

Figure 33. - Correlation of Carlson airfoil design procedure using the Lockheed-Georgia LG4-612 airfoil.

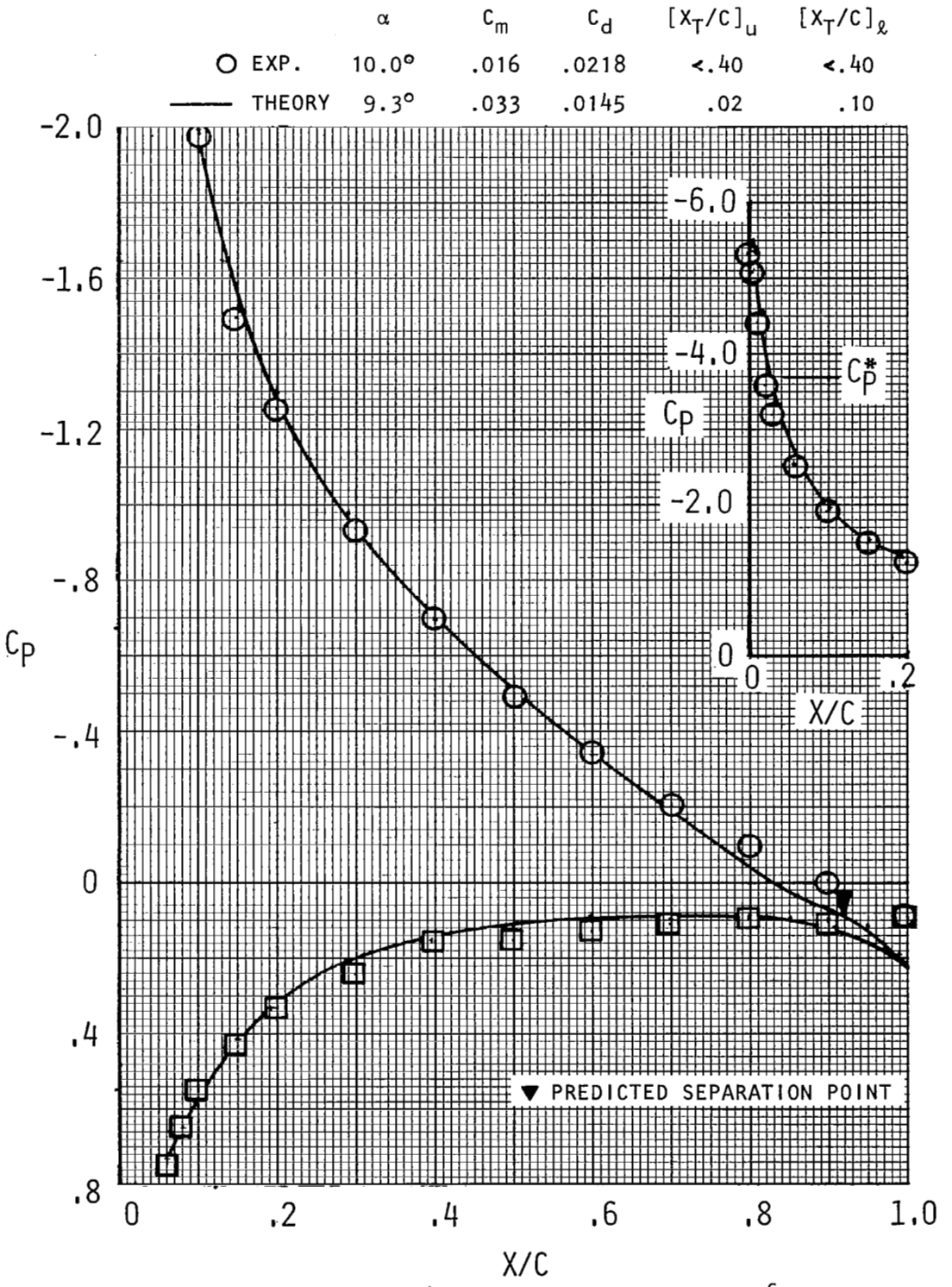

a. $M = 0.40$, $C_n = 1.03$, $R_N = 2.1 \times 10^6$.

Figure 34. - Correlation of NYU transonic airfoil analysis program using experimental data (ref. 25) for the NACA 0012 airfoil.

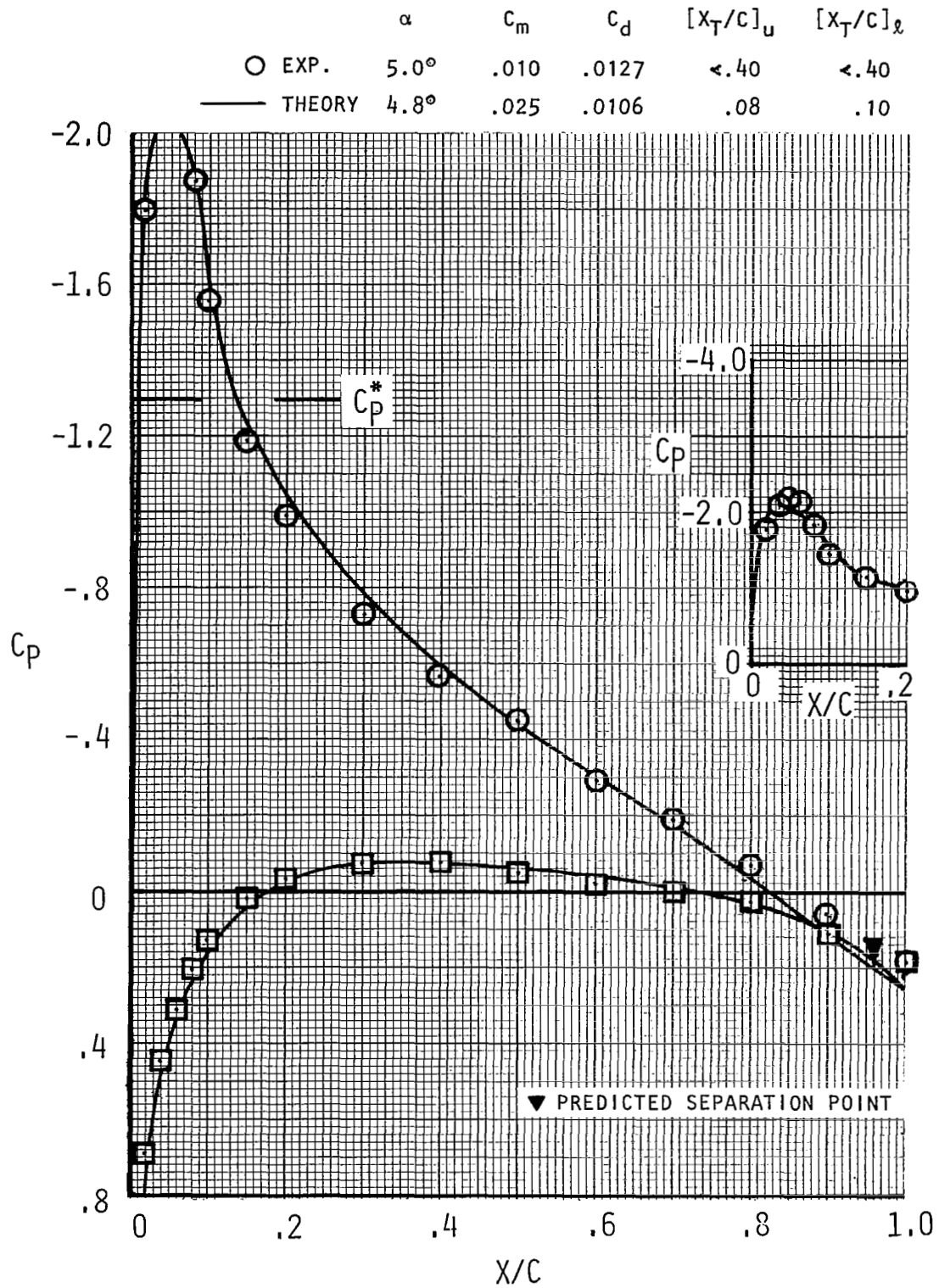

b. $M = 0.60$, $C_n = 0.63$, $R_N = 2.8 \times 10^6$.

Figure 34. - Continued.

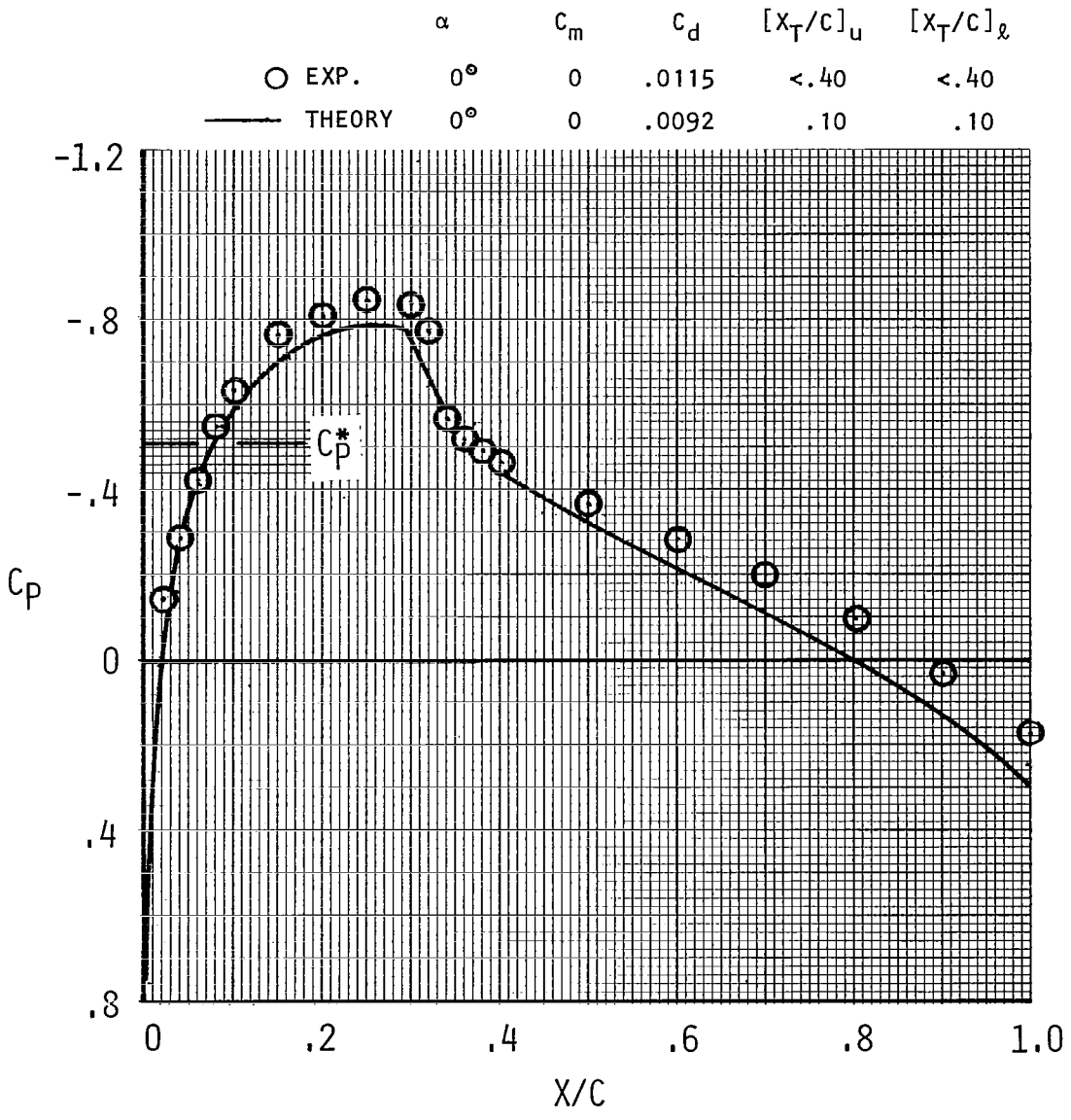

c. M = 0.775, C_n = 0, R_N = 3.5x10^6.

Figure 34. - Concluded.

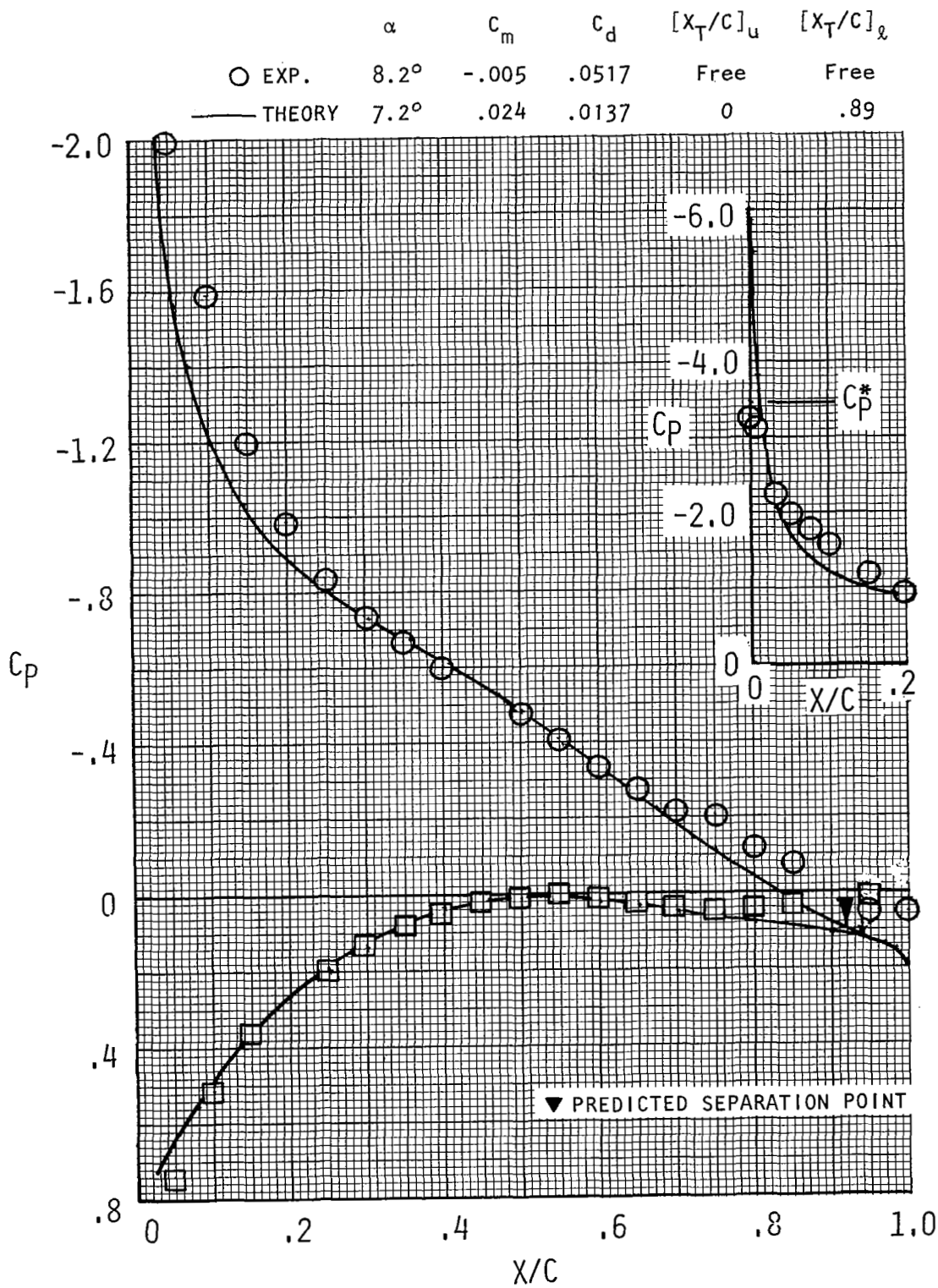

a. M = 0.41, C_n = 0.77, R_N = 1.2x10^6.

Figure 35. - Correlation of NYU transonic airfoil analysis program using experimental data (ref. 26) for the NACA 64A010 airfoil.

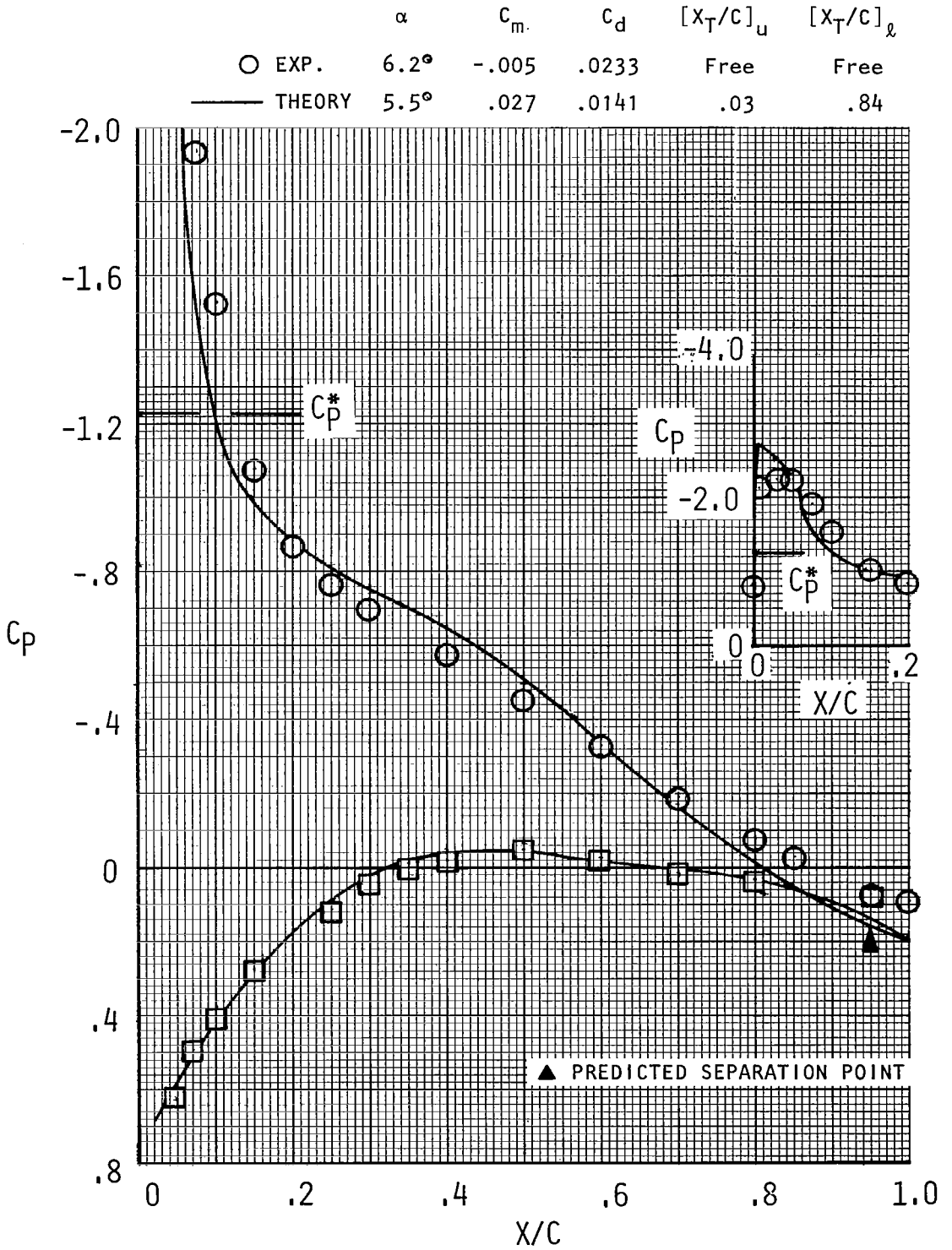

b. M = 0.61, C_n = 0.69, R_N = 1.6x10^6.

Figure 35. - Continued.

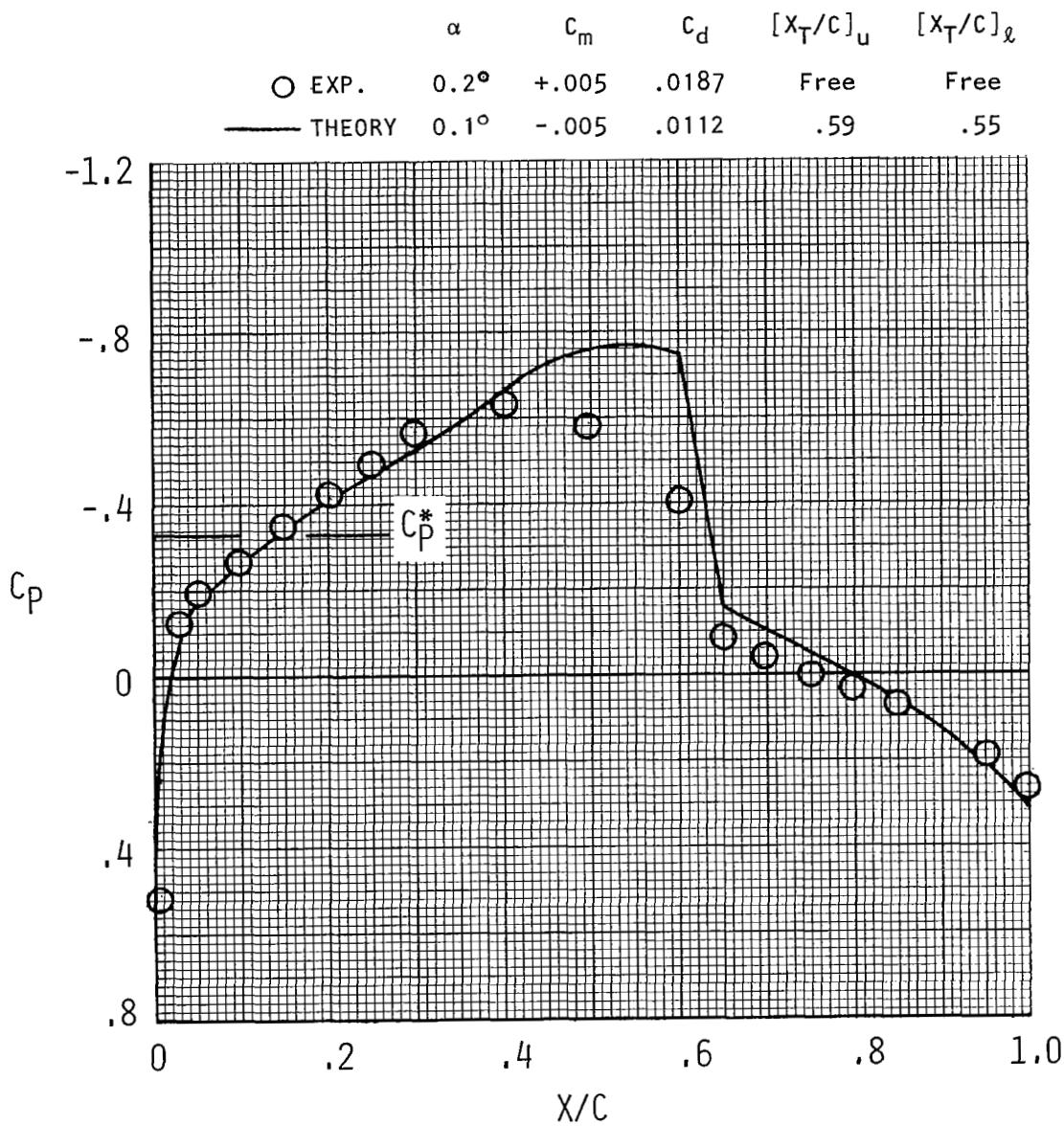

c. M = 0.84, C_n = 0.03, R_N = 1.8x10^6.

Figure 35. - Concluded.

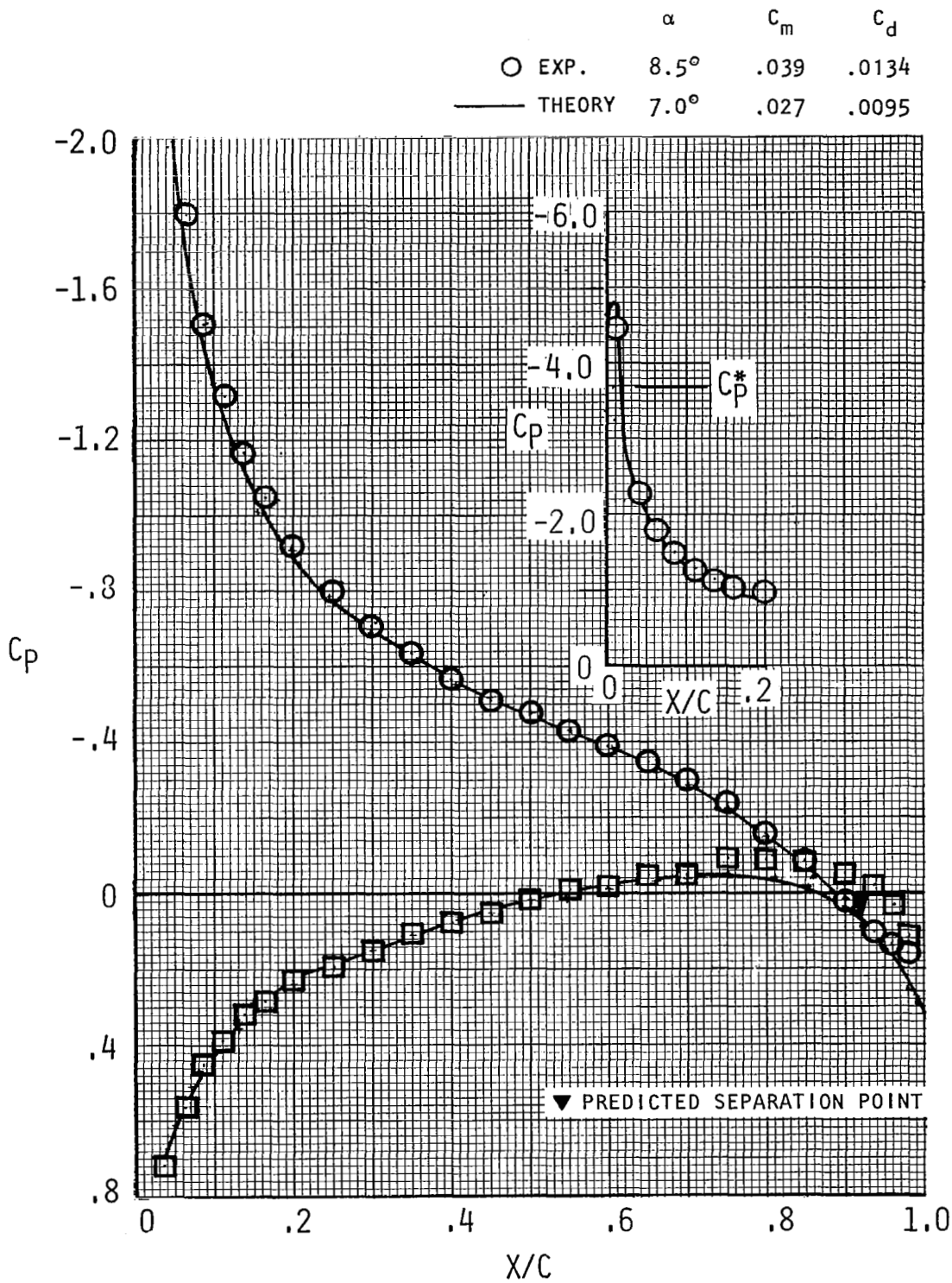

a. $M = 0.40$, $C_n = 0.77$, $R_N = 4.6 \times 10^6$.

Figure 36. - Correlation of NYU transonic airfoil analysis program using experimental data (ref. 2) for the NASA 11% symmetrical supercritical airfoil. $[X_T/C] = .05$.

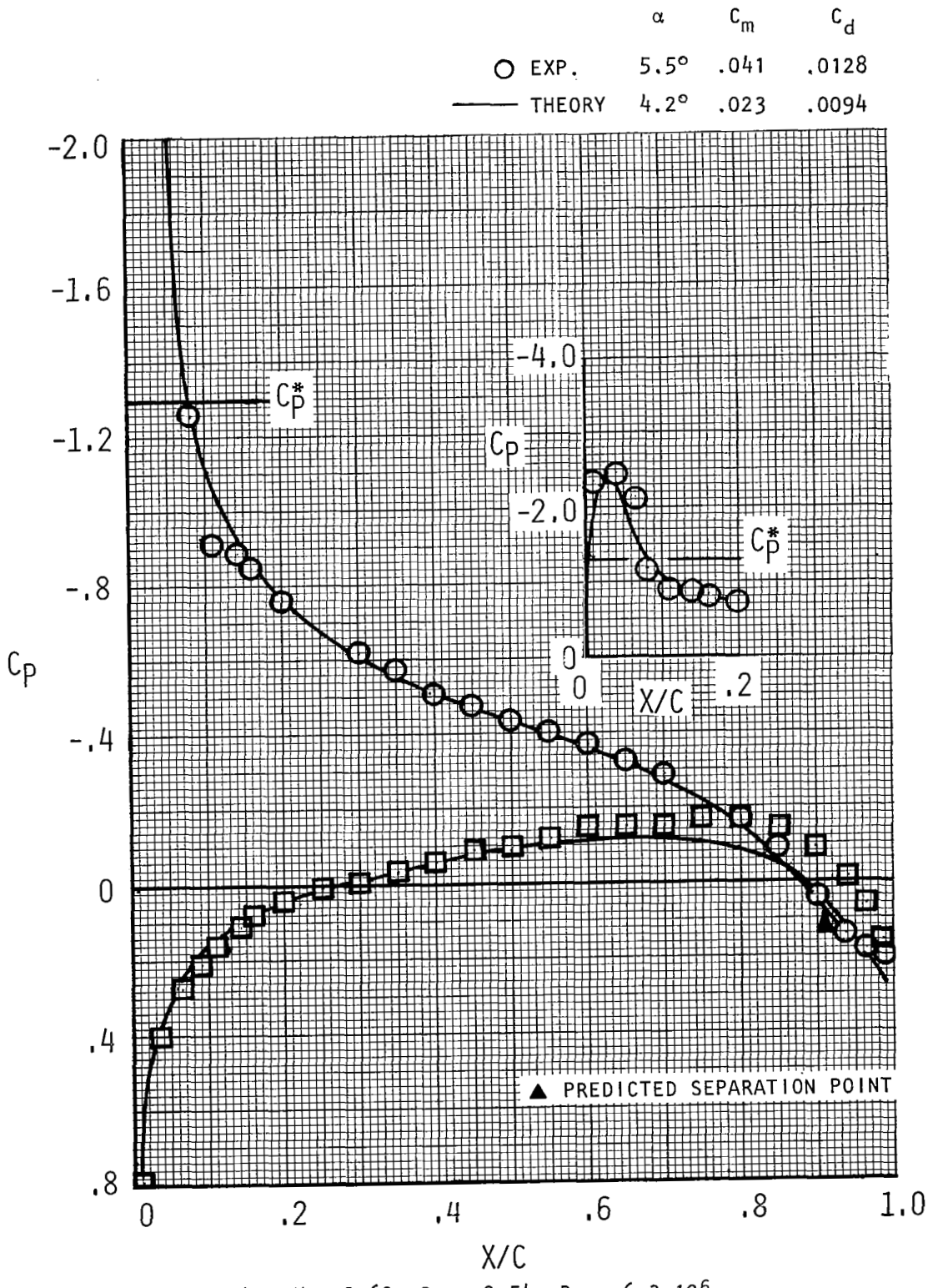

b. M = 0.60, C_n = 0.54, R_N = 6.3x10^6.

Figure 36. - Continued.

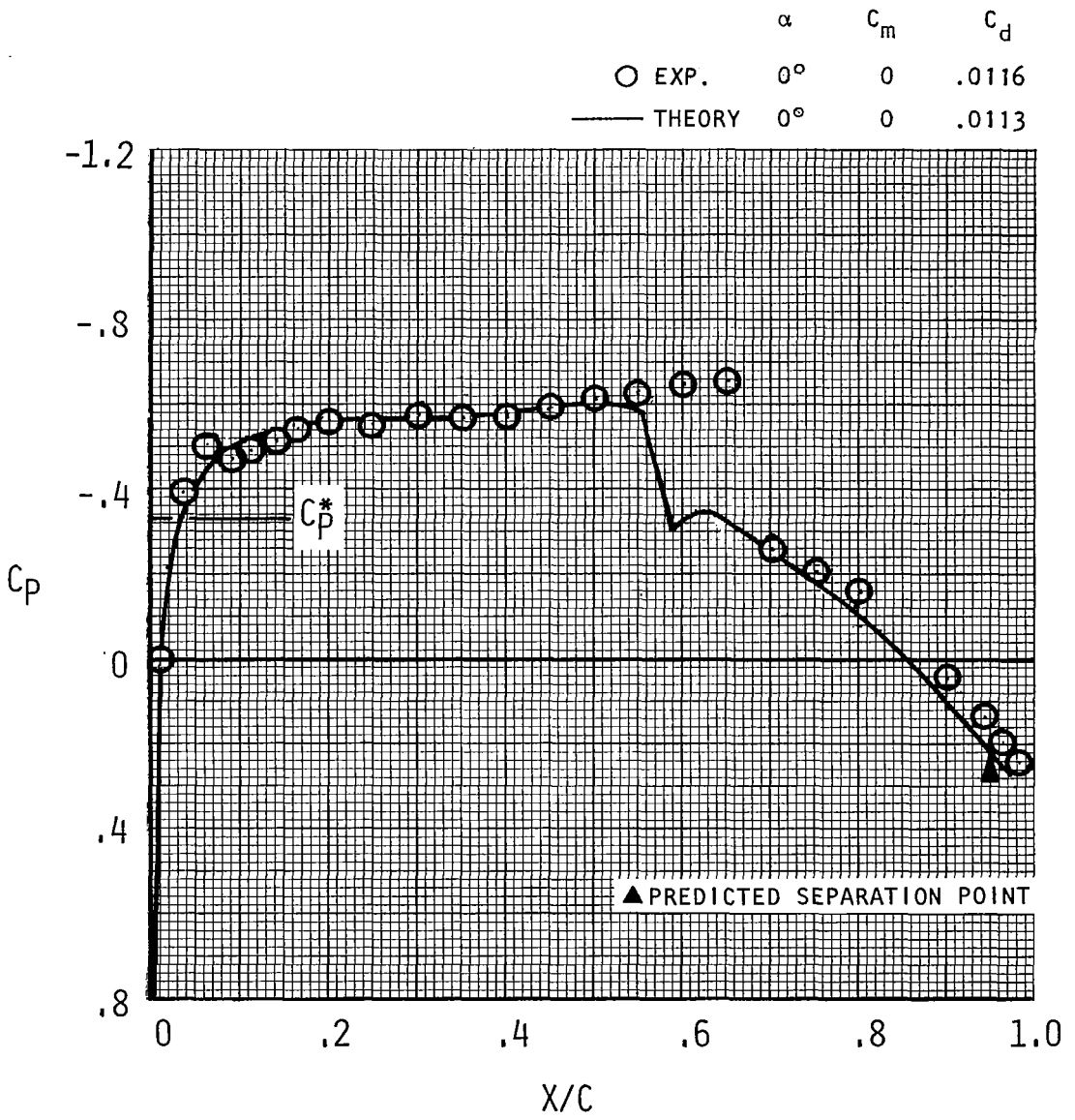

c. $M = 0.84$, $C_n = 0$, $R_N = 7.7 \times 10^6$.

Figure 36. - Concluded.

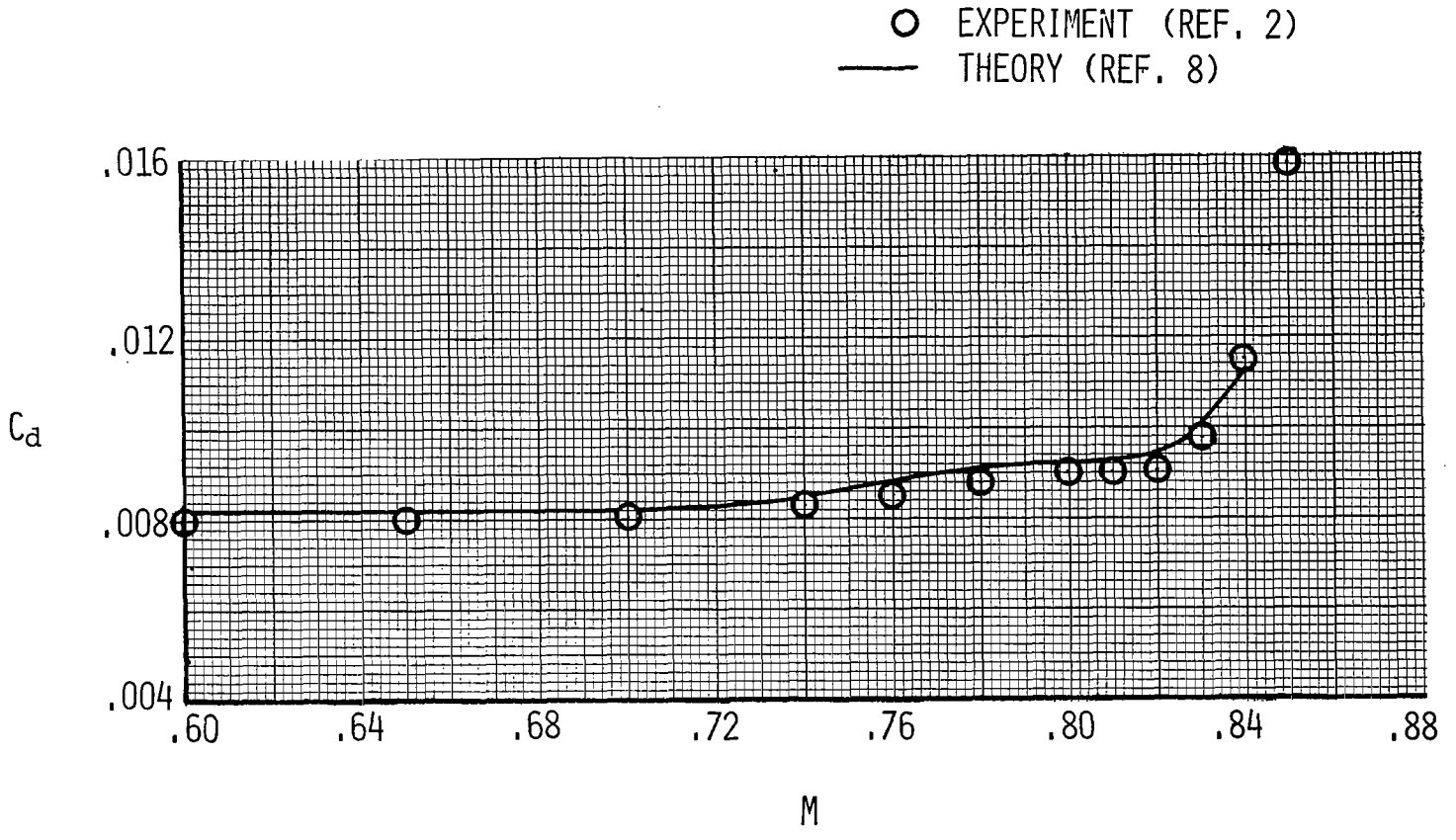

Figure 37. - Comparison of theoretical and experimental drag rise characteristics on an 11-percent thick symmetrical supercritical airfoil. $C_n = 0$; $R_N = 6.3$ to 7.7×10^6; $[X_T/C] = .05$.

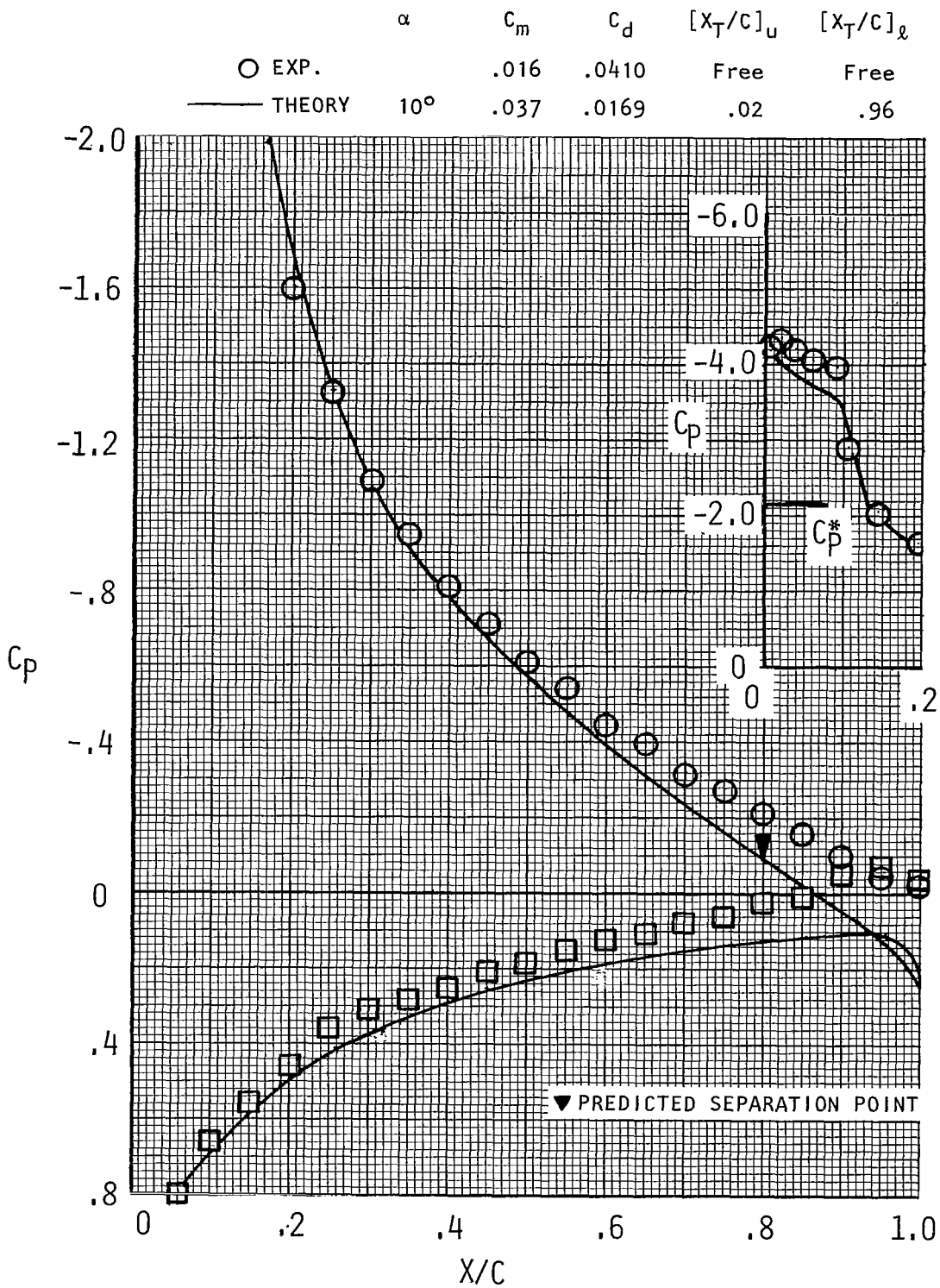

a. M = 0.50, C_n = 1.33, R_N = 4.0x10^6.

Figure 38. Correlation of NYU transonic airfoil analysis program using experimental data (ref. 23) for the FX69-H-098 airfoil.

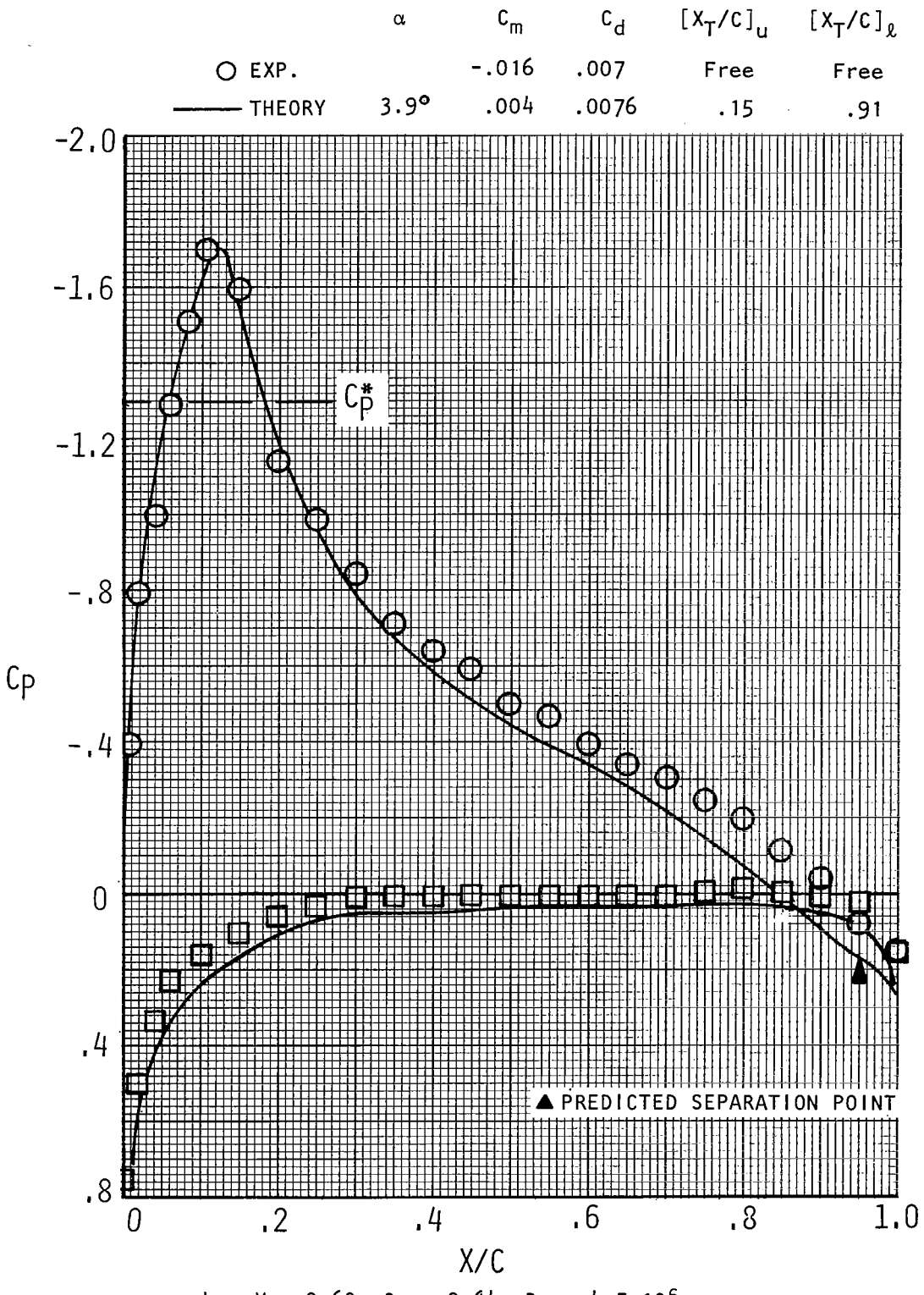

b. M = 0.60, C_n = 0.64, R_N = 4.5×10^6.

Figure 38. - Continued.

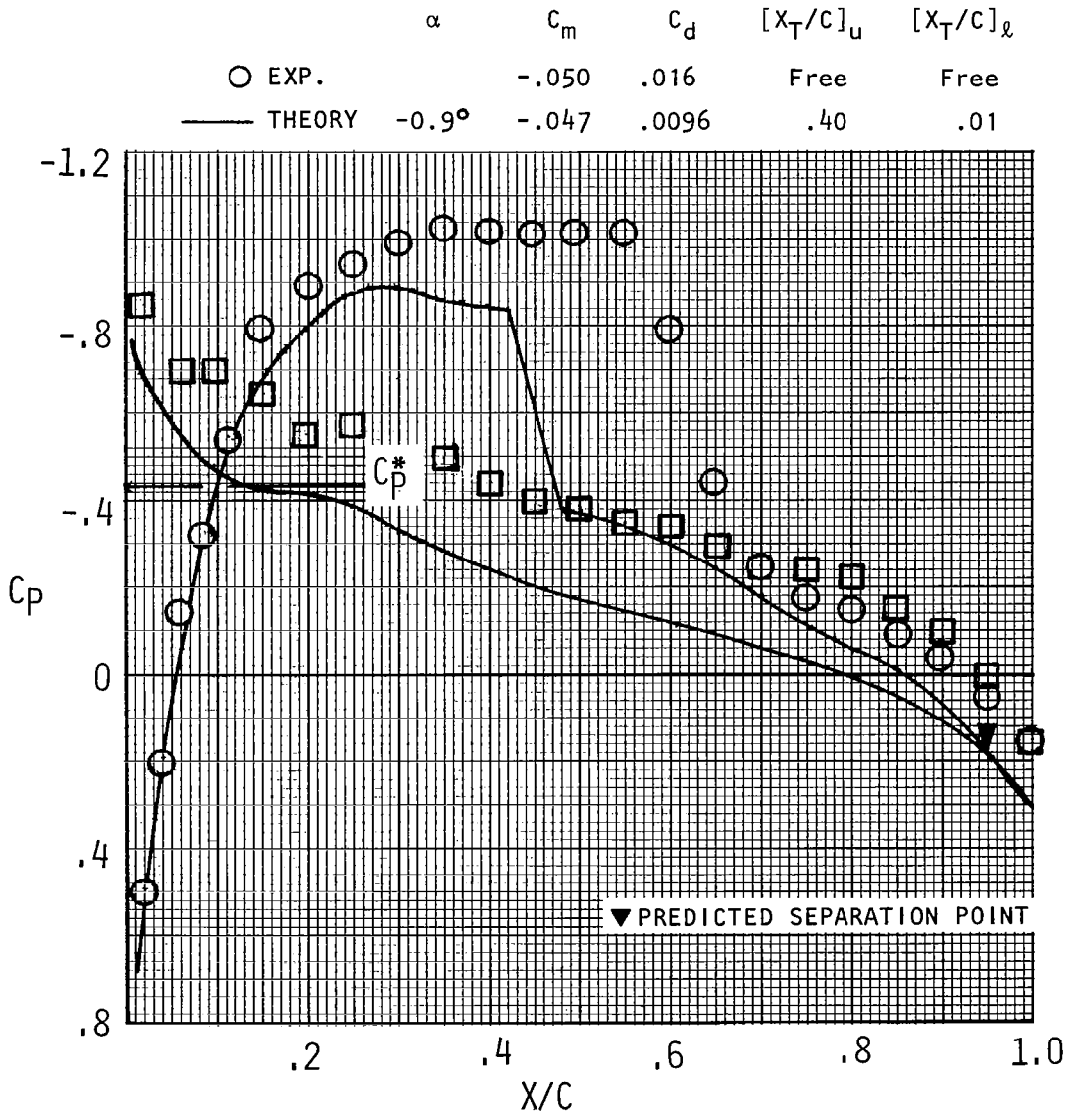

c. $M = 0.80$, $C_n = 0.15$, $R_N = 5.2 \times 10^6$.

Figure 38. - Concluded.

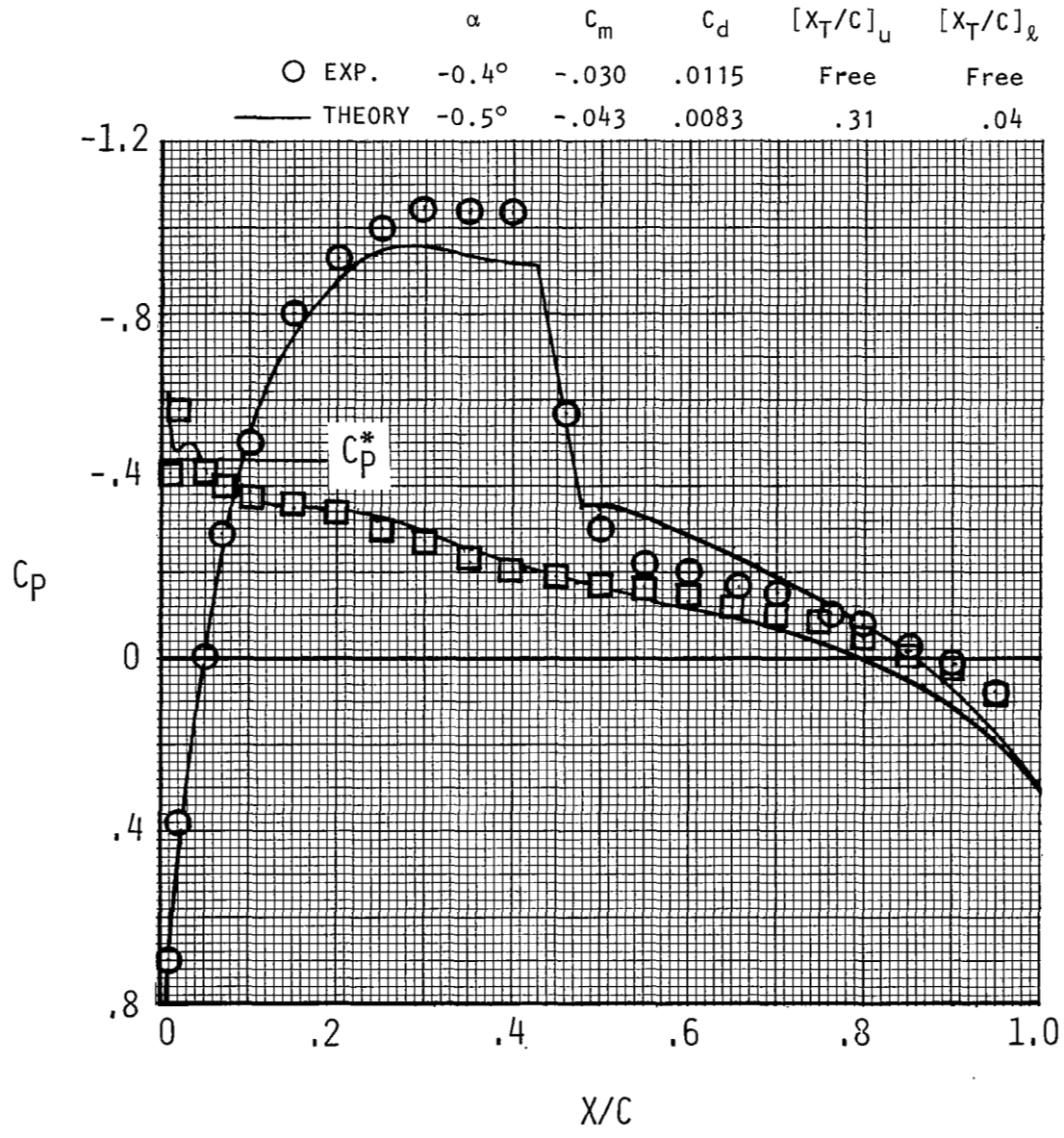

Figure 39. - Correlation of NYU transonic airfoil analysis program using experimental data (ref. 27) for the FX69-H-098 airfoil. $M = 0.79$, $C_n = 0.21$, $R_N = 8.9 \times 10^6$.

1. Report No.	2. Government Accession No.	3. Recipient's Catalog No.
NASA CR-2961		

4. Title and Subtitle	5. Report Date
THE AERODYNAMIC DESIGN OF AN ADVANCED ROTOR AIRFOIL	March 1978
	6. Performing Organization Code

7. Author(s)	8. Performing Organization Report No.
James A. Blackwell, Jr., and Bobby L. Hinson	LG77ER0208
	10. Work Unit No.

9. Performing Organization Name and Address	11. Contract or Grant No.
Lockheed-Georgia Company Marietta, Georgia	NAS1-14597
	13. Type of Report and Period Covered
12. Sponsoring Agency Name and Address	Contractor report
National Aeronautics and Space Administration Washington, DC 20546	14. Sponsoring Agency Code

15. Supplementary Notes

NASA-Langley Research Center Technical Monitor - Charles E. K. Morris, Jr.
The contract research effort which has led to the results in this report was financially supported by USARTL (Langley Directorate).

16. Abstract

An advanced rotor airfoil has been designed utilizing supercritical airfoil technology and advanced design-and-analysis methodology. The new airfoil was designed subject to stringent aerodynamic design criteria for improving the performance over the entire rotor operating regime. The design was accomplished using a physical-plane, viscous, transonic inverse-design procedure, and a constrained function-minimization technique for optimizing the airfoil leading-edge shape. The section is predicted to achieve most of the aerodynamic performance objectives which insure an improved design.

17. Key Words (Suggested by Author(s))	18. Distribution Statement
airfoils, rotors	FEDD Distribution Subject Category 02

19. Security Classif. (of this report)	20. Security Classif. (of this page)	21. No. of Pages	22. Price*
Unclassified	Unclassified	110	

Available: NASA's Industrial Application Centers

NASA-Langley, 1978